

Democratic and Popular Republic of Algeria

وزارة التعليم العالي والبحث العلمي

Ministry of Higher Education and Scientific Research

University of Mohamed Khider –
Biskra
Faculty of Exact Sciences and
Science of Nature and life.
Department of Material Sciences



جامعة محمد خيضر - بسكرة
كلية العلوم الدقيقة وعلوم الطبيعة والحياة
قسم علوم المادة

Thesis presented to obtain the degree:

Doctorate LMD

Option:

Physics of semiconductors

Entitled:

**Investigation of solar cell devices based on Indium Gallium Nitride
(InGaN) ternary alloy.**

Presented by:

Benslim Amina

In front of the jury composed of:

Nouredine Sengouga	professor	U.M.K. Biskra	President
Meftah Amjad	Professor	U.M.K. Biskra	Supervisor
Meftah Afak	Professor	U.M.K. Biskra	Co-Supervisor
Nouadji Malika	M.C.A	U.M.K. Biskra	Examiner
Filali Walid	M.R.A	C.D.T.A. Algiers	Examiner

Acknowledgement

First of all, thank to *Allah* who enabled me to complete this work and facilitated this path for me. Countless people supported my effort on this work, I would like to thank Professors Amjad Meftah and Afak Meftah for their help and guidance during the research process. Also, I would like to thank Professor Nouredine Sengouga and my colleague Madani Labeled for their valuable assistance. My thanks also go to the members of the discussion committee for agreeing to judge this work and honoring me with their presence. And last, but not least, I would like to thank my family, for their patience and support during my research period, and All of my friends whose support has helped me. We do not forget to present the generous form to all the respected professors at the University of Mohamed Khider in Biskra, we say thank you very much for all your efforts.

Dedication

This thesis is dedicated to:

My great parents, who never stop giving of themselves in countless ways,

My beloved brothers and sisters,

To all my friends who encourage and support me,

All the people in my life who touch my heart, I dedicate this research.

ملخص

توفر سبيكة نيتريد الغاليوم الإنديوم (InGaN) إمكانية كبيرة لتصميم وتصنيع خلايا شمسية فائقة الكفاءة نظراً لمجموعتها الواسعة من فجوات النطاق المباشر والامتصاص القوي والخصائص الكهروضوئية الأخرى. نجري في هذا العمل عمليات محاكاة عددية باستخدام برنامج محاكاة جهاز Silvaco Atlas ، ركزنا أولاً على اختيار المعلمات المناسبة بما في ذلك تركيبة الإنديوم x_{In} ووظيفة عمل المعدن ϕ_M التي تقدم أفضل أداء. مع دراسة المعدن المناسب لتشكيل تقاطع شوتكي مع InGaN بين المعادن التالية: Pt، Ni، Au و Pt.

تنقسم التحسينات التي أجريناها على الخلية الشمسية الحاجز Schottky المستندة إلى InGaN إلى مرحلتين. تتكون المرحلة الأولى من إضافة طبقة جوهريّة من نفس تركيز الإنديوم بين أشباه الموصلات والمعدن. ندرس تأثير سماكة هذه الطبقة وتأثير العيوب على معاملات الخرج لهذه الخلية الشمسية. بعد ذلك، استبدلنا هذه الطبقة الجوهريّة المنتظمة بطبقة تدريجية من حيث تكوين الإنديوم وقارننا نتائج الخليتين الشمسيّتين. حصلنا على نتائج ممتازة في حالة الطبقة الجوهريّة التدريجية حتى مع وجود عيوب.

المرحلة الثانية من التحسينات تضمنت تدعيم حاجز شوتكي (بين المعدن والنصف الناقل) بطبقة اوكسيد عبر زيادة ارتفاعه، مع دراسة عدة اوكاسيد وهي: SiO_2 ، Al_2O_3 و HfO_2 . ثم درسنا تأثير تركيز الشحنات الثابتة والسماحية.

الكلمات المفتاحية: سبيكة InGaN ، الخلايا الشمسية ، النمذجة العددية ، كفاءة التحويل.

Abstract

The indium gallium nitride (InGaN) alloy offer a great possibility of designing and fabricating ultra-high efficiency solar cells due to its wide range of direct band gaps, strong absorption and other optoelectronic properties. This work is numerical simulation using Silvaco Atlas software to study InGaN-based Schottky barrier solar cell. First, we focused on the suitable parameters including the indium composition x_{In} and the metal work function ϕ_M that gives the best performances, followed by the study of the appropriate metals among Pt, Ni, Au and Pd to form a Schottky junction with InGaN.

Optimizations we have made to the InGaN-based Schottky barrier solar cell are divided into two steps. The first one consists of adding an intrinsic layer (with the same concentration of indium as the doped region) between the semiconductor and the metal. We study the effect of the thickness of this layer and the effect of defects on the output parameters of the solar cell. Then, the uniform intrinsic layer is replaced by a gradual one in terms of indium composition. We found that the gradual intrinsic layer, even in the presence of defects, provides the best performance.

In the second step of the optimizations, between the metal and the semiconductor was inserted an oxide layer and several oxides was studied: SiO₂, Al₂O₃ and HfO₂, including the effect of negative fixed charge density and the permittivity.

Keywords: InGaN alloy, Solar cell, Numerical modeling, Conversion efficiency

Table of Contents

Acknowledgement	i
<i>Dedication</i>	ii
ملخص	iii
Abstract	iv
Table of Contents	v
List of figures	viii
List of tables	xi
General Introduction	1
Chapter I: Schottky barrier solar cell and InGaN material.	5
I.1. Introduction	6
I.2. Basics of Schottky barrier junction	6
I.2.1 Under equilibrium condition.....	7
I.2.2. Effect of biasing.....	8
I.2.3. Current-Voltage characteristics ($I - V$)	9
I.2.4. Effect of traps in schottky junctions	12
I.3. Schottky barrier solar cell.....	12
I.3.1. Working principle	13
I.3.2 ($I - V$) Characteristics of a Solar Cell	14
I.3.3 Suitable materials for Schottky electrodes.....	15
I. 3.4 MIS (Metal-Insulator-Semiconductor) solar cell.....	17
I.4 InGaN for solar cells	18
I.4.1 InGaN material properties.....	18
I.4.2 Growth techniques	25
I.4.3 Challenges of InGaN alloys	26
I.4.4 Studied InGaN-based solar cell structures	29

Chapter II: Silvaco Atlas Simulation Software	30
II.1 Introduction	31
II.2 Device modeling	32
II.2.1 Basic semiconductor equations	32
II.2.2 Numerical methods.....	33
II.3 Deckbuild	34
II.4 Definition of the structure	36
II.4.1 Specifying mesh	36
II.4.2 Specifying regions	37
II.4.3 Specifying electrodes.....	39
II.4.4 Specifying doping.....	39
II.5 Definition of material parameters and models	40
II.5.1 Specifying material properties.....	40
II.5.2 Specifying physical models.....	41
II.5.3 Specifying contact characteristics	41
II.5.4 Specifying interface properties	42
II.6 The choice of the numerical method.....	42
II.7 Obtaining solutions	43
II.8 Interpreting results	44
II.9 Luminous.....	45
II.10 Solar cell simulation.....	46
II.11 Tonyplot	48
II.11.1 2D Mesh plot	48
11.2 X-Y plots	50
Chapter III: Results and discussions	52
III.1 Introduction.....	53
III.2. Device structure and modelling	53
III.3 Initial study to determine the suitable parameters of the solar cell.....	55
III.3.1 Part 1	55
III.3.2 Part 2	60
III.4 Optimizations.....	63

III.4.1 Adding a uniform Intrinsic Layer.....	63
III.4.2 The effect of interfacial layer defect	64
III.4.3 Adding gradual intrinsic layer.....	66
III.4.4 Influence of an insulating layer on the Schottky solar cell	70
III.4.5 Changing the Schottky solar cell to a MIS solar cell	72
III.5. Summary	76
General Conclusion	78
References.....	80
Publications and conferences.....	90

List of figures

Chapter I: Schottky barrier solar cell and InGaN material.

Figure I. 1: Energy band diagrams of metal contact to n-type semiconductor with (a) materials separated from each other and (b) after contact.	7
Figure I. 2: Energy band diagrams of metal on contact n-type semiconductor under (a) forward bias (b) reverse bias.	9
Figure I. 3: Schematic $I - V$ characteristics of Schottky diodes.....	10
Figure I. 4: Energy band diagram of a forward biased Schottky barrier junction on n-type semiconductor showing different transport processes.....	11
Figure I. 5: Energy band diagram of Schottky barrier solar cell under illumination.	13
Figure I. 6: $I - V$ and $P - V$ characteristics of a solar cell under illuminated conditions.	14
Figure I. 7: Schematic wurtzite lattice of InGaN material.	19
Figure I. 8: Bandgaps of wurtzite GaN, AlN and InN.....	20
Figure I. 9: (a) Refractive index dispersion relations and (b) absorption coefficient spectra of InGaN films	23
Figure I. 10: Energy band diagram of (a) an ideal material, and (b) a phase separated material.	28

Chapter II: Silvaco Atlas Simulation Software

Figure II. 1: Atlas inputs and outputs.	31
Figure II. 2: Screenshot from Deckbuild.	34
Figure II. 3 Atlas command groups and primary statements.....	35
Figure II. 4: Example of the mesh.	36
Figure II. 5: Tonyplot screenshot showing regions example.	38
Figure II. 6: Tonyplot screenshot showing electrodes examples.....	39
Figure II. 7: Optical Beam Geometry.....	46
Figure II. 8: Mesh plot dialog.....	48
Figure II. 9: Description of the display buttons in Tonyplot.....	49
Figure II. 10: Tonyplot screenshot showing outline tool.....	50
Figure II. 11: Screenshot of an X-Y plot in Tonyplot.	51

Figure III. 1: Structure of the InGaN based Schottky barrier solar cell studied in the simulation.	54
Figure III. 2: Band gap and the electronic affinity as function of the indium composition.	54
Figure III. 3: ($J - V$) characteristic for schottky solar cell with $x = 0.6$ and $\phi_M = 6.3$ eV.	55
Figure III. 4: (a) Short-circuit current density J_{SC} , (b) open-circuit voltage V_{oc} , (c) conversion efficiency η and (d) fill factor FF , as function of the indium composition with various metal.	56
Figure III. 5: Band gap energy diagram at equilibrium of the InGaN Schottky solar cell for different metals and 0.4 Indium composition.	57
Figure III. 6: External quantum efficiency (EQE) variation with Indium composition in $In_xGa_{1-x}N$ compound for Pt metal.	57
Figure III. 7: Band gap energy diagram at equilibrium of the InGaN Schottky solar cell for different metals and 0.8 Indium composition.	58
Figure III. 8: External quantum efficiency (EQE) for different metals and 0.8 Indium composition.	59
Figure III. 9: Electrical output parameters for the different reported values of ϕ_M versus In composition: (a) J_{SC} , (b) V_{oc} , (c) efficiency η and (d) FF.	61
Figure III. 10: ($J - V$) characteristic for different Indium compositions.	62
Figure III. 11: ($J - V$) characteristic for different Pt work function.	63
Figure III. 12: J_{SC} , V_{oc} , FF and η as a function of intrinsic layer thickness.	64
Figure III. 13: Effect of trap levels on (a) J_{SC} , (b) V_{oc} , (c) η and (d) FF	65
Figure III. 14: InGaN based Schottky barrier solar cell with gradual intrinsic layer structure.	66
Figure III. 15: Band gap energy diagram at equilibrium of the InGaN Schottky solar cell with gradual band gap energy of the intrinsic layer.	67
Figure III. 16: ($J - V$) characteristic for InGaN Schottky solar cell with a uniform intrinsic layer and gradual intrinsic layer.	68
Figure III. 17: External quantum efficiency (EQE) for InGaN Schottky solar cell with a uniform intrinsic layer and gradual intrinsic layer.	69
Figure III. 18: The gradual intrinsic layer solar cell efficiency η versus defect densities.	70
Figure III. 19: InGaN based MIS solar cell structure.	70
Figure III. 20: ($J - V$) characteristic for InGaN Schottky solar cell and MIS solar cell.	71

Figure III. 21: $(J - V)$ characteristics of simulated structure for different oxides.....	73
Figure III. 22: Reflectance factor of the oxides used in the simulation.....	74
Figure III. 23: External quantum efficiency (EQE) for different oxides.....	74
Figure III. 24: J_{SC} , V_{oc} , FF and η as a function of negative fixed charge density in Al_2O_3 oxide.	75
Figure III. 25: J_{SC} , V_{oc} , FF and η as a function of permittivity of Al_2O_3 oxide.....	76

List of tables

Chapter I: Schottky barrier solar cell and InGaN material.

Table I. 1: Values of work function and electrical conductivity of some common metals.	15
Table I. 2: The lattice parameters values (a and c) of InN and GaN.	19
Table I. 3: Experimental electrical parameters of GaN and InN.	20
Table I. 4: GaN, InN material mobility parameters.	22
Table I. 5: Experimental values of C and D for different indium composition x	24
Table I. 6: Crystallographic data of various materials that can act as a substrate for InGaN films.	26

Chapter III: Results and discussions

Table III. 1: The Indium composition corresponding to the maximum efficiency for Au, Ni, Pd and Pt Schottky contacts.	60
Table III. 2: The optimum Indium composition for the different Pt work function values.	62
Table III. 3: Traps related to InGaN layer.	64
Table III. 4: J_{SC} , V_{OC} , FF and η for InGaN schottky solar cell with uniform intrinsic layer and gradual intrinsic layer.	68
Table III. 5: J_{SC} , V_{OC} , FF and η for InGaN schottky solar cell and MIS solar cell.	71
Table III. 6: Parameters of oxides: Band gap, Affinity, Permittivity, electron and hole effective masses and fixed charge.	72
Table III. 7: J_{SC} , V_{OC} , FF and η for InGaN MIS solar cell with different oxides.	73

List of acronyms

J_{sc}: Short Circuit Current density

V_{oc}: Open Circuit Voltage

FF: Fill Factor

PCE: Power conversion efficiency

P_{in}: Input Power

P_{max}: Maximum Power

TE: Thermionic emission

TFE: Thermionic field emission

FE: Field emission

EQE: External quantum efficiency

MIS: Metal-Insulator-Semiconductor

MBE: molecular beam epitaxy

MOCVD: metal organic chemical vapor deposition

MOVPE: metal organic vapor phase epitaxy

PECVD: plasma enhanced evaporation deposition process

HVPE: hydride vapor phase epitaxy

PAMBE: Plasma-assisted molecular beam epitaxy

SRH: Shockley-Read-Hall recombination

DLTS: deep-level transient spectroscopy

General Introduction

General Introduction

Energy is used extensively in our daily lives, and the need for it increases with the continued advancement of technology. Therefore, the world began to exploit renewable energy, since it is non-permeable and free energy, in addition to being clean. There are many renewable energy sources, but solar energy is much larger than other renewable energies[1]. Electric power is generated by photovoltaic cells, whether for small systems such as homes and buildings, or central generating stations connected to the electrical grid[2].

Researchers are racing to improve the performance of solar cell devices, whether by improving the device's composite materials or designing the device's structure to generate more power. Schottky barrier solar cell is based on one type of semiconductor (N or P) and a metal that replaces the second type, and that is why it is considered the simplest type of solar cell. It is characterized by being inexpensive and easy to manufacture, in addition to that it gives a better spectral response in the shorter-wavelength region due to the close surface depletion region[3].

Among the semiconductors that have received significant interest recently are III-nitride materials due to their attractive properties. Among these materials is InGaN, which has a crystal structure (Wurtzite) and a direct energy band gap[4], which allows for efficient absorption of light. Also, its energy range can be engineered by changing the indium content to cover the entire electromagnetic spectrum from the visible region to the ultraviolet region[5]. It has exhibited a higher resistance against proton irradiation damage in comparison with traditional GaAs and GaInP solar cell materials[6]. Among the drawbacks that make InGaN difficult to manufacture is that it is difficult to achieve P-type doping and it is difficult to grow in good quality, and on which ohmic contacts are difficult to realize[7].

- **Objective**

Schottky junction solar cells are a good alternative to PN solar cells since the metal compensates for the P-type semiconductor which is the most important drawback for InGaN. Therefore, the aim of this work was to model a Schottky barrier solar cell based on InGaN and study its performance in different conditions, in addition to optimizing the structure to give high performance and good efficiency, using Silvaco Atlas TCAD simulation software.

- **Previous work**

III-V nitride materials and their alloys have been widely used in several compounds including photodetectors, LEDs, and laser diodes[8]. But it was not used in solar cells until 2007, publications were reported about two InGaN solar cell type PN[9,10]. Many works have been carried out on InGaN-based PN devices, PIN devices and it was reported that the p-type doping of high Indium composition is very difficult[3,11].

However, few works were done on n-InGaN Schottky barrier solar cells, Jun-Jun published a study in 2009 [6], and another publication by Chen et al.[12]. Later on, a solar cell of the same type was manufactured by S. Lin and al[13].

The high In composition is required for high efficiency of InGaN-based solar cells[14], But most of the solar cells manufactured in previous years do not exceed 0.35 indium content[15]. While alloys with a high In content of 0.68[16] and 0.69-0.89[17] were reported.

The difficulty of developing Schottky InGaN solar cell with high barrier height and low leakage current has also been reported due to the difficulty of accessing suitable metal with high work function.[18]. Chen et al.[12] have fabricated Au/Pt/n-In_{0.2}Ga_{0.8}N Schottky barrier solar cell and reported experimental effect of doping levels on its photovoltaic performances[3].

Mahala et al. [3] have studied the effects of indium composition, thickness and donor doping density of the n-InGaN layer on n-InGaN-GaN Schottky barrier solar cell performance using platinum as Schottky contact. Then another numerical study was published by Sidi Ould Saad Hamady et al[14]. for a simple Schottky solar cell with an efficiency of 18.2 % at an indium composition of 0.6 with a work function of 6.3 eV.

Recently, Khetrou et al. [19] have performed numerical study by Silvaco-Atlas of the Schottky n-InGaN/n-GaN solar cell with compositionally graded layer between GaN and InGaN, and reported an expected conversion efficiency of 21.69% at indium composition 0.54 and work function 6.3 eV.

- **Organization**

This thesis is organized as follows. In Chapter I, we cover the basics on schottky junction, then schottky solar cell fundamentals, and introduce the properties of InGaN and the Growth

Techniques, in addition to its drawbacks. In chapter II we give details of the modeling software Silvaco ATLAS. In Chapter III, we present the design, simulation, and optimization of the InGaN Schottky solar cell. The results and potential future work are discussed in this chapter.

Chapter I: Schottky barrier solar cell and InGaN material.

Chapter I: Schottky barrier solar cell and InGaN material

I.1. Introduction

Schottky barrier solar cells are receiving a lot of attention recently, due to their simplicity in manufacturing and also because the conductor is a good alternative to the second semiconductor layer. This type of cell is the simplest in terms of structure compared to other solar cells (PN and PIN). It can also be fabricated easily and at low cost[3].

Recent researches have demonstrated the feasibility of wide band gap semiconductor such as InGaN and GaN as alternative materials for next-generation solar cells. III-N materials are the best candidates for high power, high frequency and high temperature applications because of their interesting material properties compared to InGaP, and GaAs[6,20]

Due to the direct band gap spanning from 0.7 eV to 3.42 eV[21], and additional advantages like high absorption coefficients, low effective electron mass, radiation tolerance, etc. InGaN films have been used in the manufacture of high-efficiency solar cells such as multiple quantum well solar cells[22] and multi-junction solar cells[23]. Despite its many advantages, this material still has many challenges that make it difficult to obtain a high-quality crystal alloy. This makes InGaN solar cells need more studies and development[24].

In order to understand the working mechanism of Schottky barrier solar cells based on InGaN material, we present, in this chapter, the principle of Schottky junction taking into account the good Schottky connection condition required for the solar cells. For that purpose, we will study the most suitable materials for schottky electrodes to form this type of connection. We will also focus on InGaN material, from its advantages and properties to its growth method and disadvantages.

I.2. Basics of Schottky barrier junction

Electronic devices usually consist of several materials with different properties (insulator, conductor, semiconductor), and due to this difference, junctions are formed with a critical interface between the materials. A Schottky junction is a junction formed between a metal and a semiconductor because of the Fermi energy mismatch between the metal and the semiconductor, which is due to the difference in their work functions[25]. Schottky junction

Chapter I: Schottky barrier solar cell and InGaN material

energy levels diagram before and after the two materials connection is represented in Figure I.1[26]

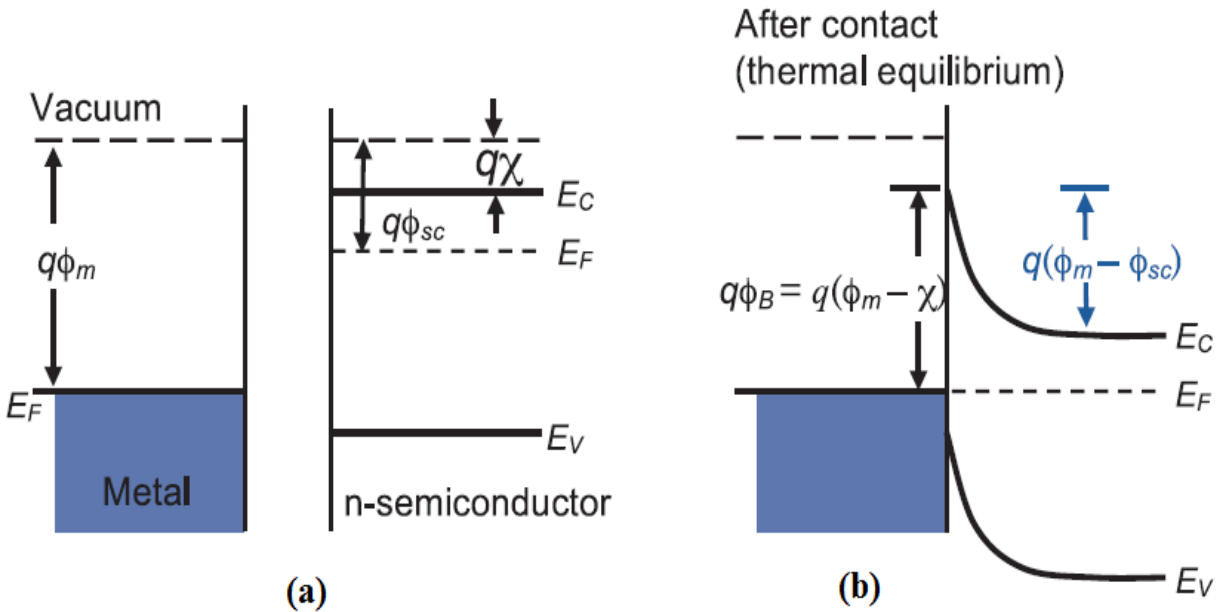


Figure I. 1: Energy band diagrams of metal contact to n-type semiconductor with (a) materials separated from each other and (b) after contact[26].

The work function ϕ is one of the properties of the metals (ϕ_m) and the semiconductors (ϕ_{sc}) and it is defined as the amount of energy required to raise an electron from the fermi level (E_F) to the vacumi level [27]. But the semiconductor work function is a variable quantity because the fermi level E_F of the semiconductor varies with the doping. The electron affinity χ is the energy difference of an electron between the vacuum level and the conductor band edge E_c (the energy required to free an electron at the bottom of the conductor band)[27]. q is the electron charge and E_v is the valence band.

I.2.1 Under equilibrium condition

In thermal equilibrium situation after the contact has been made, electrons flow from the semiconductor (which has higher energy than the metal electrons) to the metal until the fermi level on the two sides is brought into coincidence as shown in Figure I.1(b). The free electrons concentration in the semiconductor near the boundary decreases and the electrons leave behind a positive charge of ionized donors and creating depletion region (this region near the metal gets

Chapter I: Schottky barrier solar cell and InGaN material

depleted of free electrons)[28]. Thus, this region becomes positively charged and on the other side of the metal, the electrons form a thin sheet of negative charge. Consequently, an electric field is established from the n-type semiconductor to the metal[29].

The energy bands in the semiconductor will bend up in the depletion region (the band gap E_g do not change by making contact with metal), the amount of band bending is equal the difference between the work function of the metal ϕ_m and the one of semiconductor ϕ_{sc} and it is given by[28]:

$$qV_i = (\phi_m - \phi_{sc}) \quad (I.1)$$

Where V_i is the contact potential difference, while qV_i is the barrier that an electron must cross to pass from the semiconductor to the metal. But the barrier from the metal to the semiconductor namely Schottky barrier height is given by the schottky-mott equation[29]:

$$q\phi_B = q(\phi_m - \chi) \quad (I.2)$$

I.2.2. Effect of biasing

The energy band diagram changes in the space charge region of the schottky junction when an external polarization is applied, and the Fermi levels no longer line up as shown in Figure I.2. The current that flow in the schottky junction depends on the value of applied potential and the type of bias[29].

Chapter I: Schottky barrier solar cell and InGaN material

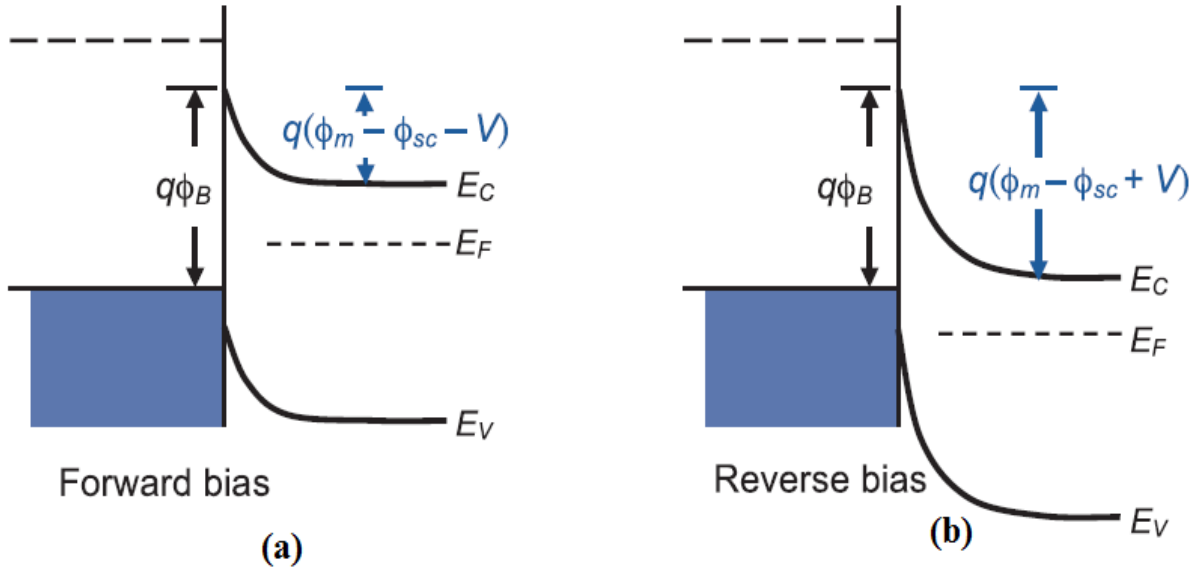


Figure I. 2: Energy band diagrams of metal on contact n-type semiconductor under (a) forward bias (b) reverse bias[26].

If the metal is connected with positive bias, the junction is considered to be in direct bias by a voltage $V = V_F$, the depletion region width decreases and the contact potential difference reduced from V_i to $(V_i - V_F)$. In this case, the electrons on the semiconductor side are easily transferred to the metal through the reduced barrier[29]. This leads to an increase in current with increasing external potential. Energy band diagram of the Schottky junction under forward bias is shown in Figure I.2 (a).

In the case of a reverse bias, the external potential is applied in the same direction as the junction potential and the applied voltage is given by $V = V_R$, the potential barrier increase to $(V_i + V_R)$ and it increase the width of the depletion region as shown in Figure I.2 (b)[30]. Under a reversed bias, only a small amount of electrons in the metal may be able to overcome the potential barrier. This leads to a current flowing in the opposite direction which is small compared to the forward current.

I.2.3. Current-Voltage characteristics ($I - V$)

The current-voltage ($I - V$) characteristic of schottky diode is shown in the Figure I.3.

Chapter I: Schottky barrier solar cell and InGaN material

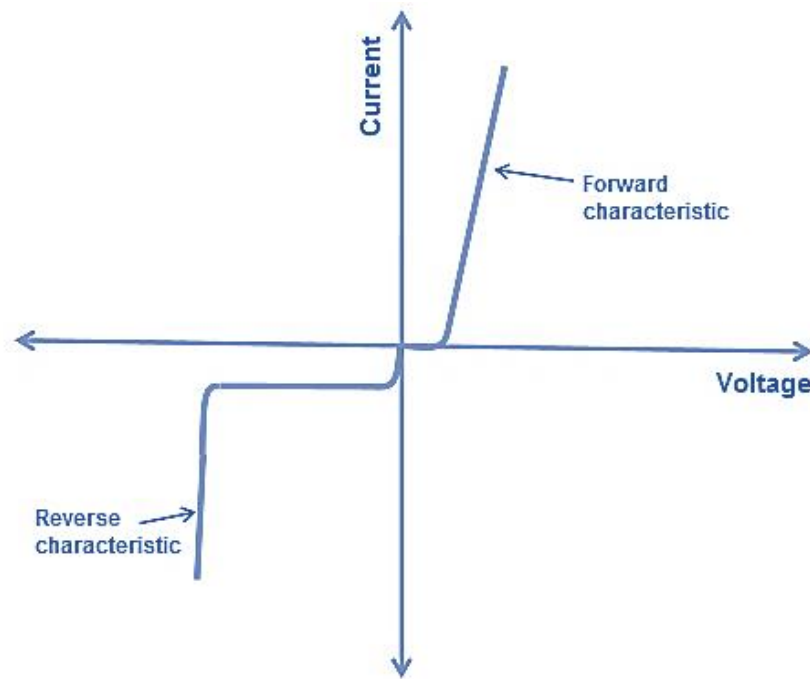


Figure I. 3: Schematic $I - V$ characteristics of Schottky diodes[26].

It is almost similar to the P-N junction diode. However, the transport mechanism of schottky junction is different from the P-N junction. There are three carrier transport for an ideal schottky contact: Thermionic emission (TE) , Tunneling through the barrier (field emission (FE)) and thermionic field emission (TFE)) [28,31], where the current flows from the semiconductor to the metal in forward bias or in the opposite direction in reverse bias. The transport mechanisms are illustrated in Figure I.4[32].

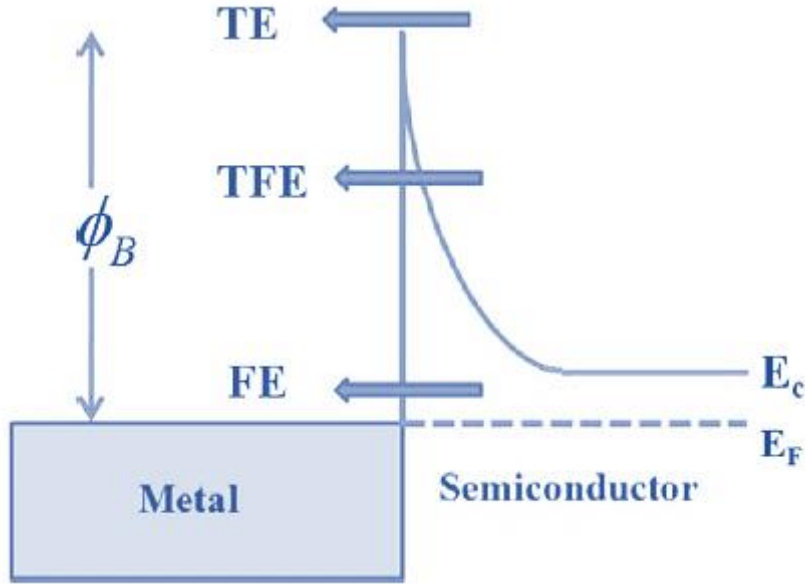


Figure I. 4: Energy band diagram of a forward biased Schottky barrier junction on n-type semiconductor showing different transport processes[32].

I.2.3.1. Diffusion and thermionic emission over the barrier

The movement of the emitter electrons over the barrier is the dominant mechanism in the schottky junction, namely the thermionic emission (TE) and this includes only electrons with an energy higher than qV_i . It comes with drift diffusion processes in the depletion region. The current-voltage ($I - V$) characteristic of schottky barrier diode in the thermionic emission (TE) regime is given by [30,33]:

$$I = I_0 \left\{ \exp \left[\frac{q(V - IR_s)}{nkT} \right] - 1 \right\} \quad (\text{I.3})$$

where I_0 is the saturation current:

$$I_0 = SA^*T^2 \exp \left(\frac{-q\phi_B}{kT} \right) \quad (\text{I.4})$$

such as the voltage (V) is applied to the semiconductor, the current (I) of electrons flow from the semiconductor into the metal through Schottky barrier height (ϕ_B), (n) is ideality factor, (A^*) is effective Richardson's constant and (R_s) is series resistance.

Chapter I: Schottky barrier solar cell and InGaN material

The forward and reverse bias currents for a Schottky junction formed between metal and n-type semiconductor which are plotted in Figure I.3 can be calculated using Eq. (I.3).

I.2.3.2. Tunneling through the barrier

In addition to the thermionic emission and drift diffusion mechanisms, there are also two other mechanisms that depend mainly on tunneling transport. Which are field emission (FE) and thermionic field emission (TFE). Electrons with energy close to the Fermi level E_F can tunnel from the semiconductor into the metal at low temperature, and because of heavy doping, the depletion region becomes very thin, this facilitates this process known as the field emission (FE)[31]. The trajectory of the carrier transport by the field emission in the energy diagram is shown in Figure I.4.

But at higher temperature, these electrons gain thermal energy, which allows them to rise above the Fermi level, where they find a thinner barrier to cross to the other side and this is known as the thermionic field emission (TFE)[28].

I.2.4. Effect of traps in Schottky junctions

Defects in Schottky junctions are usually localized in the interface of the semiconductor in contact with the metal in the form of electron traps because of the mismatch between the two materials. These traps may adversely affect the performance of Schottky devices, especially on large band gap semiconductors. It has been proven in previous studies that the Schottky barrier height can be changed by changing the occupancy of the traps, so that the more traps occupied at the interface[34], the barrier height begins to increase, thus a decrease in electrons traveling above the barrier (TE). Therefore, the performance of Schottky devices depends largely on the method of surface preparation. by treating the interface to create an interface trap distribution. The defects are also mitigated by adding an insulating layer in the interfacial region (MIS structure), and this can be attributed to tunneling assisted by the traps in the interface between oxides and semiconductor to improve the performance of the cell[35].

I.3. Schottky barrier solar cell

As is well known, Solar cells are devices that convert sunlight into ready-to-use electrical energy, and its energy is a form of clean renewable energy. Usually solar cells consist of two layers N-type and P-type doped semiconductors attached to external electrodes but, in Schottky

Chapter I: Schottky barrier solar cell and InGaN material

solar cells, one of the layers is dispensed and replaced with metal. Researchers have resorted to this type of solar cell for several reasons, including compensating semiconductors that are difficult to doping. Also, using metal instead of the semiconductor may be less expensive to manufacture solar cells[13]. In addition, Schottky junction solar cells are expected to give better spectral response in the shorter wavelength region due to the near surface depletion region[3].

I.3.1. Working principle

Most of the solar cells have the same working principle based on 3 important steps: (i) Of the absorbed photons, only photons with higher energy than the bandgap energy of the semiconductor will create the free photo-generated electron-hole pairs. (ii) Separation of the photo-generated pairs by the electric field in the space charges region. (iii) Minority carrier assembly across external electrodes to form a current-voltage ($I - V$) characteristic. However, Schottky barrier solar cells differ from the classical solar cells in the step (iii); as it is known on Schottky devices, it depends on the majority carriers unlike PN junction solar cell [36,37], because the current of the majority carriers mainly contributes to the thermionic emission (TE) so that the electrons in the metal move over the Schottky barrier height (ϕ_B) if they have sufficient energy as shown in Figure I.5.

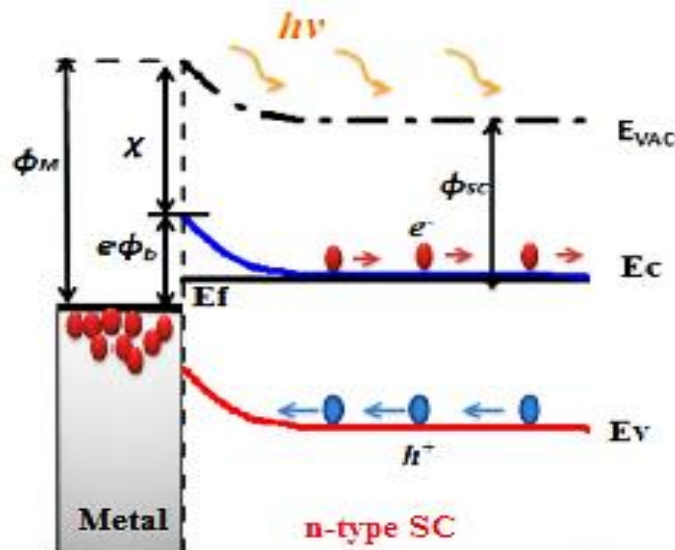


Figure I. 5: Energy band diagram of Schottky barrier solar cell under illumination[19].

Chapter I: Schottky barrier solar cell and InGaN material

A Schottky barrier solar cell has advantages over the standard designs. For example, the space charge region extends in the semiconductor, the same applies to the associated electric field. This removes the need for a window layer to prevent carrier flow in the wrong direction and also enhances collection of carriers generated by higher energy photons which are absorbed very close to the surface [38].

I.3.2 ($I-V$) Characteristics of a Solar Cell

Under illumination the photo-generated current flows in the opposite direction to the forward current under dark conditions (diode). Therefore, the current through the solar cell under illumination is given by[6,39]:

$$I_L = I_D - I_{sc} = SA^*T^2 \cdot \exp\left(\frac{-q\phi_b}{kT}\right) \left[\exp\left(\frac{qV}{nkT}\right) - 1 \right] - I_{sc} \quad (I.5)$$

where I_{sc} denotes the short circuit current of the solar cell under illumination.

There are four important parameters for a solar cell device extracted from the $I-V$ characteristic, it helps us to know the performance of the cell:

The short-circuit current (I_{sc}): the maximum current that can be extracted from the solar cell when the voltage equal to zero as shown in Figure I.6. I_{sc} is affected by several factors, including the area of the cell, the spectrum of incoming light and the carrier lifetime...etc.[39]

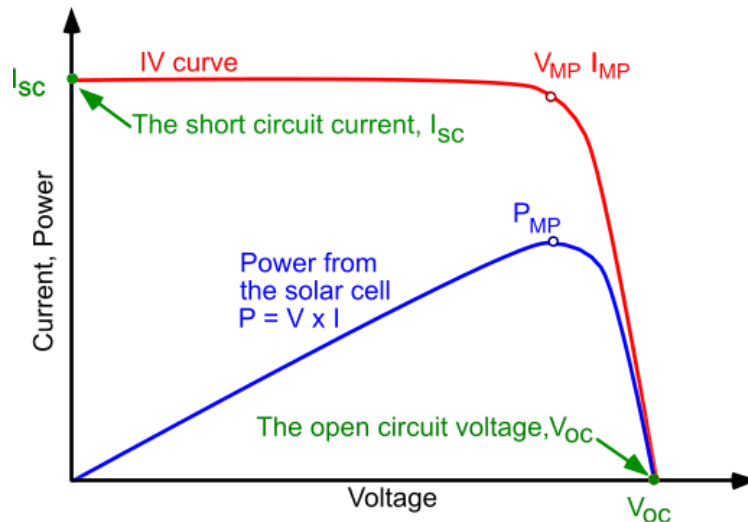


Figure I. 6: $I-V$ and $P-V$ characteristics of a solar cell under illuminated conditions.

Chapter I: Schottky barrier solar cell and InGaN material

The open-circuit voltage (V_{oc}): is the maximum voltage generated by the solar cell, and this occurs at zero current as shown in Figure I.6. In schottky barrier solar cell the open circuit voltage is given by[39]:

$$V_{oc} = \frac{KT}{q} \left(\ln \left(\frac{J_{sc}}{A^*T^2} \right) \right) + \phi_B \quad (I.6)$$

V_{oc} is dependent on the Schottky barrier height, as opposed to being dependent on E_g as in the PN solar cell.

Fill factor (FF): Represents a measure of the area of the largest rectangle that occupies the area of the property voltage current and it is a relation between 4 characteristics of $I - V$ curve. Therefore, the FF is defined as[39,40]:

$$FF = \frac{V_{mp}I_{mp}}{V_{oc}I_{sc}} \quad (I.7)$$

Conversion efficiency (η): is defined by the ratio of generated power over the total power of the incident light P_{in} on the solar cell per unit area, conversion efficiency is defined as[39,40]:

$$\eta = \frac{\text{Output power}}{\text{Input power}} = \frac{V_{mp}I_{mp}}{P_{in}} \quad (I.8)$$

The value of $P_{in} = 100 \text{ mWcm}^{-2}$ in the standard AM1.5 condition[41].

I.3.3 Suitable materials for Schottky electrodes

Wide bandgap semiconductors set a condition for selecting the appropriate metal to form a Schottky junction with, it requires the metal to have a work function (ϕ_m) higher than the electron affinity (χ) of the semiconductor to form Schottky contacts with appreciable Schottky barrier heights.

We present some metals and their electronic properties in Table I.1. Most metals conduct electricity to a certain extent. Some metals are more highly conductive than others. The most highly conductive metals are silver (Ag), copper (Cu), and gold (Au).

Chapter I: Schottky barrier solar cell and InGaN material

Table I. 1: Values of work function and electrical conductivity of some common metals.[42–45]

<i>Element</i>	Work function (eV)	Electrical Conductivity (S/m)	<i>Element</i>	Work function (eV)	Electrical Conductivity (S/m)
<i>Ag</i>	4.26 – 4.74	66.7×10^6	<i>Ni</i>	5.04 – 5.35	16.4×10^6
<i>Cu</i>	4.53 – 5.1	64.1×10^6	<i>Fe</i>	4.67 – 4.81	11.2×10^6
<i>Au</i>	5.47	49.0×10^6	<i>Pt</i>	5.64 – 6.35	10.2×10^6
<i>Al</i>	4.28	40.8×10^6	<i>Pd</i>	5.12 – 5.6	9.3×10^6
<i>Cr</i>	4.5	7.9×10^6	<i>Ti</i>	4.33	2.3×10^6

Another property to consider is the transparency of the used metal, the metal must cover the entire surface of the semiconductor to form a uniform, one-dimensional electric field profile[38], and to ensure a low series resistance. This reduces the number of photons passing through the absorbing layer, as well as a decrease in the amount of the photo-generation current. The appropriate thickness of the metal to be considered semi-transparent and pass the largest amount of photons to the absorbing layer is 5 nm [46]. The first transparent Schottky electrode of interest is an oxidized Ni/Au bilayer (5 nm Ni / 5 nm Au) with low sheet resistance [47,48]. Later, a more transparent electrode with good electrical conductivity was found; which is a thin oxidized layer of ruthenium and nickel (5 nm Ru / 5 nm Ni)[49].

Another material, that is distinguished by its transparency, is Indium Tin Oxide (ITO)[50], but it has a low work function (4.6-4.75 eV[51]) that is not suitable for use with Wide band gap semiconductor materials.

Currently, graphene (Gr) is considered a good alternative to metals because of its good properties such as high transparency (~97% optical transmissivity[52]) and good conductivity, in addition to flexibility. Although it has a small work function ($\phi=4.56$ eV[53]), it can be widely tuned by: (i) doping, where the work function changes from 4.2 eV to 5.14eV[54,55]. (ii) Tuning the work function of graphene in contact with noble metal it may reach to $\phi_m = 6.13$ eV[56]. (iii) Oxidation (graphene oxide GO or reduced graphene oxide rGO) is the largest impact on work function (6.7 eV) relative to all other groups[56].

Chapter I: Schottky barrier solar cell and InGaN material

I. 3.4 MIS (Metal-Insulator-Semiconductor) solar cell

MIS solar cells are a promising candidate for the cost effective photovoltaic devices due to the low temperature device process, and because oxides are abundant in resources, and can be chemically synthesized with good electrical properties[57]. This type of cell is one of the ways to improve Schottky barrier solar cells by adding a thin oxide layer between the metal and the semiconductor, where it has been proven to increase schottky barrier height in devices that use an oxide layer at the interface[58,59]. The insulating layer brings an additional advantage of minimizing the interactions between metal and the semiconductor[39].

In the presence of such an oxide layer, the carrier transport is modified and the current through the cells can be represented by an equation of the form[60]:

$$I_D = SA^*T^2 \exp(-X^{1/2}\delta) \exp\left(\frac{-\phi_b}{kT}\right) \exp\left(\frac{eV}{nkT}\right) \quad (I.9)$$

Where χ (eV) is the mean barrier presented by the thin oxide layer whose thickness δ (Å). The device ideality factor n also increases and an appropriate expression for n to take into account the oxide layer is given by[61]:

$$n = 1 + \frac{\delta\epsilon_s}{W\epsilon_{ox}} \quad (I.10)$$

Where ϵ_{ox} is the permittivity of the oxide, ϵ_s is the permittivity of the semiconductor and W is depletion width. The modified V_{OC} after adding the oxide is given by the following expression[60]:

$$V_{OC} = n \left[\phi_B + \left(\frac{kT}{q}\right) X^{1/2}\delta + \left(\frac{kT}{q}\right) \ln(J_{SC}/A^*T^2) \right] \quad (I.11)$$

This layer also prevents chemical reactions between the two materials (the metal and the semiconductor). This leads to an increase in the device lifetime. This is an ideal way to improve performance, stability, and lifetime of PV solar cells[39].

Insulating films usually contain charges which affect the semiconductor surface potential. These charges may be positive in some oxides such as SiO₂, Si₃N₄ and HfO₂, and may be negative in other oxides such as Al₂O₃ and TiO₂. These negative charges strip electrons from the surface of the semiconductor, thus preventing surface recombination. Through the added oxide layer, the open circuit voltage and efficiency of the solar cell are improved[62]. And the positive charges indicate the possibility of reduced diffusion in the n-type semiconductor[61].

Chapter I: Schottky barrier solar cell and InGaN material

I.4 InGaN for solar cells

Ternary Indium Gallium Nitride (InGaN) alloy is a group III-V semiconductor material with direct band gap, it is made of a mix of gallium nitride (GaN) and indium nitride (InN). The ability to control the optical and electrical properties of InGaN (bandgap (E_g), refractive index (n), absorption coefficient (α)...etc.), that provides a good spectral match to sunlight, makes InGaN promising material for photovoltaic devices[1]. Among the most important advantages of this material are:

- The presence of a direct and changeable band gap makes it suitable for use in photovoltaic devices[1].
- Due to the high absorption coefficient values, even thin layers of InGaN material are able to exploit photons of solar radiation [63].
- InGaN alloys have the ability to withstand high amounts of radiation while retaining their properties compared to other materials[7].
- InGaN also has an apparent insensitivity to high dislocation densities as the strong internal fields, due to the presence of spontaneous and piezoelectric polarization, may counter the effect of dislocations[64,65].
- InGaN has low effective mass of electron and hole, which makes carrier transport easier[24].
- InGaN material does not contain any toxic elements (such as Cd, As...etc.), which has positive impact on environmental concern.

I.4.1 InGaN material properties

I.4.1.1 Structural properties

Since nitride semiconductors have a high degree of ionicity, the III-nitrides materials typically crystallize in a wurtzite crystal structure (Figure I.7), unlike Si, Ge, and GaAs, which crystallize in a diamond or zinc-blend structure [21]. The crystal structures with high degree of ionicity has tendency to go for wurtzite structure[66]. This leads to unique material properties, thus changing the lattice parameter (a and c). These parameters of the InGaN are calculated by using the Vegard's law, which is given by Eqs.(I.12) and (I.13)[67] where x is the indium composition. The values of these parameters for InN and GaN are shown in Table I.2[68].

$$a_{\text{InGaN}} = xa_{\text{InN}} + (1 - x)a_{\text{GaN}} \quad (\text{I.12})$$

Chapter I: Schottky barrier solar cell and InGaN material

$$c_{\text{InGaN}} = x c_{\text{InN}} + (1 - x) c_{\text{GaN}} \quad (\text{I.13})$$

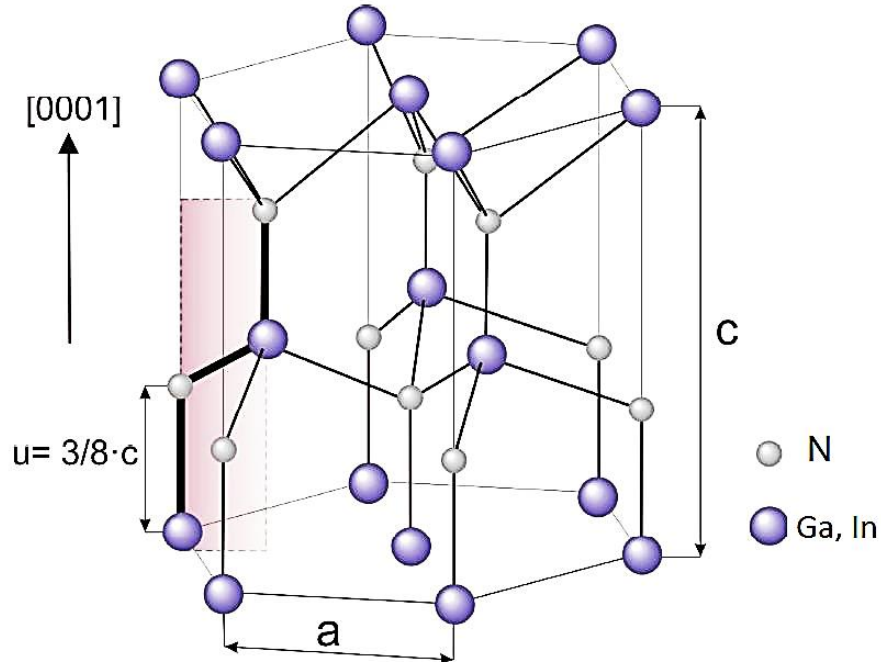


Figure I. 7: Schematic wurtzite lattice of InGaN material [27].

Table I. 2: The lattice parameters values (a and c) of InN and GaN[68].

Parameter ($T = 300 \text{ K}$)	InN	GaN
$a \text{ (nm)}$	0.3533	0.3189
$c \text{ (nm)}$	0.5693	0.5185

The III-V nitride material, which consists of AlN, GaN and InN are among the materials that can offers a wide range of bandgaps. InGaN material bandgap can be tuned by varying the amount of indium (In) in the alloy. Depending on the alloy composition, the direct bandgap varies from about 0.7 eV (at $\lambda = 1770 \text{ nm}$) to 3.42 eV (at $\lambda = 360 \text{ nm}$), covering a wide wavelength range from the infrared to the ultraviolet[5]. This benefit is accompanied, however, by an enormous lattice mismatch between InN and GaN as shown in Figure I.8.

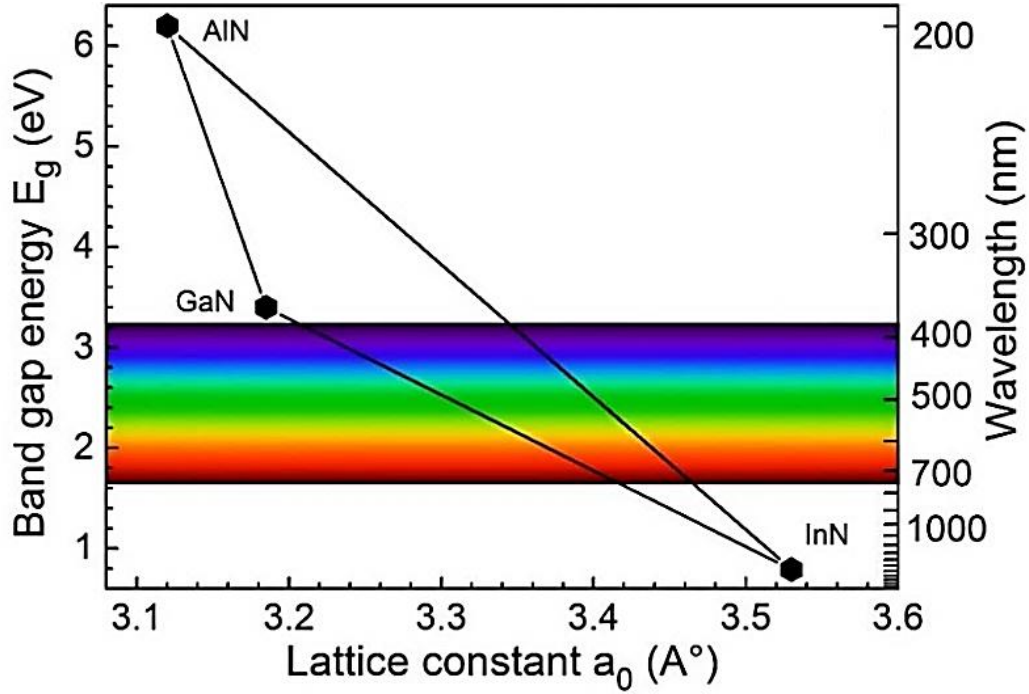


Figure I. 8: Bandgaps of wurtzite GaN, AlN and InN[69].

I.4.1.1 Electrical properties

The electrical properties of InGaN are a mix of those of InN and GaN, they can be calculated using Vegard's law (linear interpolation)[70] as it has been determined from ab initio calculations studies[71]. The bowing parameter (b) must be added to calculate bandgap and electron affinity, and it is equal to 1.43 and 0.8, respectively [19]. The electrical properties values are calculated via Eq. (I.14)[20], where A represents the properties in Table I.3.

$$A^{\text{In}_x\text{Ga}_{1-x}\text{N}} = xA^{\text{InN}} + (1-x)A^{\text{GaN}} - bx(1-x) \quad (\text{I.14})$$

Table I. 3: Experimental parameters of GaN and InN[19,20,72].

Electric properties	E_g (eV)	χ (eV)	N_c (cm^{-3})	N_v (cm^{-3})	ϵ
GaN	3.42	4.1	2.3×10^{18}	4.6×10^{19}	8.9
InN	0.7	5.6	9.1×10^{17}	5.3×10^{19}	15.3

Chapter I: Schottky barrier solar cell and InGaN material

Table I.3 shows bandgap (E_g), electron affinity (χ), the density of states in the conduction band and valance band (N_C) and (N_V) respectively and the dielectric permittivity (ϵ) respectively.

The bowing parameter b is significant factor for determining the bandgap of InGaN alloys and is a function of optical quality of the material [7].

InGaN alloy has low effective mass of carriers due to which they do possess high electron mobility. The mobility carriers for ternary materials is expressed using Caughey and Thomas model who take into consideration the temperature and the doping concentration[70]. The mobility carriers are determined by the following expression[14]:

$$\mu_m = \mu_{1m} \left(\frac{T}{300} \right)^{\alpha_m} + \frac{\mu_{2m} \left(\frac{T}{300} \right)^{\beta_m} - \mu_{1m} \left(\frac{T}{300} \right)^{\alpha_m}}{1 + \left(\frac{N}{N_m^{crit} \left(\frac{T}{300} \right)^{\gamma_m}} \right)^{\delta_m}} \quad (I.15)$$

where m presents either electrons or holes, μ_m is the mobility of electrons or holes, N is the doping concentration [cm^{-3}], N_m^{crit} is the critical doping concentration [cm^{-3}]. T is the absolute temperature in degrees Kelvin ($^{\circ}K$). α_m , β_m , δ_m and γ_m are model parameters and depend on the Indium content (α_m , β_m and γ_m have been estimated to 1). The linear interpolation between the experimental values of GaN and InN set in Table I.4., allows the estimation of the InGaN parameters.

Chapter I: Schottky barrier solar cell and InGaN material

Table I. 4: GaN, InN material mobility parameters [20,71].

Parameter	<i>GaN</i>	<i>InN</i>
$\mu_{1n} (cm^2V^{-1}s^{-1})$	295	1982.9
$\mu_{2n} (cm^2V^{-1}s^{-1})$	1460	10885
δ_n	0.71	0.7439
$N_n^{crit} (\times 10^{16} cm^{-3})$	7.7	10
$\mu_{1p} (cm^2V^{-1}s^{-1})$	3	3
$\mu_{2p} (cm^2V^{-1}s^{-1})$	170	340
δ_p	2	2
$N_p^{crit} (\times 10^{17} cm^{-3})$	10	8

I.4.1.2 optical properties

Among the parameters influencing the performance of a photovoltaic devices, absorption coefficient, and refractive index are of utmost importance. The spectral variation of the refractive index and absorption coefficient of the InGaN samples with varying Indium composition are shown in Figure I.9. InGaN alloys also exhibit near bandgap absorption coefficients up to an order of magnitude larger than semiconductors used in present-generation high efficiency solar cells. Therefore, InGaN alloy films have the ability to absorb 90% of the photons lying above bandgap within the first 500 nm thickness of the film[7].

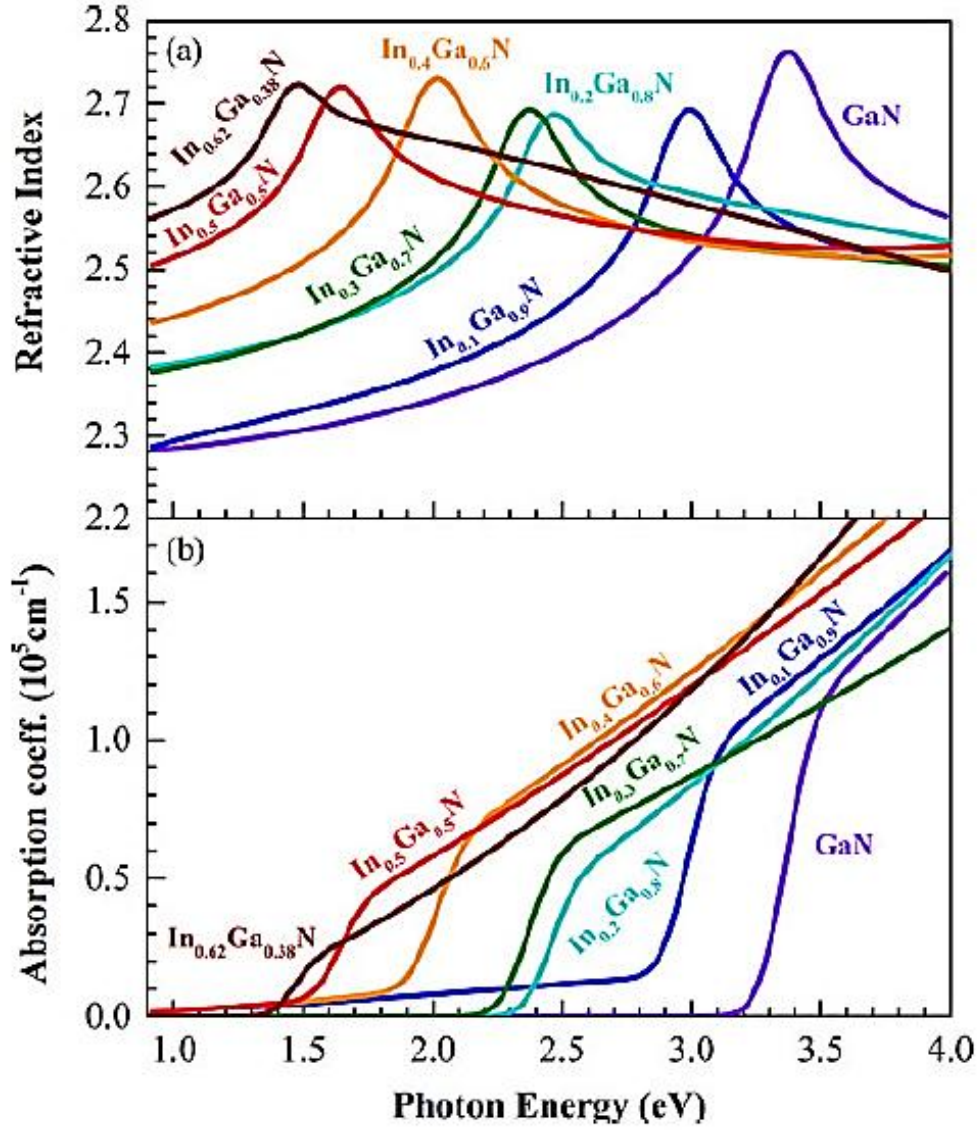


Figure I. 9: (a) Refractive index dispersion relations and (b) absorption coefficient spectra of InGaN films [73].

- **Absorption coefficient**

The absorption coefficient (α) is an important factor in photovoltaic devices; it expresses the quantity of absorbed photons and consequently the number of produced carriers. The absorption coefficient is expressed as the following equation[70] with defined photon energy (E_{ph}) and indium composition (x):

$$\alpha(\text{cm}^{-1}) = 10^5 \sqrt{C(E_{ph} - E_g(x)) + D(E_{ph} - E_g(x))^2} \quad (\text{I.16})$$

Chapter I: Schottky barrier solar cell and InGaN material

where E_{ph} is the energy of the incident photons. C and D are the parameters measured experimentally and reported in Table I.5. C and D can be expressed as [19]:

$$C_{InGaN}(eV^{-1}) = 3.525 - 18.29x + 40.22x^2 - 37.52x^3 + 12.77x^4 \quad (I.17)$$

$$D_{InGaN}(eV^{-2}) = -0.6651 + 3.616x - 2.460x^2 \quad (I.18)$$

Table I. 5: Experimental values of C and D for different indium composition (x) [42, 45].

Indium composition (x)	$C(eV^{-1})$	$D(eV^{-2})$
1	0.69642	0.46055
0.83	0.66796	0.68886
0.69	0.58108	0.66902
0.57	0.60946	0.62182
0.5	0.51672	0.46836
0	3.52517	-0.65710

- **Refractive index**

The index of refraction (n) also determines the amount of light that is reflected when reaching the interface, as well as the critical angle for total internal reflection. It is also a primordial factor for optical devices, we used the Adachi's refractive index model given by Eq. (I.19)[20].

$$n(E_{ph}) = \sqrt{\frac{A}{\left(\frac{E_{ph}}{E_g}\right)^2} \left[2 - \sqrt{1 + \frac{E_{ph}}{E_g}} - \sqrt{1 - \frac{E_{ph}}{E_g}} \right] + B} \quad (I.19)$$

The compositional dependence of the A and B parameters are given in Eqs. (I.20) and (I.21)[20].

$$A_{InGaN} = 13.55x + 9.31(1 - x) \quad (I.20)$$

$$B_{InGaN} = 2.05x + 3.03(1 - x) \quad (I.21)$$

Chapter I: Schottky barrier solar cell and InGaN material

I.4.2 Growth techniques

The semiconductor devices based on InGaN alloys are usually grown by various basic growth techniques, the various techniques are reported for the growth of these alloys are[7]:

- *MOCVD (metal organic chemical vapor deposition)* [74,75]: under N-rich growth conditions and medium growth temperature, it is the most suitable technique for the growth of InGaN alloys as it creates high uniform layer. Also, the drawback of MOCVD growth technique is that it involves the use of dangerous materials such as NH_3 , H_2 and Silane SiH_4 .

- *MBE (molecular beam epitaxy)* [76,77]: It is a high vacuum technique and the growth temperature in MBE are lower than that required for the MOCVD. The growth by MBE MME-growth (Metal Modulated Epitaxy Technique) of InGaN material on sapphire substrate had shown highly crystalline quality with lower dislocation density and excellent compositional uniformity[78].

- *MOVPE (metal organic vapor phase epitaxy)* [79,80]: This method is the most used to grow InGaN thin films with a full range of Indium composition, and can also be controlled to optimize the growth temperature, molar ratio and pressure .

- *PECVD (plasma enhanced evaporation deposition process)* [16]: It is suitable for photovoltaic devices to enable it to develop high quality InGaN layers with high indium content.

- *HVPE (hydride vapor phase epitaxy)*: This method has been used to grow GaN and InN materials with low defects, but fails to make high quality InGaN alloys[81,82].

- *PAMBE (Plasma-assisted molecular beam epitaxy)*: in this method the incorporation of active nitrogen at the growth front is independent of the substrate temperature, which allows lower growth temperature than the other techniques[83,84].

We can control the indium composition (x) of the InGaN layer by changing the growth temperature or indium source flow rate[85]. However, the films of Indium rich InGaN alloy with high quality are difficult to synthesize as there is a solid phase immiscibility gap between InN and GaN phases due to the large difference in interatomic spacing between InN and GaN[24]. Growth of high quality defect free InGaN thin film with high Indium content is still a challenging task for research community[86].

Chapter I: Schottky barrier solar cell and InGaN material

I.4.3 Challenges of InGaN alloys

Until now, it is difficult to form high quality InGaN alloys due to several reasons during the growth process, these reasons are limited to 3 points: (i) the large difference in interatomic spacing between InN and GaN[87]. (ii) the high vapor pressure of InN in comparison to GaN leading to low indium incorporation in the InGaN alloy[88]. (iii) low thermodynamic stability of InN at higher temperatures[89].

I.4.3.1 Substrate

The lattice-mismatched epitaxial growth causes a large number of dislocations in nitride devices, with dislocation densities higher than in other compound semiconductor devices. The process of selecting the right substrate is one of the important challenges of making high quality InGaN based devices[86]. Often, sapphire (Al_2O_3) or 6H-SiC is used as good substrates for the growth of GaN material, despite the difference in the lattice parameter (0.476 nm and 0.308 nm, respectively) and Thermal Expansion Coefficient as shown in Table I.6[7].

Table I. 6: Crystallographic data of various materials that can act as a substrate for InGaN films [7].

Substrate	Lattice parameter a (Å)	Thermal Expansion Coefficient along a (10^{-6} c^{-1})
Sapphire	4.758	7.5
6H-SiC	3.081	4.2
ZnO	3.250	4.75
GaN	3.189	5.6
InN	3.545	5.7
Si	5.431	3.59

InGaN epitaxial films on sapphire shows a high dislocation density typically in the $10^7 - 10^{10} \text{ cm}^{-2}$ range due to the large lattice and thermal mismatches between sapphire and InGaN[24]. From Table I.6, it appears that the most suitable substrates are 6H-SiC and ZnO, however 6H-SiC is more expensive than sapphire, and ZnO have similar dislocation densities and Thermal Expansion Coefficient mismatch[86]. Silicon is also a good substrate at a low cost

Chapter I: Schottky barrier solar cell and InGaN material

and is available in large sizes, the Si cut perpendicular to (111) direction is feasible for growing Wurtzite nitrides[90].

I.4.3.2 P-Type Doping and Contact

Actually the intrinsic GaN is N-type semiconductor due to the presence of native defects such as: nitrogen vacancies and impurities (Si and O) during the growth process. Due to highest electron affinity ($\chi = 5.6 \text{ eV}$), InN tends also to behave as an N-type semiconductor[7]. Since the properties of InN and GaN affect the properties of the mixture between them, InGaN also has an N-type behavior. Therefore, to form an intrinsic semiconductor of InGaN, P-type doping must be introduced to remove the n-type charge[1].

It is theoretically possible to achieve higher acceptor concentrations at higher indium compositions, because the activation energy of Mg in GaN is around 204 meV[91], but decreases with the increase in indium composition[92]. moreover, at very high indium compositions, the acceptor concentrations decrease due to degradation in crystal quality[93].

The p-type doping of InGaN is very difficult to achieve due to the presence of high density of defects and a low activation efficiency. Therefore, achieving P-type behavior of InGaN is one of the major challenges which are hindering the progress of P-N junction solar cells based on InGaN alloys[86].

Achieving good P-type InGaN contacts is difficult due to its low acceptors concentration, which leads to high contact resistance. there is no readily available metal that can form an Ohmic contact with p-type InGaN. As mentioned previously, these composite materials with a high electron affinity χ require metal with a high work function ϕ_m . However, most of the recognized metals tend to form a Schottky junction or have high ohmic resistance[94]. There have been several efforts to improve the surface, such as treatment[95] and annealing[96].

I.4.3.3 Phase segregation

Due to the immiscibility of InN and GaN (10% lattice mismatch between InN and GaN[97]), the lattice mismatch in InGaN increases with increasing Indium composition (x) of InGaN, and InGaN with high Indium content will be separated into indium clusters. When the thickness and In composition of InGaN materials increase, In-rich clusters in InGaN films easily induce phase separation., which reduces domains of the bandgap[98] as shown in Figure I.10.

Chapter I: Schottky barrier solar cell and InGaN material

this leads to low V_{oc} , low fill factor (FF). also, the Indium clusters formed can act as recombination centers which in turn decrease J_{sc} of InGaN based solar cell [1].

Phase separation in InGaN layer is also among the major challenges to obtain high performance solar cells. growing indium rich InGaN layers with high quality is difficult, this negatively affects the efficiency of the solar cell.

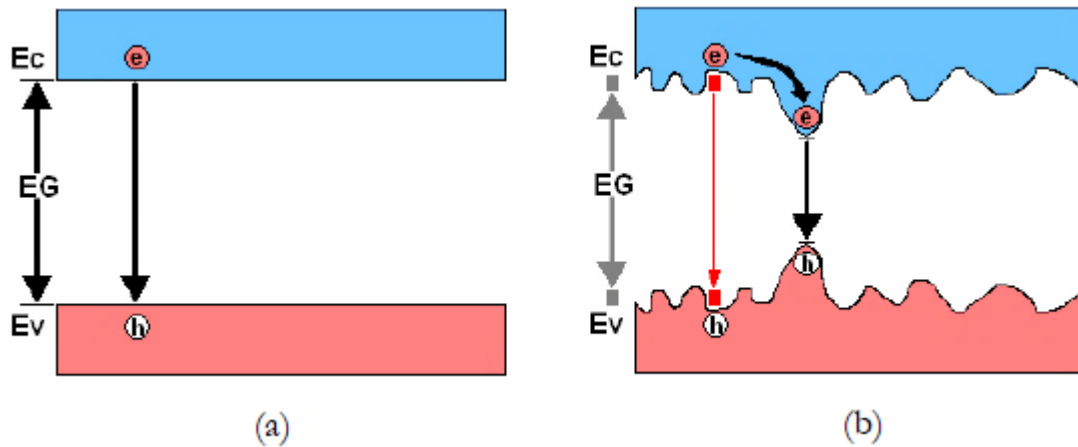


Figure I. 10: Energy band diagram of (a) an ideal material, and (b) a phase separated material[10].

I.4.3.4 Polarization

Although III-V nitrides semiconductors have many features that make them the best for photovoltaic devices, they are the only ones that show a property called spontaneous polarization. which means they possess spontaneous polarization without interference of an external electric field, due to non-centric symmetry of charges in wurtzite structure and large ionicity of covalent bonds[99].

The presence of polarization in the absorption layer can decrease the charge carrier collection significantly. The spontaneous polarization P_S of InGaN is related to its constituents InN and GaN by the non-linearly relation[64]:

$$P_S^{InGaN} = xP_S^{InN} + (1 - x)P_S^{GaN} - b_{InGaN}x(1 - x) \quad (I.22)$$

Materials that exhibit spontaneous polarization also exhibit piezoelectric polarizations. The piezoelectric polarization is caused by lattice mismatch and thermal expansion coefficients mismatch of substrate and the InGaN alloy, and its relation is given as[64]:

Chapter I: Schottky barrier solar cell and InGaN material

$$P_p^{InGaN} = xP_p^{InN} + (1 - x)P_p^{GaN} \quad (I.23)$$

The polarization can cause polar discontinuities at nitride hetero-interfaces where fixed charges occur leading to free charge accumulation[100], thus significantly reducing the charge carrier collection. Which makes it an obstacle to the advancement of optical devices based III-V nitrides semiconductors. However, Polarization can be engineered in the III-Nitride solar cell to improve electric field and thus carriers collection efficiency[86].

I.4.4 Studied InGaN-based solar cell structures

The researchers are focused on different device configurations to obtain a High performance solar cells. Due to the band gap variation feature in InGaN material, solar cells can be designed with different bandgap based junction to harvest the largest amount of solar light and achieve the largest amount of absorption. A number of different structures such as InGaN PN homojunction[101], PIN homojunction[102], InGaN/ Si tandem solar cell[103], p-GaN/i-InGaN/n-GaN heterojunction[63], AlGaIn/ InGaIn heterojunction[104], n-ZnO/InGaIn/p-GaN heterojunction[105], Au/Pt/InGaIn/GaN Schottky[6], Ni/InGaIn/GaN schottky junction[13], p-InGaIn/i-InGaIn/n-GaN double heterojunction[106] and InGaIn/GaN multiple quantum wells solar cells[107] have been reported so far. Most of the studied cells consist of InGaIn alloys with indium concentration not exceeding $x=0.35$ with poor performance. But success in making solar cells based on high-quality indium-rich InGaIn will allow to achieve higher efficiency of solar cells as predicted by simulation[70,108]

Chapter I: Schottky barrier solar cell and InGaN material

Chapter II: Silvaco Atlas Simulation Software

II.1 Introduction

Silvaco Atlas is a software environment for designing and predicting the performance of semiconductor devices, which can be modeled in either two dimensions (2D) or three dimensions (3D). This program gives the user the ability to simulate the production process to manufacture a semiconductor device and test its characteristics. Using Silvaco Atlas, we can define any material and model any simple or complex device, because it contains many models, numerical methods and types of materials included in the program.

There are many subprograms that contribute to the simulation that serve more specific functions. Deckbuild, Devedit and Athena are used to designate the input. And Tonyplot for output. As shown in diagram in Figure II.1.

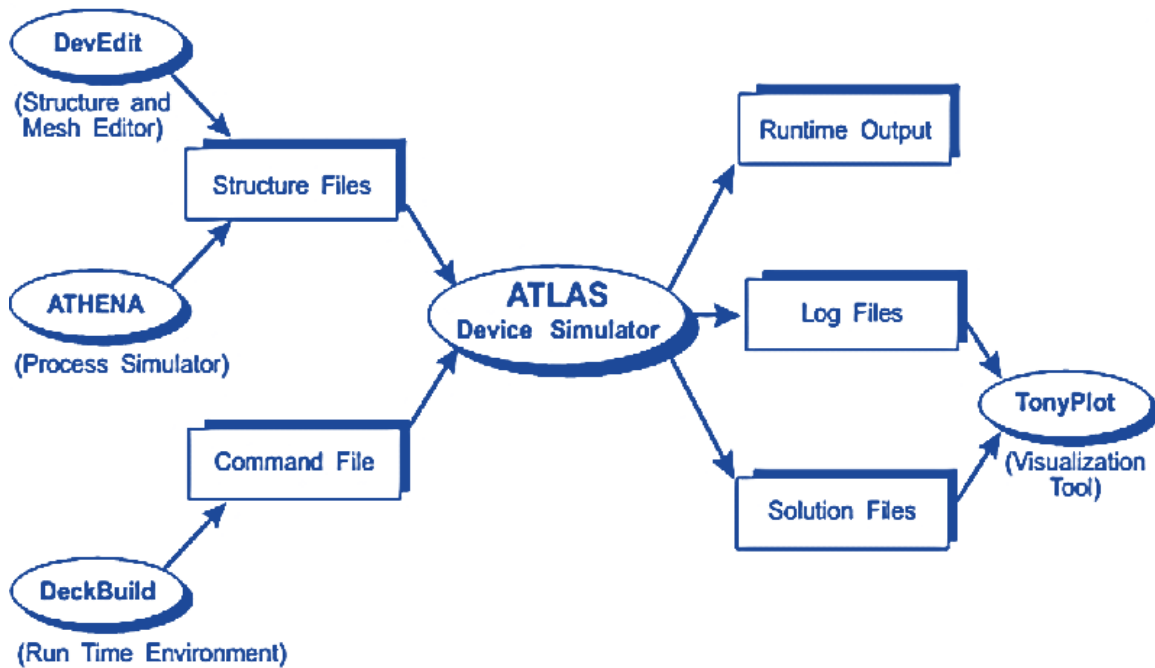


Figure II. 1: Atlas inputs and outputs[109].

In most Atlas simulations two input files are used. Input text file to specify commands, and an input file specifying the structure of the device to be simulated. The process of simulation any device must specify in the input file: the device structure, Physical models that must be taken into account, numerical methods and the type of electrical bias applied to the device.

Chapter II: Silvaco atlas simulation software

The output files that Atlas gives are divided into: the run-time output, which gives you the progress and the error and warning messages as the simulation proceeds. the log file, which stores all terminal voltages and currents from the device analysis. the solution file, which stores 2D and 3D data relating to the values of solution variables within the device at a given bias point.

II.2 Device modeling

Silvaco Atlas software is based on the process of entering parameters and working conditions of the device, and it solves a set of equations in each node of the grid covering the device, so choosing the solving method is important to obtain satisfactory results.

II.2.1 Basic semiconductor equations

Several lengthy studies on semiconductors have reached three basic equations that are solved to understand any semiconductor-based device. These equations are derived from Maxwell's laws, which are: Poisson's Equation, Carrier Continuity Equations and The Transport Equations. Poisson's Equation relates the electrostatic potential to the space charge density, and it is given by[109]:

$$\text{div}(\epsilon \nabla \Psi) = -\rho \quad (\text{II.1})$$

where ϵ is the local permittivity, Ψ is the electrostatic potential, and ρ is the local space charge density.

The continuity equations for electrons and holes are defined by equations[109]:

$$\frac{\partial n}{\partial t} = -\frac{1}{q} \text{div} \vec{J}_n + G_n - R_n \quad (\text{II.2})$$

$$\frac{\partial p}{\partial t} = -\frac{1}{q} \text{div} \vec{J}_p + G_p - R_p \quad (\text{II.3})$$

where n and p are the electron and hole concentrations, \vec{J}_n and \vec{J}_p are the electron and hole current densities, G_n and G_p are the generation rates for electrons and holes, R_n and R_p are the recombination rates for electrons and holes and q is the magnitude of the charge on an electron.

The transport equations are usually obtained by applying approximations and simplifications to the Boltzmann Transport Equation. This leads to the production of a number of different

Chapter II: Silvaco atlas simulation software

transport models such as the drift-diffusion model, the Energy Balance Transport Model or the hydrodynamic model.

The drift diffusion model is the simplest model, however; it becomes less accurate for device with smaller feature sizes. it is then necessary to use the energy-balance or hydrodynamic models.

The current densities in the continuity equations may be approximated by a drift-diffusion model as shown the derivations based upon the Boltzmann transport theory. Therefore, the drift-diffusion model is used in this thesis to model the current density. It given by[109]:

$$\vec{J}_n = qn\mu_n\vec{E}_n + qD_n\nabla n \quad (\text{II.4})$$

$$\vec{J}_p = qp\mu_p\vec{E}_p - qD_p\nabla p \quad (\text{II.5})$$

where μ_n and μ_p are the electron and hole mobilities, \vec{E}_n and \vec{E}_p are the electric field strengths, D_n and D_p are the diffusion coefficients for electrons and holes, ∇n and ∇p are the electron and hole concentration gradients.

II.2.2 Numerical methods

The simulation of semiconductor-based devices in the Silvaco Atlas requires solving the above-mentioned set of equations, depending on the models selected. Therefore, choosing the optimal solution method is one of the importance of simulating the devices. For each model type there are three techniques, decoupled Gummel, fully-coupled Newton, and Block[109].

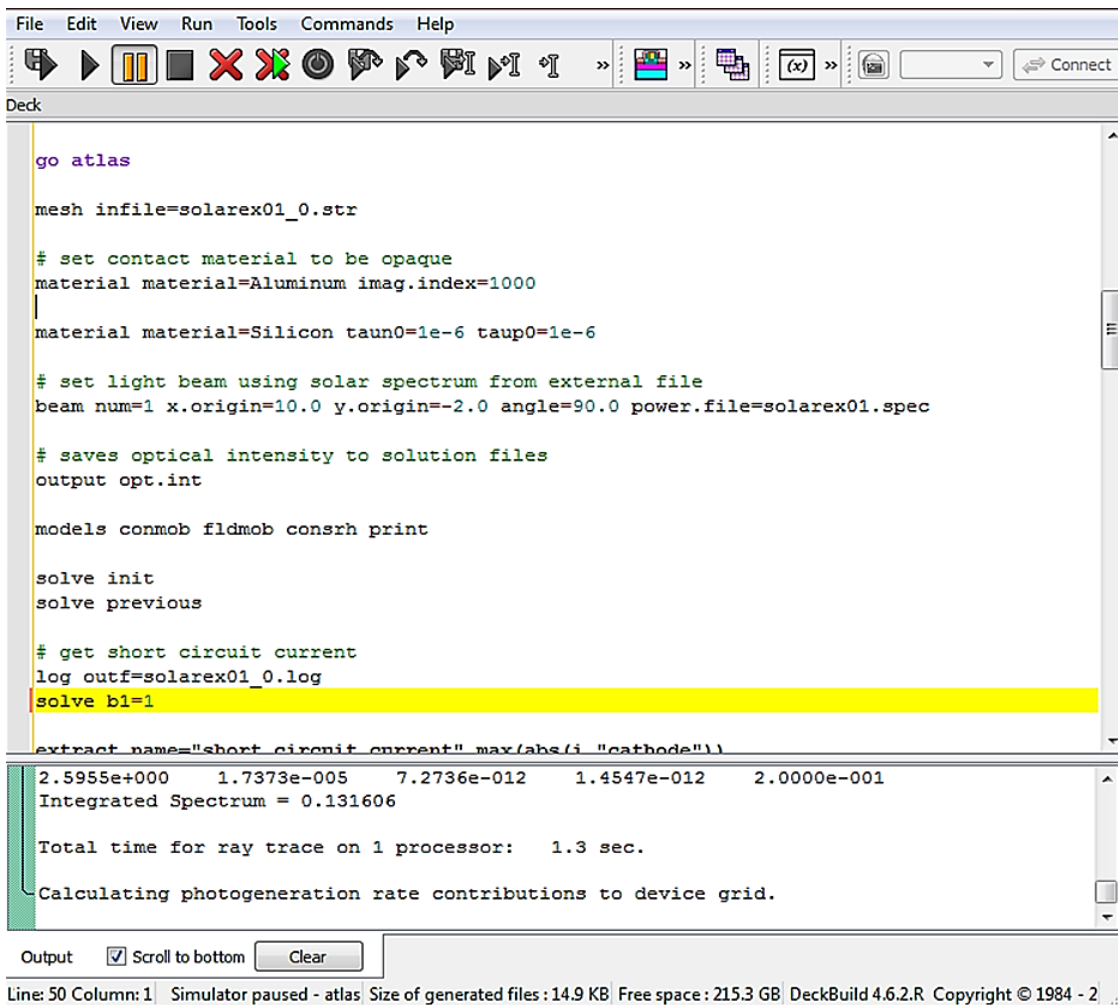
The Gummel method solves each unknown while keeping the other variables constant. It continues to do this until a stable solution is found. And this method is useful where the system of equations is weakly coupled but has only linear convergence. The Newton method solves the total system of equations together to find a solution. The Newton method is useful when the system of equations is strongly coupled and has quadratic convergence. This method may require additional time, but it gives more accurate results. The Block method solves the equations using a combination of the Newton and Gummel methods, in that some equations are solved fully coupled and the rest are decoupled[110].

Chapter II: Silvaco atlas simulation software

II.3 Deckbuild

Deckbuild is the main program that runs the simulation and receives input files as needed. through which it is possible to control all the simulations (Its interface is shown in Figure II.2). Deckbuild consists of two windows; Top window for entering and editing commands. And a lower window is to give the exit modes and simulation results. The code entered in the input file calls Atlas to run with the following command:

```
go atlas
```



The screenshot displays the Deckbuild software interface. The top window, titled 'Deck', contains a list of commands for running a simulation. The command 'go atlas' is highlighted in yellow. Below the command list, the output window shows the results of the simulation, including the integrated spectrum value and the total time for ray trace.

```
File Edit View Run Tools Commands Help
[Icons] [Connect]
Deck
go atlas
mesh infile=solarex01_0.str
# set contact material to be opaque
material material=Aluminum imag.index=1000
material material=Silicon taun0=1e-6 taup0=1e-6
# set light beam using solar spectrum from external file
beam num=1 x.origin=10.0 y.origin=-2.0 angle=90.0 power.file=solarex01.spec
# saves optical intensity to solution files
output opt.int
models conmob fldmob consrh print
solve init
solve previous
# get short circuit current
log outf=solarex01_0.log
solve b1=1
extract name="short circuit current" max(abs(i "cathode"))
2.5955e+000 1.7373e-005 7.2736e-012 1.4547e-012 2.0000e-001
Integrated Spectrum = 0.131606
Total time for ray trace on 1 processor: 1.3 sec.
Calculating photogeneration rate contributions to device grid.
Output [x] Scroll to bottom Clear
Line: 50 Column: 1 Simulator paused - atlas Size of generated files : 14.9 KB Free space : 215.3 GB DeckBuild 4.6.2.R Copyright © 1984 - 2
```

Figure II. 2: Screenshot from Deckbuild.

Next a certain order is used to set the device parameters as shown in Figure II.3. Otherwise, the program may not work properly or may not give accurate results. Generally, the format is:

Chapter II: Silvaco atlas simulation software

<STATEMENT> <PARAMETER>=<VALUE>

The following line of code serves as an example:

```
DOPING UNIFORM N.TYPE CONCENTRATION=1.0e16 REGION=1 OUTFILE=my.dop
```

Statements can have more than one parameter defined. The statement is DOPING. The parameters are UNIFORM, N.TYPE, CONCENTRATION, REGION, and OUTFILE.

Deckbuild also contains ready-made examples of simulators for different semiconductor compounds (solar cells, transistors, diodes...etc.).

<i>Group</i>		<i>Statements</i>
1. Structure Specification	————	MESH REGION ELECTRODE DOPING
2. Material Models Specification	————	MATERIAL MODELS CONTACT INTERFACE
3. Numerical Method Selection	————	METHOD
4. Solution Specification	————	LOG SOLVE LOAD SAVE
5. Results Analysis	————	EXTRACT TONYPLOT

Figure II. 3 Atlas command groups and primary statements[111].

Chapter II: Silvaco atlas simulation software

II.4 Definition of the structure

II.4.1 Specifying mesh

To build any device on atlas you must first define the mesh that will be the framework of the model. The mesh is made of triangles covering the device, and each corner of these triangles forms a node. The equations used to solve are calculated at each node, and the upper limit for the number of nodes is 100000 (in 2D)[109].

The number of nodes increases as the mesh is accurate, to give more accurate results, but this requires an increase in the time taken to run the simulation. A lower number of nodes leads to simulation results that are slightly further from the correctness and a shorter run time. The best way to create a mesh is to increase the number of nodes at the important junctions and depletion regions. To keep every information in this part of the device, and for the rest of the device, it is not important to make the mesh accurate (See Figure II.4).

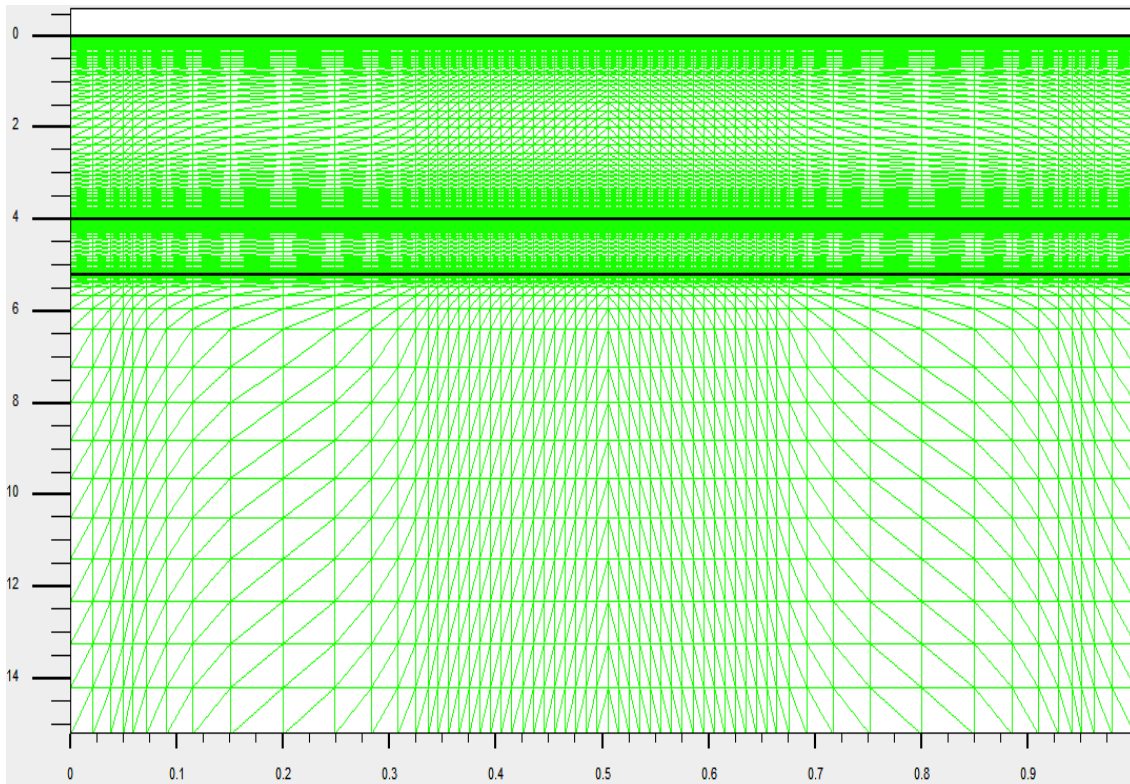


Figure II. 4: Example of the mesh.

Chapter II: Silvaco atlas simulation software

A structure can be created in the atlas in three ways. The first method is to create a structure in advance and save it in a separate file and then give a command to read it, the command is by typing:

```
MESH INFILE=<filename>
```

The second method is to use the automatic interface and this feature allows to transfer all the characteristics of the structure by running Athena or Devedit from inside the Deckbuild using the input of commands go Athena or go Devedit. After building the structure in Athena or Devedit run Atlas to run the simulation. And automatically receives the information between Athena and Dave and Atlas.

The third method is a direct method. So we simply use the command language directly in Deckbuild to define the structure. The command language is:

```
MESH SPACE.MULT=<value>
```

Space.mult is a scaling factor that controls the granularity of the mesh. The default value is 1. The value greater than 1 gives a coarser mesh, and a value less than 1 results in a finer mesh. The next statements define where mesh lines in the x and y direction will be:

```
X.MESH LOCATION=<value> SPACING=<value>
```

```
Y.MESH LOCATION=<value> SPACING=<value>
```

The X. MESH and Y. MESH statements are used to specify the locations in microns of vertical and horizontal lines, respectively, together with the vertical or horizontal spacing associated with that line. An alternate method to the space.mult command is to use the automatic mesh function:

```
MESH AUTO
```

This statement is followed by x.mesh statements. The locations of y.mesh lines will be automatically determined by the parameters of the REGION statements.

II.4.2 Specifying regions

After defining the mesh, the materials in each piece of the mesh must be defined, so first the division and regions must be determined, and defining the regions is as follows:

Chapter II: Silvaco atlas simulation software

```
REGION NUMBER=<integer> <material_type> <position_parameters>
```

The regions are identified by numbers, starting from 1 and up to 15,000 different regions in the Atlas. Also it contains many materials known for their properties, they can be changed in a material statement in the code.

The position parameters are specified in microns using the X.MIN, X.MAX, Y.MIN, and Y.MAX parameters as shown in Figure II.5. If no mesh point is defined in the structure, the code will not run successfully. Therefore, position parameters must be accurate to ensure proper results. If the position parameters of a new statement overlap those of a previous REGION statement, the overlapped area is assigned as the material type of the new region. we can express the location of a region by define it with respect to other regions in the device such as:

```
REGION NUM=4 BOTTOM THICKNESS=10 MATERIAL=InGaN DONOR=1e17
```

```
REGION NUM=5 TOP THICKNESS=$bulk MATERIAL= InGaN
```

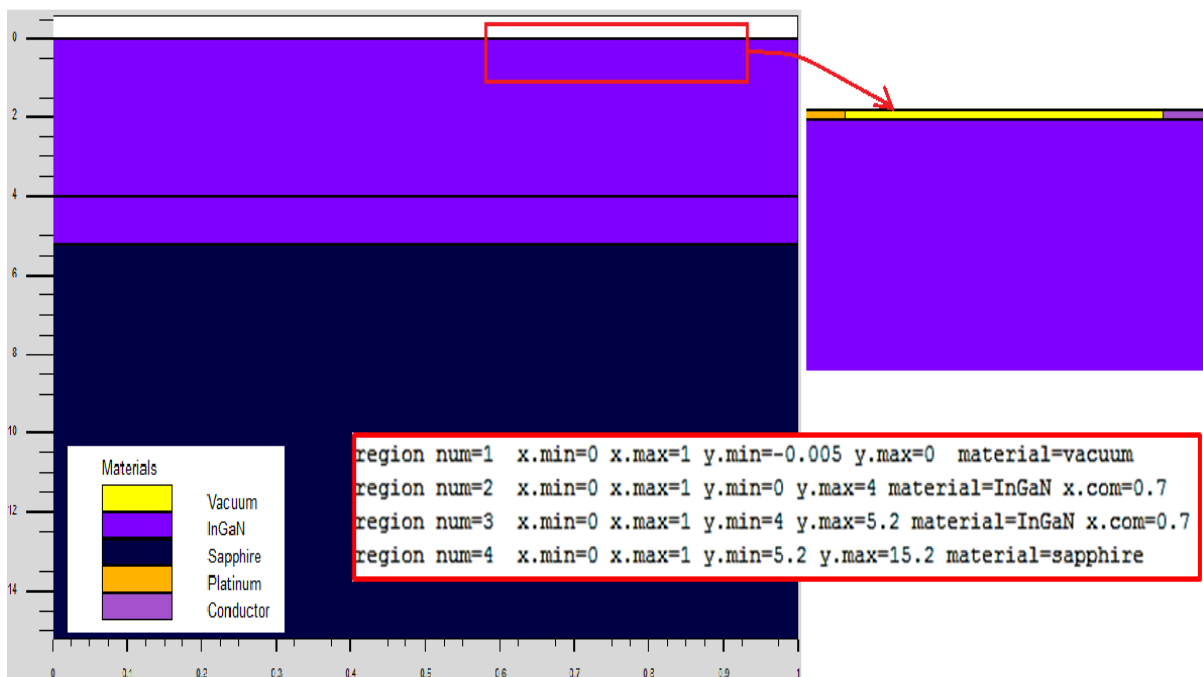


Figure II. 5: Tonyplot screenshot showing regions example.

Chapter II: Silvaco atlas simulation software

II.4.3 Specifying electrodes

To simulate any device, the electrodes must be identified, where we can identify from 1 to 50 electrodes in Atlas. And if any of the defined electrodes are given the same name, the electrodes are considered electrically connected. A typical electrode statement is:

```
ELECTRODE NAME=<electrode name> <position_parameters>
```

The position parameters are specified in microns using the X.MIN, X.MAX, Y.MIN, and Y.MAX parameters as shown in the example Figure II.6. If no y-coordinate is given, then the electrode is placed at the top of the device. The top, bottom, right and left parameters can be used to define the location as well.

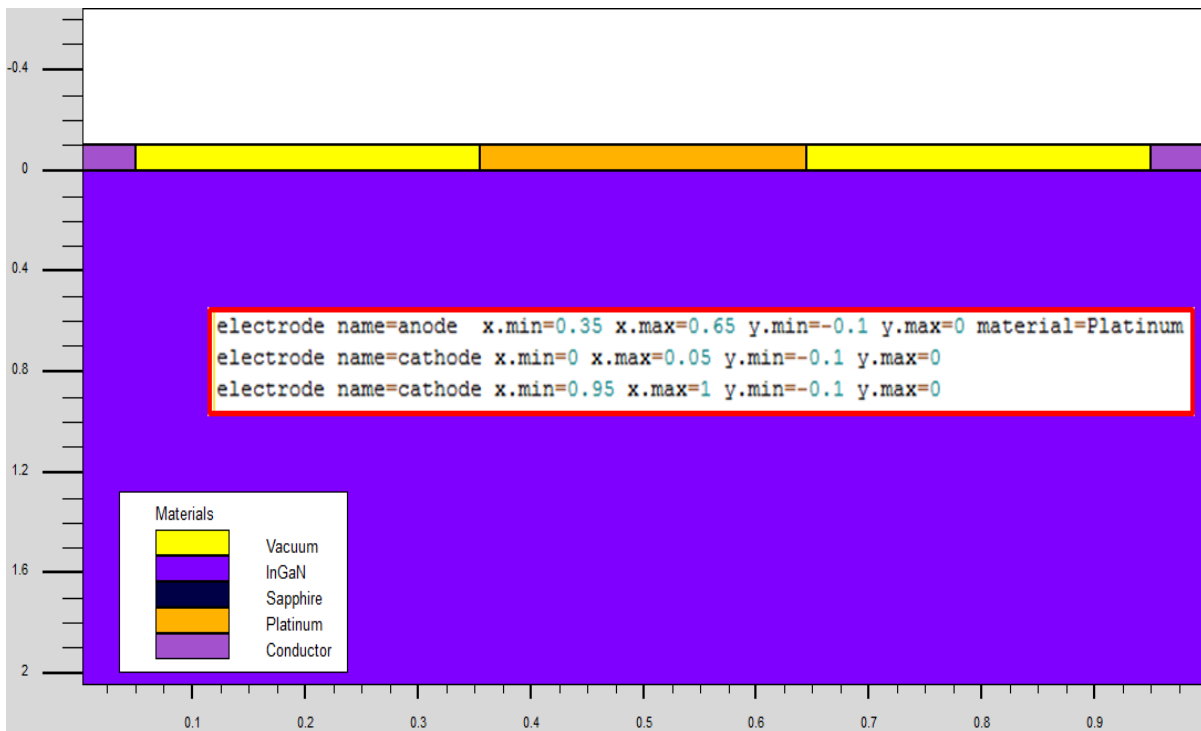


Figure II. 6: Tonyplot screenshot showing electrodes examples.

II.4.4 Specifying doping

After specifying the above, the parameters of the doping are determined and are in the form:

```
DOPING <distribution_type> <dopant_type> <postion_parameter>
```

Chapter II: Silvaco atlas simulation software

The dopant type can be specified as n. type or p.type, and the concentration amount can be defined. The distribution type can be uniform, Gaussian, or complementary error function. The position parameter can be specified by region number or the minimum/maximum parameters. As shown in the two following examples:

```
DOPING UNIFORM CONCENTRATION=1E16 N.TYPE REGION=1
```

```
DOPING GAUSSIAN CONCENTRATION=1E18 CHARACTERISTIC=0.05 P.TYPE \  
X.LEFT=0.0 X. RIGHT=1.0 PEAK=0.1
```

II.5 Definition of material parameters and models

II.5.1 Specifying material properties

You can use the MATERIAL statement to specify the material properties of the defined regions. But you must complete the entire mesh and doping definition before any MATERIAL statements can be used. this statement allows you to specify your own values for these basic parameters. For example, the statement:

```
MATERIAL MATERIAL=GaN EG300=3.42 MUN=1100
```

EG300 is the bandgap at 300K, and MUN is electron mobilities. We can find the identification codes for all the parameters in the user manual of Silvaco.

To define the index of refraction and the index of extinction for any material, it is by using one of the two methods. The first method is to use refractive index data from the SOPRA database. To do this, you must specify the appropriate index file (in the user manual) on the SOPRA parameter of the MATERIAL statement. As the following example shows:

```
MATERIAL MATERIAL=Platinum SOPRA =Pt.nk
```

The second method is to enter a text file that contains ordered triplets of wavelength, refractive index, and extinction coefficient. It is as shown in this example:

```
MATERIAL MATERIAL=GaN INDEX.FILE=GaN.nk
```

Chapter II: Silvaco atlas simulation software

II.5.2 Specifying physical models

Physical models are specified using the MODELS statements. They can be grouped into five classes[109]: mobility, recombination, carrier statistics, impact ionization, and tunneling. To specify the physical models in the simulation of any device, use the models statement followed by the name of the models. For example, the statement:

```
MODELS BGN CONMOB SRH AUGER FERMI PRINT
```

specifies that Bandgap narrowing, the standard concentration dependent mobility, Auger recombination, Shockley-Read-Hall recombination with fixed carrier lifetimes, the Fermi-Dirac statistics[19,70]. Adding print in the model statement allows the user to ensure the correct parameters were used by displays the models and parameters used during the simulation into the runtime output. These models are among those used in our simulation.

The Shockley-Read-Hall (SRH) recombination model is used to model the indirect recombination of charge carriers that occurs in the presence of traps (or defects) within the semiconductors bandgap. That is to model the losses in our structure[20].

$$R_{SRH} = \frac{np - n_i^2}{\tau_p(n + n_i e^{(ETRAP/kT)}) + \tau_n(p + n_i e^{(-ETRAP/kT)}} \quad (II.6)$$

where ETRAP is the difference between the trap energy level and the intrinsic Fermi level $ETRAP = E_t - E_i$, τ_n and τ_p are the electron and hole lifetimes. This model only presumes one trap level which is $ETRAP = 0$ and it corresponds to the most efficient recombination center.

The second indirect recombination model we took into consideration is the Auger recombination, given by the expression[20]:

$$R_{Auger} = C_{Augn} (pn^2 - nn_i^2) + C_{Augp} (np^2 - pn_i^2) \quad (II.7)$$

Where C_{Augn} and C_{Augp} are the Auger coefficients.

II.5.3 Specifying contact characteristics

Atlas assumes that the electrode in contact with the semiconductor is ohmic. If the work function is defined, the electrode is treated as a Schottky contact. We give the value of the work function by the WORKFUNCTION parameter. For example, the statement:

Chapter II: Silvaco atlas simulation software

```
CONTACT NAME=gate WORKFUNCTION=4.8
```

To specify a thermionic emission schottky contact with tunneling and barrier lowering, the command would be:

```
CONTACT NAME=ANODE SURF.REC E.TUNNEL BARRIER
```

The SURF.REC parameter to enable surface recombination, E. TUNNEL specifies that the Schottky tunneling model for electrons will be used and BARRIER to enable barrier lowering.

II.5.4 Specifying interface properties

The INTERFACE statement is used to define surface recombination velocity and the interface charge density at interfaces between semiconductors and insulators. For example, the statement:

```
INTERFACE QF=3e10
```

In this example, the fixed charge on all interfaces between semiconductors and insulators is set to $3 \cdot 10^{10} \text{ cm}^{-2}$. And to determine the interface parameter in a specific region we use the X.MIN, X.MAX, Y.MIN, and Y.MAX parameters on the INTERFACE statement. For example, the statement:

```
INTERFACE X.MIN=-4 X.MAX=4 Y.MIN=-0.5 Y.MAX=4 QF=1E10 S.N=1E4 S.P=1E4
```

In this example, in addition to the fixed charge QF, both S.N (electron surface recombination velocity) and S.P (holes surface recombination velocity) are specified.

II.6 The choice of the numerical method

After the device is built, the numerical solution that should be used to calculate the solutions to the device equations must be determined. Numerical methods are given in statement METHOD of the input file; thus defining the program which numerical methods to use. There are 3 methods, each of which uses a different method to solve equations. They are: (i) GUMMEL (decoupled), (ii) NEWTON (fully coupled) and (iii) BLOCK[109].

The Gummel method solves for each unknown while keeping the variables constant. It continues doing this until a stable solution is found. The Newton method solves the total system of unknowns together, and the Block method solves some of the equations the Gummel way and

Chapter II: Silvaco atlas simulation software

the rest the Newton way. Generally, the Newton method is preferred and is the default if the method statement is not used, it is the method used for simulation in this work. Specification of the solution method is carried out as follows:

```
METHOD GUMMEL BLOCK NEWTON
```

Atlas can solve both electron and hole continuity equations, or only for one or none. You can make this choice by using the CARRIERS parameter. For example:

```
METHOD CARRIERS=2
```

```
METHOD CARRIERS=1 HOLE
```

We can change all parameters associated with the solution process, and among the most important of these parameters are: CLIMIT or CLIM.DD, which specify the values of the minimum concentrations that will be resolved by the solver.

II.7 Obtaining solutions

In simulation of any device Atlas can calculate DC, AC, small signal, and transient solutions. After determining the voltages on the electrodes, Atlas calculates both currents and the internal quantities. the device starts with zero bias on all electrodes. Solutions are obtained by stepping the biases on electrodes from this initial condition. To set the voltage of an electrode named anode:

```
SOLVE VANODE=0 VSTEP=0.2 VFINAL=5 NAME=anode
```

```
SOLVE VSTEP=0.5 VFINAL=10 NAME=anode
```

The voltage extends in the first statement from 0 to 5 V with a step of 0.2 and in the second statement from 5 to 10 V with a step of 0.5. The first guess is very important so that there are no convergence problems. Therefore, a good initial guess must be made of the variables to be evaluated at each bias point. The initial guess comes from the two previous solutions, and if none are available convergence problems can arise. like the following example:

```
SOLVE VGATE=1 VDRAIN=1 VSUBSTRATE=1
```

In this example, the voltage is set to 1 volt on all three electrodes. The program may find the solution, but it also may not get convergence, so it is better to write it as follows:

Chapter II: Silvaco atlas simulation software

```
SOLVE VGATE=1
```

```
SOLVE VDRAIN=1
```

```
SOLVE VSUBSTRATE=1
```

In the first solve statement, vgate set to 1 V, while the other two electrodes are at 0 V. The second solve statement sets vdrain at 1 V with vgate remaining at 1 V from the previous solve and vsubstrate remaining at 0 V. last statement sets all the electrodes to 1 V, this statement solves with all three electrodes at 1 V. The difference is that, in this case, Atlas has two previous solutions to use as the initial guess, this reduces the possibility of a convergence problem. When previous solutions are not available, the initial guess for potential and carrier concentrations must be made from the doping profile. To do this the initial solution must be made at zero bias which is done by:

```
SOLVE INIT
```

If this statement is not included, Atlas automatically evaluates an initial solution prior to the first solve statement.

II.8 Interpreting results

After running the simulation, it is important to save the simulation characteristics, so a log file must be opened to save the terminal characteristics. And to open a log file, the following statement must be entered:

```
LOG OUTFILE=<filename>
```

A log file is opened with the chosen name, then Terminal characteristics from all SOLVE statements after the LOG statement are then saved to this log file, until another log statement is opened or the log is closed with Off parameter. In general, the values of electric current are saved in units of amperes per micron in Tonyplot, because Atlas is a two-dimensional simulator, and sets the third dimension Z to be 1 micron. If a three-dimensional device is simulated, the units of current are in Amperes, and when the WIDTH parameter is used in the mesh statement, Atlas scaled the current by this factor and it is also in amperes. The extract parameters can also be extracted from the log file using the extract command and it is as follows:

Chapter II: Silvaco atlas simulation software

```
EXTRACT INIT INF=<filename>
```

The user can make calculations on the data saved in the file for later use for viewing in TonyPlot. The extraction results display in the run-time output and are stored in a file called results.final. To store the results in a different file at the end of EXTRACT command, use the following option:

```
EXTRACT..... DATAFILE=<filename>
```

A solution file or structure file is another type of file provided by Atlas, which contains an image of the device at a particular bias point and gives us the ability to display any device parameters, from doping profiles and band parameters to electron concentrations and electric fields. It enables the user to know what is going on at any point in the device, and helps to discover errors in any part of the code to fix them. These files should be plotted using TonyPlot. To create these files, we use one of the statements:

```
SAVE OUTFILE=<filename>
```

```
SOLVE .... OUTFILE=<filename>.sta MASTER [ONEFILEONLY]
```

II.9 Luminous

luminous is a program integrated into the Atlas system for the study of optoelectronic devices, used for light diffusion and absorption. It calculates the optical intensity within the semiconductor devices, so that the density is converted to photo-generation rates and integrated into the continuity equations. There are 4 physical models to describe the propagation of light and they include the following[109]:

- Ray tracing (RT). It is a general method of resolving 2D and 3D non-planar geometries but ignores diffraction and coherence effects.
- The transfer matrix method (TMM). This method is a 1D method that includes interference effects. It is recommended for large area devices such as thin film solar cells.
- The beam propagation method (BPM). BPM is a general 2D method that is computationally intensive because it includes diffraction effects.

Chapter II: Silvaco atlas simulation software

- Finite difference time domain (FDTD) methods, it is the most general 2D and 3D method that is the most computationally intensive because it accounts for both diffraction and coherence by direct solution of Maxwell's equations.

If we want to specify different propagation models for different portions of the optical spectrum, we specify the same beam index for more than one beam statement. The parts of the spectrum in a beam statement are specified by: WAVEL.START and WAVEL.END or E. START and E.END.

Any optical beam is modeled and its source controlled using a beam statement. To determine the origin of the beam we use the parameters X.ORIGIN and Y.ORIGIN. To determine the direction of propagation angle of the beam we use the ANGLE parameter, which is relative to the x-axis. MIN.WINDOW/MAX.WINDOW parameters specify the illumination window. As shown in Figure II.7.

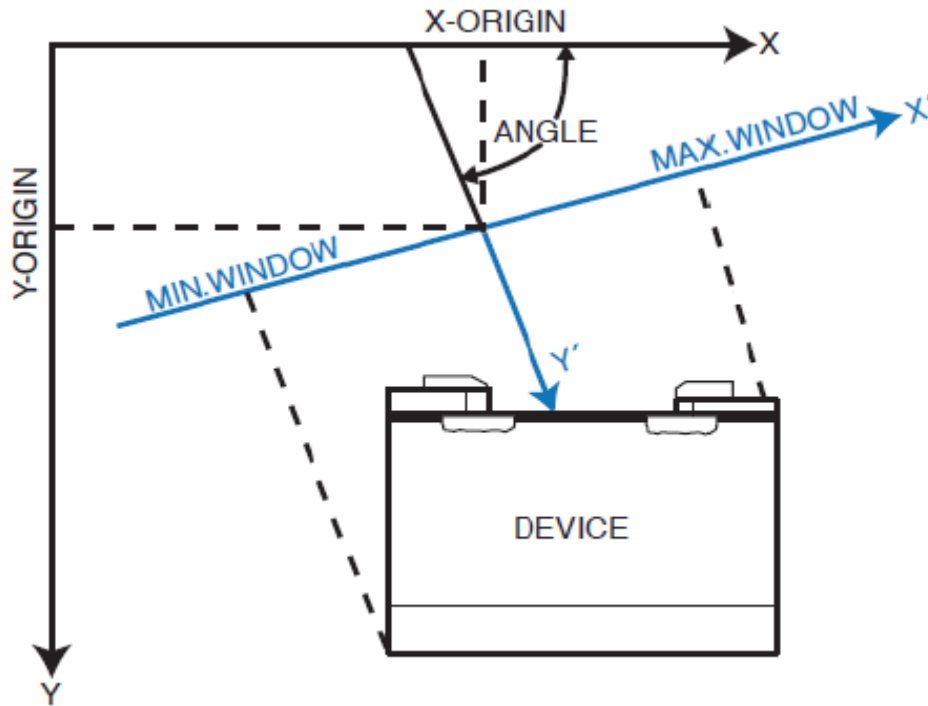


Figure II. 7: Optical Beam Geometry[109].

II.10 Solar cell simulation

To simulate solar cells, we need the properties of propagation and absorption of light, and this is what The Luminous simulators provides us. The user can also specify the spectra used in

Chapter II: Silvaco atlas simulation software

the simulation or to use the built-in spectra for AM0 and AM1.5. We use the following statement to determine the beam:

```
BEAM NUM=1 AM1.5 WAVEL.START=0.3 WAVEL.END=1.2 WAVEL.NUM=50
```

In this example, the AM1.5 spectrums was selected and sampled between 0.3 microns and 1.2 microns at 50 samples. To get the simulation data, solve statements are used. The first statement is:

```
SOLVE B1=1
```

This command line turns on the light beam and obtains a solution of optical density of 1 W/cm² (full intensity). In some cases, we may encounter difficulties in convergence, so we need to gradually increase the intensity of the light as follows:

```
SOLVE B1=0.01
```

```
SOLVE B1=0.1
```

```
SOLVE B1=1.0
```

A log file must be opened to save the current and voltage characteristics, and the voltage of one of the electrodes of the solar cell must be set. To extract data and characteristics of solar cells represented by the fill factor, efficiency, maximum output power, open circuit voltage, and short circuit current, we use the following extraction statements:

```
EXTRACT NAME="Isc" Y.VAL FROM CURVE (V."anode", I."cathode") WHERE  
X.VAL=0.0
```

```
EXTRACT NAME="Voc" X.VAL FROM CURVE (V."anode", I."cathode") WHERE  
Y.VAL=0.0
```

```
EXTRACT NAME="Pm" MAX (CURVE (V."anode", (V."anode" * I."cathode")))
```

```
EXTRACT NAME="Vm" X.VAL FROM CURVE(V."anode", (V."anode"*I."cathode")) \
```

```
WHERE Y.VAL=$"Pm"
```

```
EXTRACT NAME="Im" $"Pm"/$"Vm"
```

Chapter II: Silvaco atlas simulation software

```
EXTRACT NAME="FF" "$Pm"/("$Jsc"*"$Voc")
```

II.11 Tonyplot

The data obtained from device simulations is plotted by saving it to a file and then loading the file into TonyPlot. If the file is a structure file; the information is displayed as a 2D mesh plot. and If it is a log file, Tonyplot displays the data in an x-y plot. TonyPlot is a graphical tool that can be called directly on your Deckbuild by typing:

```
TONYPLOT <filename> -overlay
```

II.11.1 2D Mesh plot

2D Mesh is a way to show the outline of the simulated device. It contains a set of options to display information about the device, and the display options can be controlled using the display (2D Mesh) feature, the display panel and the control buttons are shown in Figure II.8. So that we can see the mesh and the shape and size of the regions in addition to the electrodes and other features such as the light beam applicable. The function of each of the display buttons is shown in Figure II.9. Some of these features have further control dialog boxes, which can be accessed from the Define button.

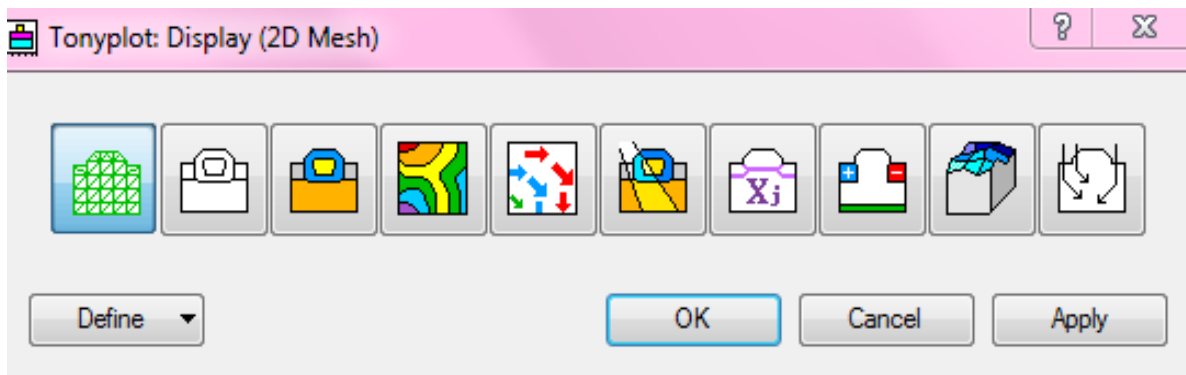


Figure II. 8: Mesh plot dialog.

Chapter II: Silvaco atlas simulation software

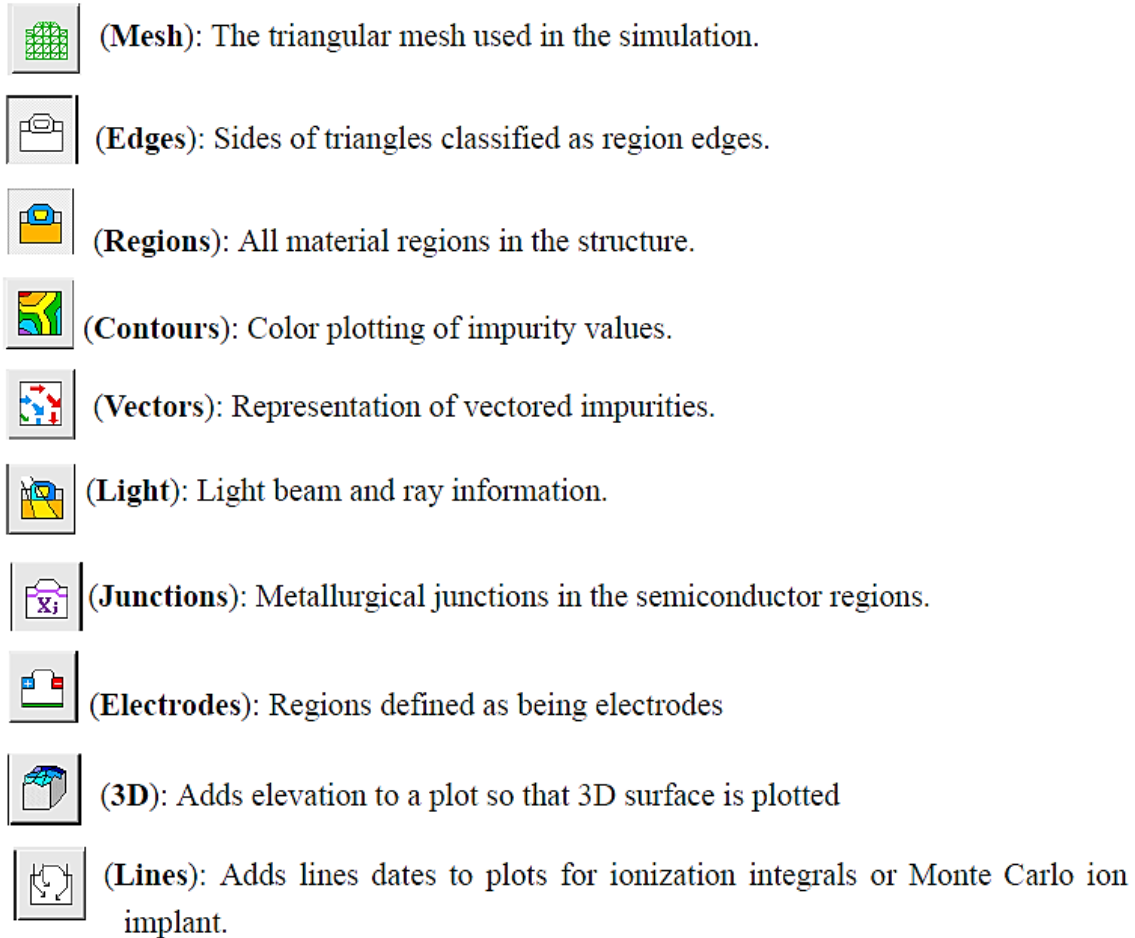


Figure II. 9: Description of the display buttons in Tonyplot[112].

One of the most important buttons is the mesh button. This button operates the mesh diagram on the device structure, and shows the location of the triangles, which helps the user to develop an accurate mesh and improve the simulation time. There is also another important button, which is the regions button, which operates the regions of the device, with each region coded in a specific color according to the material. Turning on the contour button will show the contour diagram on the device, and it is the most used method for visualizing data on two-dimensional meshes.

2D mesh plot has the ability to display several types of information about the device, as shown in Figure II.10. So that it can display the doping concentration, the electrical field, the optical intensity, the generation rate and the recombination rate and some other information. This is

Chapter II: Silvaco atlas simulation software

done by using the cutline tool and cutting the cross section of the device. This tool also has the ability to move cutlines through the device and watch the profile move and shift as the cutline position updates.

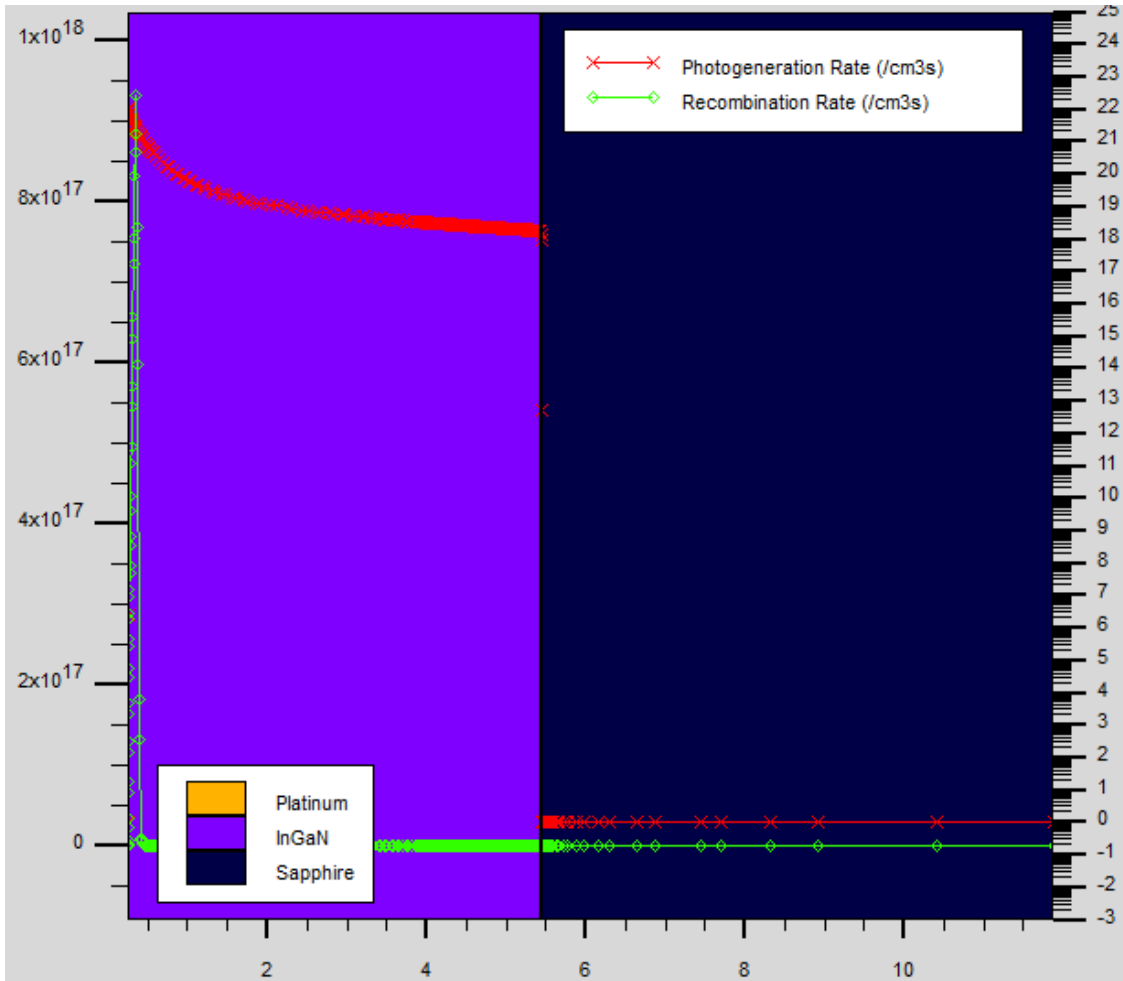


Figure II. 10: Tonyplot screenshot showing cutline tool.

11.2 X-Y plots

This displays the data as x-y as shown in the Figure II.11. And we have several quantities to choose from to display on the X-axis and Y-axis. We can also change the data display scales (linear or logarithmic). Multiple x-y plots can be opened in the same window; they can also be overlaid for comparison of data, to do this you can use the Overlay option from the edit menu or in the command line when invoking TonyPlot. In addition, we can measure different distances

Chapter II: Silvaco atlas simulation software

from the plot using the ruler tool, such as measuring the distance between two points or intercepts and the slope of a curve.

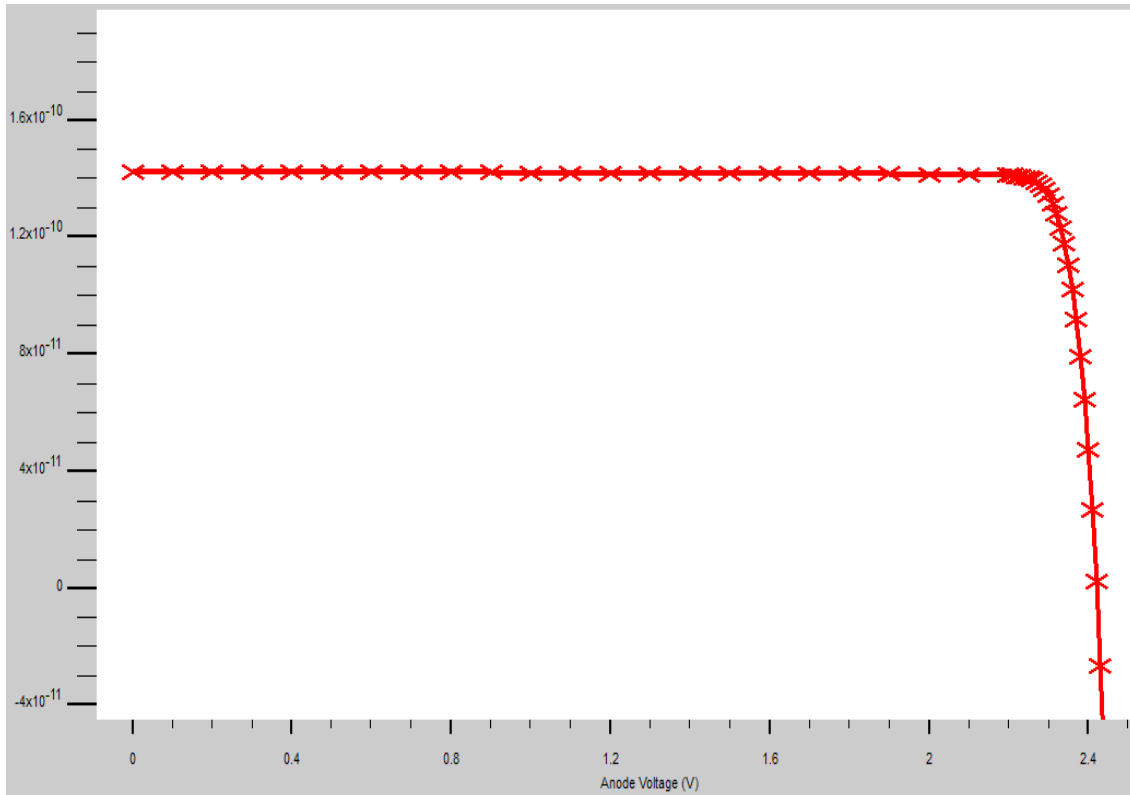


Figure II. 11: Screenshot of an X-Y plot in Tonyplot.

Chapter III: Results and discussions

III.1 Introduction

Recently, InGaN-based solar cells have attracted the attention of many researchers, both in simulation and experimental[113,114]. Recent research for this type of cell includes simultaneous optimization of the design in order to improve its efficiency[20]. InGaN solar cells have many challenges, with the difficulty of developing a P-type doping layer, and the difficulty of achieving the electrode over this type[1]. Many researchers have favoured Schottky solar cells by replacing the P-type layer with metal [13,19,115] as a good solution to some problems of InGaN solar cells.

In this work, Numerical simulation is carried out using Silvaco TCAD software to design an InGaN-based Schottky solar cell and selected the suitable parameters for it, starting from searching for the best metal to form the Schottky junction to the most suitable indium composition for high efficiency. We also focused on improving its performance by modifying the cell structure, adding a uniform intrinsic layer and then a gradual intrinsic layer between the metal and the semiconductor. We also studied the effect of defects in this layer in order to obtain more accurate and reliable results. Finally, we added to the Schottky solar cell an oxide layer between the metal and the semiconductor and then turns into a MIS solar cell, this is the aim to improve more the cell's performance.

III.2. Device structure and modelling

The device is consisted of a $1.2 \mu\text{m}$ n-type InGaN layer (n-doping concentration $6.5 \times 10^{16} \text{ cm}^{-3}$). The indium composition of the InGaN active layer (x_{In}) was set to vary in the range [0.1-0.8]. The Schottky contact is a 5 nm thin metallic semi-transparent layer to facilitate the transit of photons into the InGaN layer and the metal occupies 30% of the illuminated area. The metals used are high work function metals (ϕ_M) such as Ni, Pd, Au, and Pt and the simulation was done under the AM1.5 solar spectrum. And finally we used sapphire substrate. Figure III.1 shows a schematic diagram of the simulated structure.



Figure III. 1: Structure of the InGaN based Schottky barrier solar cell studied in the simulation.

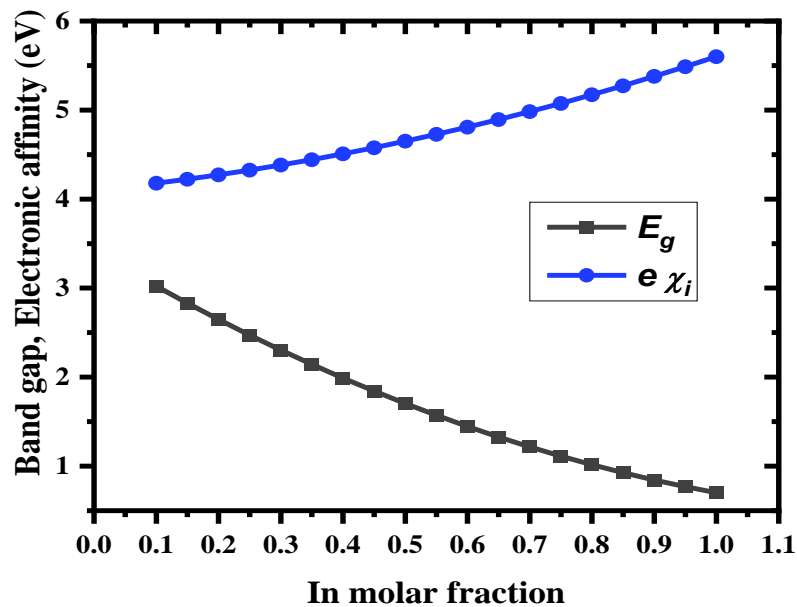


Figure III. 2: Band gap and the electronic affinity as function of the indium composition.

The properties of InGaN material change with changing the indium composition in the material and this applies to E_g , χ , N_C , N_V , μ All the properties of the semiconductor for concentrations from 0.1 to 0.8 were calculated using MATLAB software that includes the equations mentioned in the first chapter. Figure III.2 shows the change in energy band gap and electronic affinity with

the change of the Indium composition x_{In} . Also, nk files (that consist wavelength, refractive index, and extinction coefficient) were calculated at each indium composition using Adachi and absorption models (Eqs I.16 and I.19)[20,70]. Thermionic emission and drift-diffusion are considered as the dominant transport models in this type of solar cell and have been used in the simulations. In addition, models as Fermi-Dirac statistics[19,70], Shockley-Read-Hall (SRH) [116], Auger recombination [117] and Bandgap narrowing [14] are also implanted. Finally, the native carrier's lifetime was taken equal to 1ns [24].

III.3 Initial study to determine the suitable parameters of the solar cell

III.3.1 Part 1

Sid Ould Saad et al.[14] have numerically studied an InGaN schottky solar cell using the Silvaco Atlas software, an optimum efficiency $\eta = 18.2\%$ was obtained. We got a similar result using the following parameters: $x_{In} = 0.6$, $\phi_M = 6.3$ eV and the $J - V$ characteristic obtained is shown in Figure III.3.

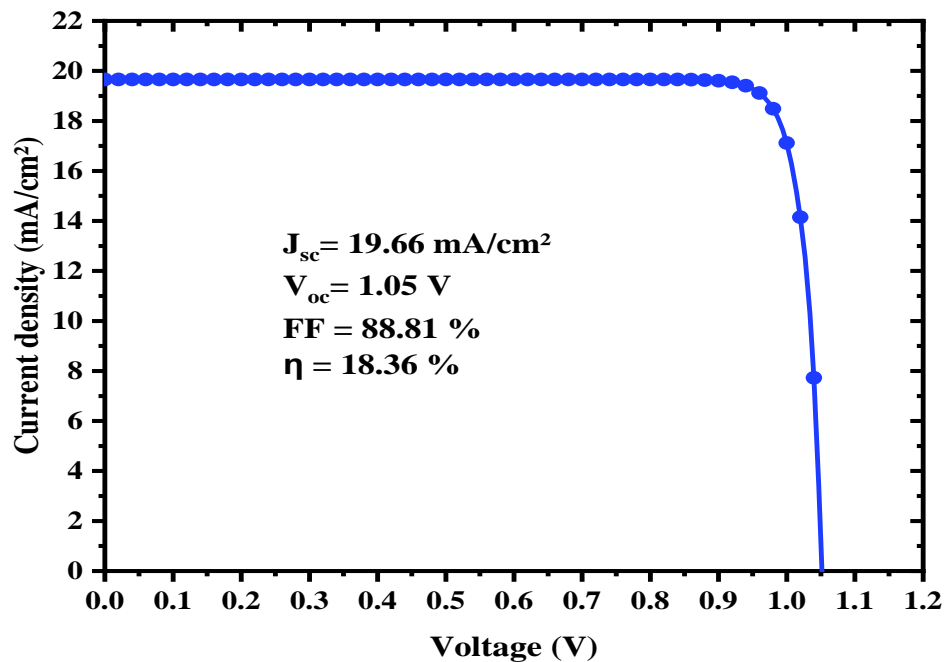


Figure III. 3: ($J - V$) characteristic for schottky solar cell with $x_{In} = 0.6$ and $\phi_M = 6.3$ eV.

Also, we have studied several Schottky junction metals by changing the indium composition. Figure III.4 presents the results obtained for J_{SC} , V_{OC} , FF and η . The selected metals have a high

work function compared to other metals and this is what InGaN requires to form a good Schottky junction. The considered metals are Pd, Ni, Au, and Pt with work functions ϕ_M of 5.12 eV[43], 5.22 eV[118], 5.47 eV[118] and 5.65 eV[43] respectively. The work function affects the equilibrium bandgap diagram as illustrated in Figure III. 5. This widens the width of the depletion region, which improves the photo-generation and carrier separation processes.

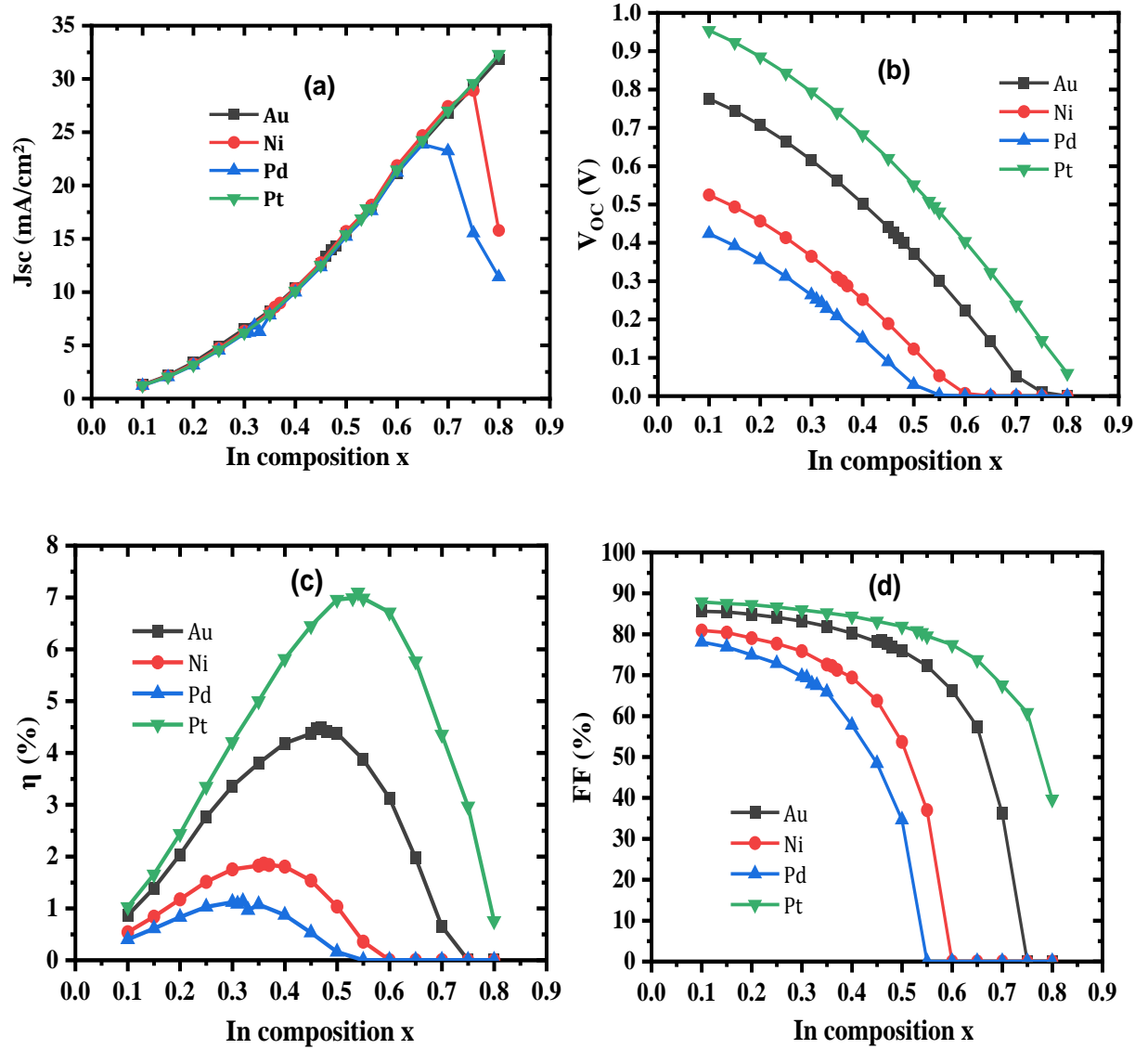


Figure III. 4: (a) Short-circuit current density J_{sc} , (b) open-circuit voltage V_{oc} , (c) conversion efficiency η and (d) fill factor FF , as function of the indium composition with various metal.

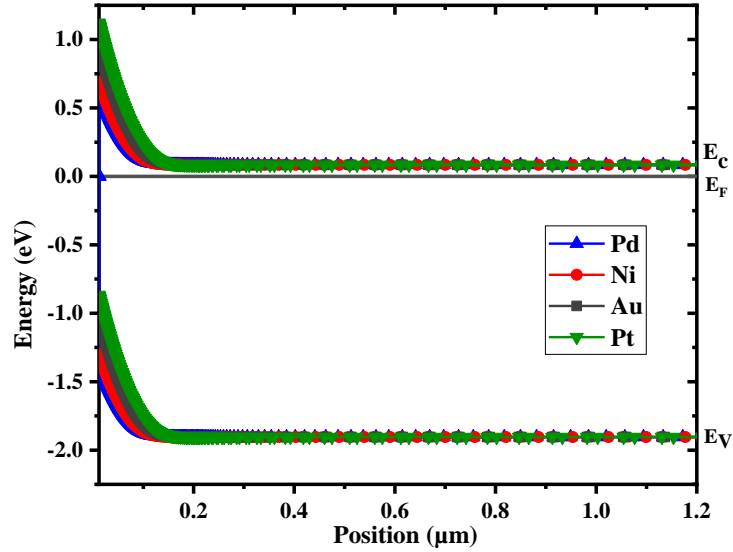


Figure III. 5: Band gap energy diagram at equilibrium of the InGaN Schottky solar cell for different metals and 0.4 Indium composition.

Now, in the aim to explain the increase in the J_{sc} when increasing the composition of indium (Figure III.4(a)), we extracted the External quantum efficiency (EQE) curves at all the studied indium composition (Figure III.6). It is easy to notice that the quantum efficiency range expands at high In composition solar cell. This is due to the low bandgap according to Vegard's law, which allows the absorption of a larger portion of the solar spectrum.

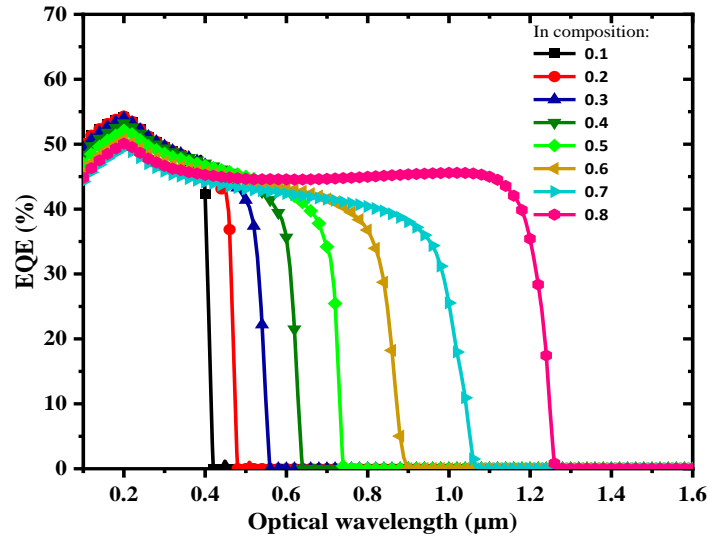


Figure III. 6: External quantum efficiency (EQE) variation with Indium composition in $In_xGa_{1-x}N$ compound for Pt metal.

The effect of the work function ϕ_M on J_{SC} appears only at high In composition (Figure III. 3(a)). As for the metals, Pt and Au, it increases continuously with the increasing Indium composition. However, it decreases for Ni and Pd metals at $x_{In}=0.75$ and $x_{In}= 0.65$, respectively. Figures III.7 and III.8 display an explanation for the current drop at these compositions.

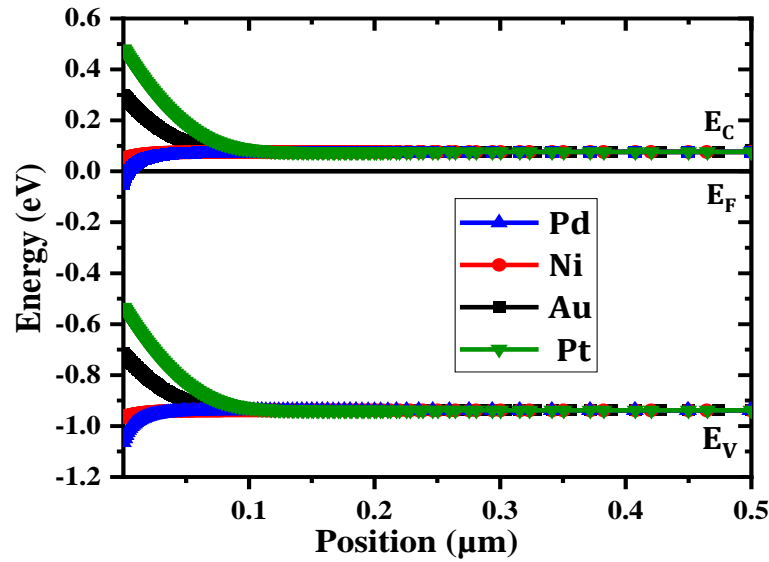


Figure III. 7: Band gap energy diagram at equilibrium of the InGaN Schottky solar cell for different metals and 0.8 Indium composition.

A high indium composition affects the electronic affinity as shown in Figure III.2. Both the increase in affinity and the decrease in the work function lead to a decrease in the Schottky barrier height according to the Schottky-Mott relation ($\phi_B = \phi_M - \chi$) and also the increase of In composition reduce the band gap energy (Figure III. 2) toward the range that coincide with the maximum of the AM1.5 spectrum. This has benefited effect on J_{SC} for the higher ϕ_M while J_{SC} drops pointedly at high In composition for Pd and Ni. This effect is presented in the external quantum efficiency spectrum (EQE) in Figure III.8.

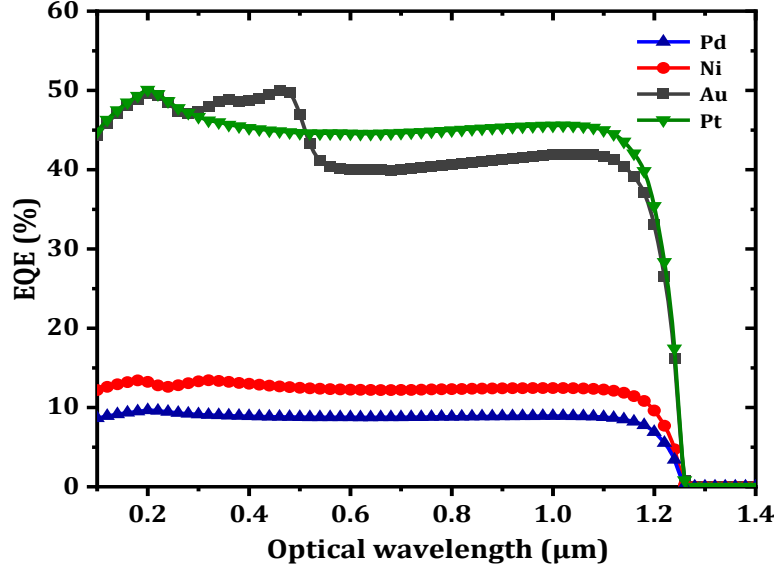


Figure III. 8: External quantum efficiency (EQE) for different metals and 0.8 Indium composition.

In Figure III.4(b), the V_{oc} changes with the metal work function and the indium composition is shown. The increase in V_{oc} is related to the increase in the work function according to the following relation [39]:

$$V_{oc} = \frac{K_B T}{q} \left(\ln \left(\frac{J_{sc}}{A^* T^2} \right) \right) + \phi_B \quad (III.1)$$

As we mentioned above, the height of the Schottky barrier is related to the work function according to the Schottky-Mott relation ($\phi_B = \phi_M - \chi$), and therefore the higher the metal with a large work function, the higher the voltage barrier and from it the V_{oc} increases. The V_{oc} decreases with increasing the Indium composition for all metals, as we notice in Figure III.4(b). This is expected because according to Vegard's law, the band gap decreases and the electronic affinity increases with an increase in the In composition (Figure III.2), and this leads to a decrease in the V_{oc} to zero.

It is clearly shown in Figure III.4(c) that the power conversion efficiency η has a peak value at certain In composition that varies from metal to another and increases with the work function. Before the peak, the efficiency increases with increasing J_{sc} and after the peak it decreases with the decrease in the V_{oc} produced by the solar cell. The indium compositions and efficiencies values for each peak of metal are given in Table III.1.

Table III. 1: The Indium composition corresponding to the maximum efficiency for Au, Ni, Pd and Pt Schottky contacts.

	<i>Au</i>	<i>Ni</i>	<i>Pd</i>	<i>Pt</i>
x_{In}	0.47	0.36	0.32	0.54
η %	4.48	1.86	1.13	7.10

The effect of the change of metal and indium composition on the fill factor FF of the solar cell is shown in Figure III.4(d). For low composition, there is a slight decrease, while in large composition, the decrease is sharp, especially in the case of the metals Pd and Ni. That is, the changes of V_{OC} values dominate the changes of FF .

For this part, which includes the study of four metals to form the Schottky junction and changing the values of indium composition in the semiconductor, we concluded that platinum metal is the most appropriate metal to form a Schottky junction in the InGaN solar cell with an indium composition of $x_{In} = 0.54$ to give an efficiency of $\eta = 7.1\%$.

III.3.2 Part 2

Since platinum represents the best metal to contact with the InGaN semiconductor and form a Schottky solar cell, in this section a comprehensive study of several values of the Pt work function that has been reported in several research works: 5.65 eV[43], 5.93 eV[118], 6.1 eV[119] and 6.35 eV[120]. Figure III. 9 shows the obtained electrical output parameters of the solar cell for the different reported values of ϕ_M versus In composition.

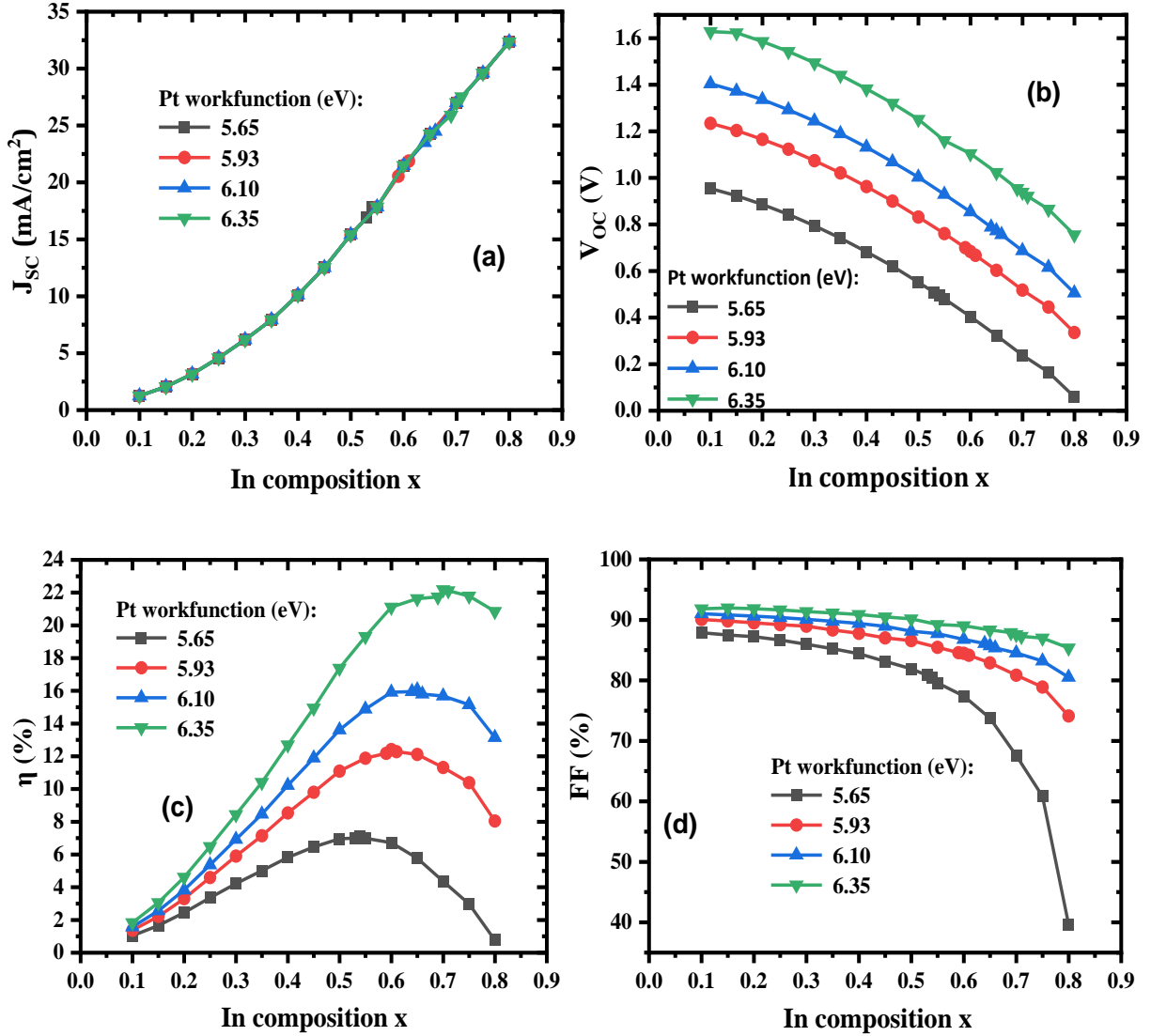


Figure III. 9: Electrical output parameters for the different reported values of ϕ_M versus In composition: (a) J_{SC} , (b) V_{OC} , (c) efficiency η and (d) FF.

J_{SC} is not affected by the change of ϕ_M , and it keeps increasing with increasing indium composition (figure III.9 (a)). Whereas in the case of V_{OC} it increases with increasing metal work function as observed in figure III.9 (b). The value of the peak efficiency improves from $\eta = 7.1\%$ to $\eta = 22.18\%$ at In composition of $x_{In}=0.54$ and $x_{In}=0.7$, respectively, as shown in Table III.2 and we notice that the deterioration of FF weakens as the work function ϕ_M increases (Figure III.9 (d)). Schottky solar cell composed of platinum metal with a work function of

$\phi_M = 6.35$ eV and a semiconductor with an indium composition of $x_{In} = 0.7$ is the cell that shows good performance and gives an efficiency of 22.18%.

Table III. 2: The optimum Indium composition for the different Pt work function values.

$\phi_M(eV)$	5.65	5.93	6.1	6.35
x_{In}	0.54	0.6	0.65	0.7
η %	7.10	12.41	16.05	22.18

Figure III.10 and Figure III.11 show the $J - V$ characteristics with respect to the In composition and Pt work function, respectively. Changing indium composition effects on both of J_{sc} and V_{oc} , While the work function affects only V_{oc} .

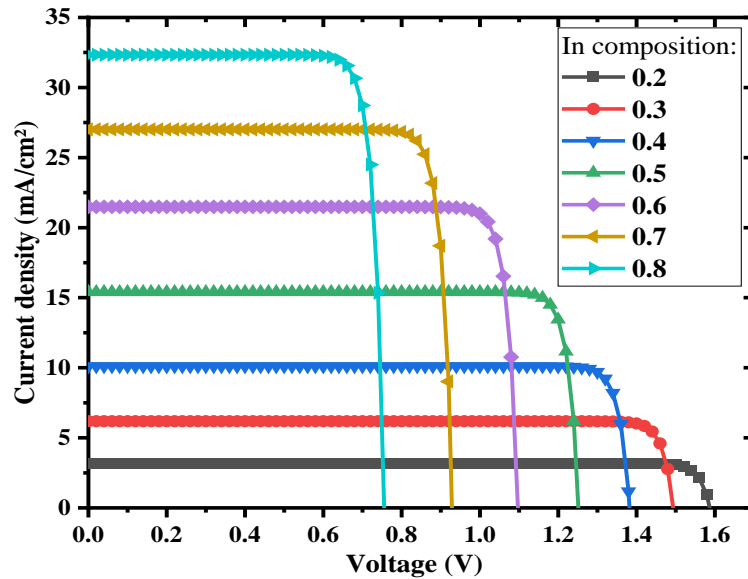


Figure III. 10: ($J - V$) characteristic for different Indium compositions.

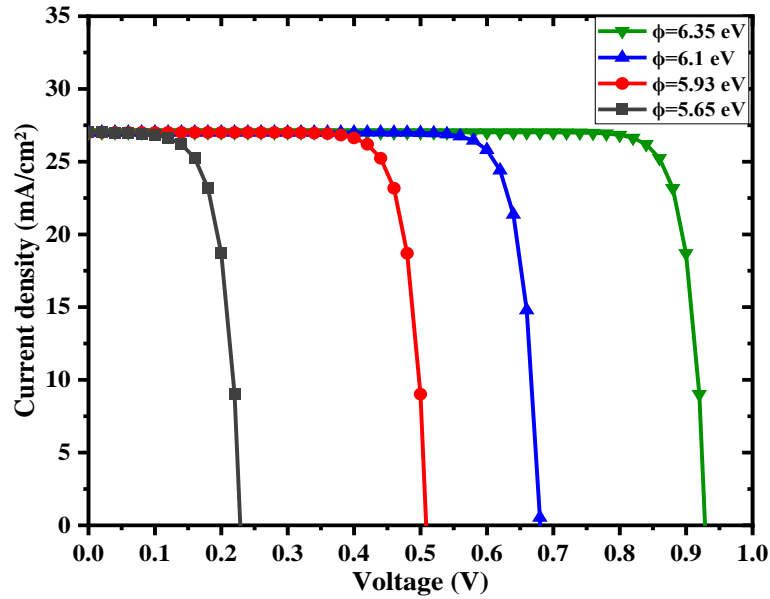


Figure III. 11: ($J - V$) characteristic for different Pt work function.

III.4 Optimizations

We suggested a number of approaches to optimize the cell performance and the first one is the following:

III.4.1 Adding a uniform Intrinsic Layer

We suggest adding an intrinsic layer to the Schottky solar cell to give better performance. The added layer is located between the metal Pt and the $\text{In}_{0.7}\text{Ga}_{0.3}\text{N}$ semiconductor. Figure III. 12 shows the effect of changing the thickness of the intrinsic layer on the output of the solar cell.

As we can see, there is an improvement in the performance of the cell as the thickness of the intrinsic layer increases with a saturated efficiency of $\eta = 23.30\%$ at $10 \mu\text{m}$. This improvement is related to the improvement of J_{SC} , by increasing the width of the space charge region. Thus an increase in photo-generation and separation of carriers[39]. The V_{OC} and FF are approximately constant. Consequently, for an efficiency of 23.09% we choose a thickness of $4 \mu\text{m}$ for the added intrinsic layer.

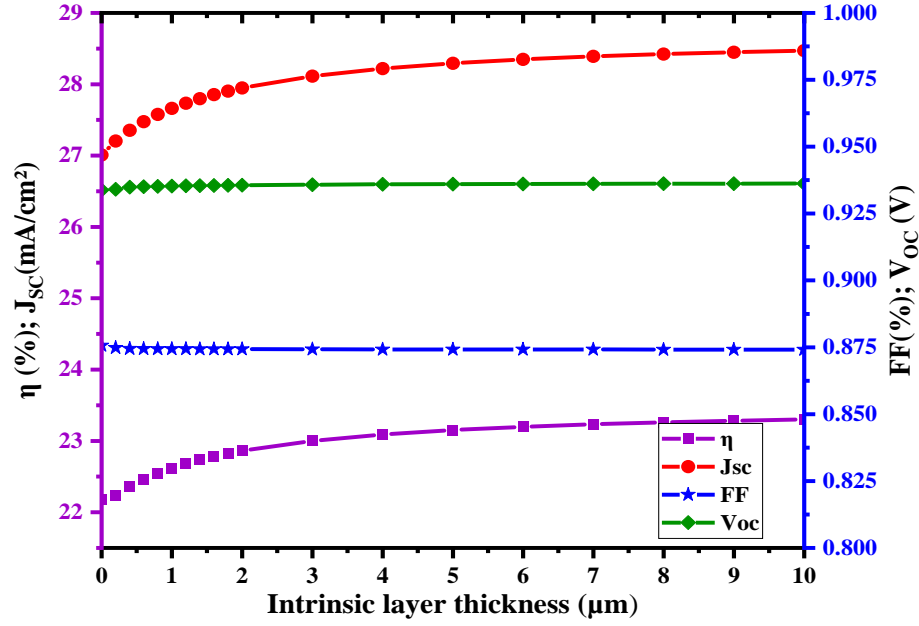


Figure III. 12: J_{sc} , V_{oc} , FF and η as a function of intrinsic layer thickness.

III.4.2 The effect of interfacial layer defect

Experimental results of the InGaN-based Schottky solar cell provided much lower performance than expected in the simulation results[6,13]. This difference may be related to the effect of traps at the interface layer between the metal and the semiconductor, and according to the results of deep-level transient spectroscopy DLTS, traps $E_c-0.18$, $E_c-0.39$ and $E_c-0.65$ eV are among the dominant traps in InGaN material[121,122]. Table III.3 presents the characteristics of these traps.

Table III. 3: Traps related to InGaN layer.

Trap level (eV)	Electron capture cross section (cm ²)	Density (cm ⁻³)
$E_c - 0.39$	1.24×10^{-16}	1.9×10^{15}
$E_c - 0.18$	2.40×10^{-20}	1×10^{15}
$E_c - 0.65$	1.00×10^{-16}	1×10^{15}

The effect of the added traps on output parameters of the solar cell is presented in Figure III.13 (a). The effect of traps with levels $E_c-0.39$ and $E_c-0.65$ on J_{sc} is clearly shown especially when

the density of traps exceed 5×10^{17} and 5×10^{16} , respectively. This is mostly due to that these defects act as recombination centres of the carriers. According to Grassa et al, $E_c-0.65$ level behave as non-radiative recombination level. The shallow level trap $E_c-0.18$ eV has a neglectful effect on J_{SC} .

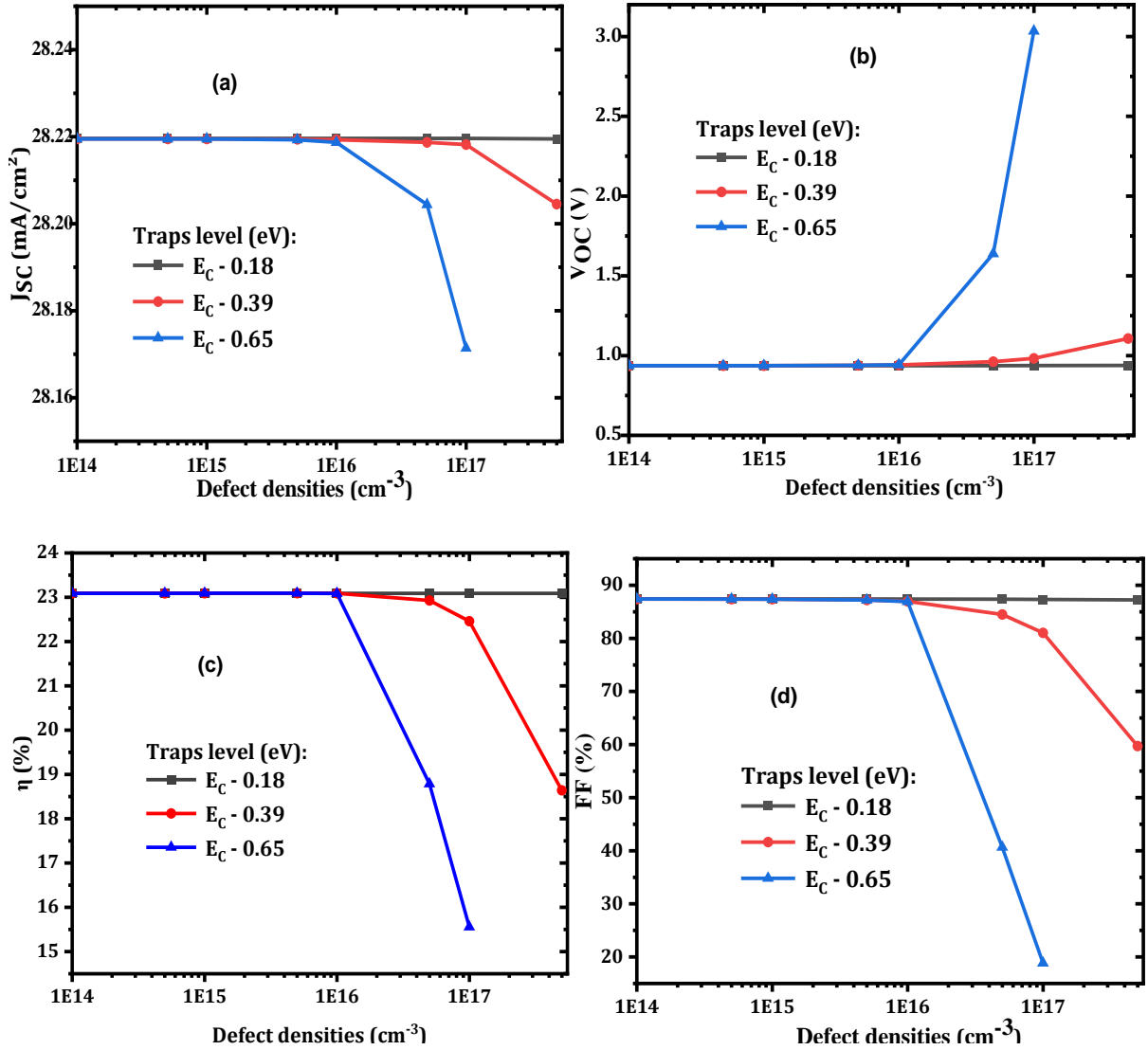


Figure III. 13: Effect of trap levels on (a) J_{SC} , (b) V_{OC} , (c) η and (d) FF .

Schottky barrier height is related to the number of traps occupied at the Pt-InGaN interface so that the height increases as the traps increase. Therefore, V_{OC} increases because it is related to the barrier height according to the relation III.1. And this is only for traps with levels $E_c-0.39$ and $E_c-0.65$, and the trap $E_c-0.18$ also does not affect V_{OC} as we can see in Figure III. 13(b).

Figure III.13(c) shows a significant decrease in η when the density of the traps Ec-0.39 and Ec-0.65 is increased to 10^{17} and 5×10^{16} , respectively. This is due to the low J_{SC} in these terms. A decrease in FF at the same intensity is shown in Figure III.13(d).

III.4.3 Adding gradual intrinsic layer

InGaN-based Schottky barrier solar cells perform well in two cases: (1) The higher the V_{OC} , and this is when the InGaN semiconductor has a low indium composition (high Schottky barrier height). (2) When the J_{SC} is high and that is when the InGaN layer has a large Indium composition.

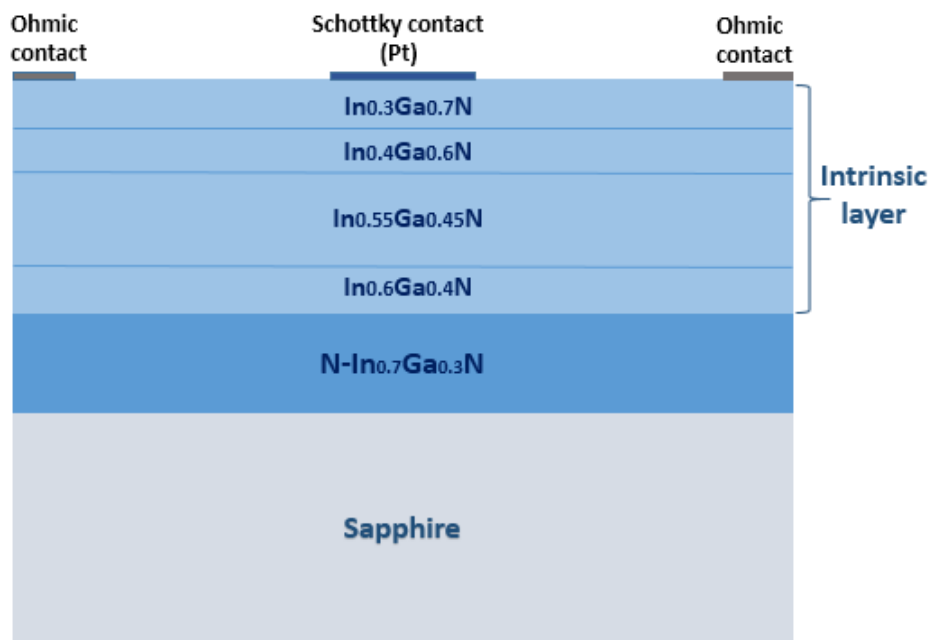


Figure III. 14: InGaN based Schottky barrier solar cell with gradual intrinsic layer structure.

In the context of enhancing the efficiency of this solar cell, we changed the uniform Indium composition of the intrinsic layer to a gradual composition, from a low in contact with the metal to high in contact with N-InGaN layer. The composition of indium is as follows $x_{In}=0.3$ (0.1 μm); $x_{In}=0.4$ (0.1 μm), $x_{In}=0.55$ (3.7 μm) and $x_{In}=0.6$ (0.1 μm). Figure III.14 shows the enhanced cell structure. This gradient in the indium composition occurs in the energy band gap, as shown in Figure III.15.

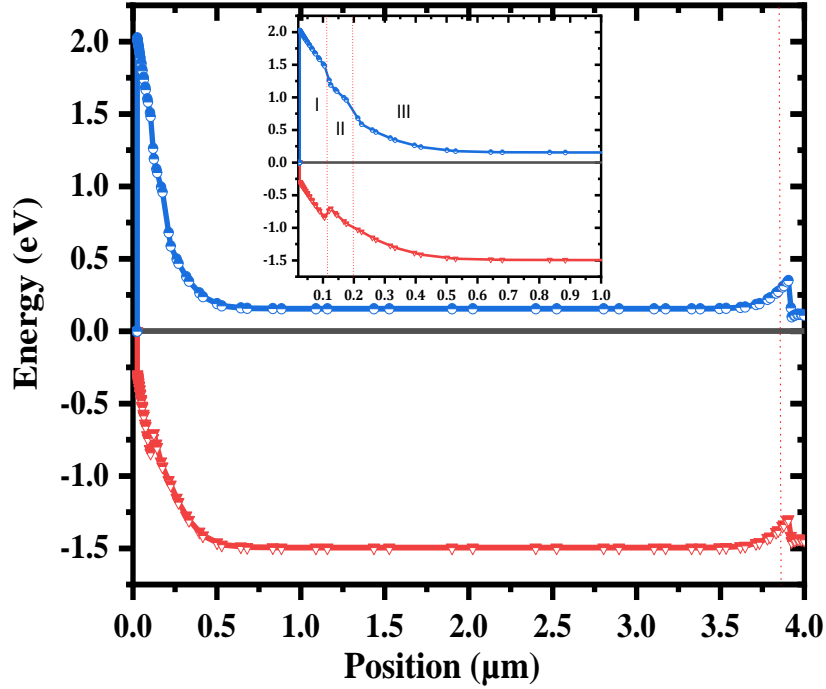


Figure III. 15: Band gap energy diagram at equilibrium of the InGaN Schottky solar cell with gradual band gap energy of the intrinsic layer.

From Figure III.16 and Table III.4, we can notice that the efficiency in the case of a solar cell with a gradual intrinsic layer is higher than that of a cell with a uniform intrinsic layer. This is due to the observed improvement in the open-circuit voltage V_{OC} . The reason for this high rise is that the InGaN layer that forms contact with the metal has a low indium composition (low electron affinity) and therefore a large Schottky barrier height. J_{sc} decreases because the larger thickness ($3.4 \mu\text{m}$) has a composition less than 0.7 which is $x_{In} = 0.55$. Figure III. 17 represents the difference in the external quantum efficiency spectrum (EQE) between a uniform intrinsic layer solar cell and a gradual layer solar cell, and shows the reason for the decrease in J_{sc} .

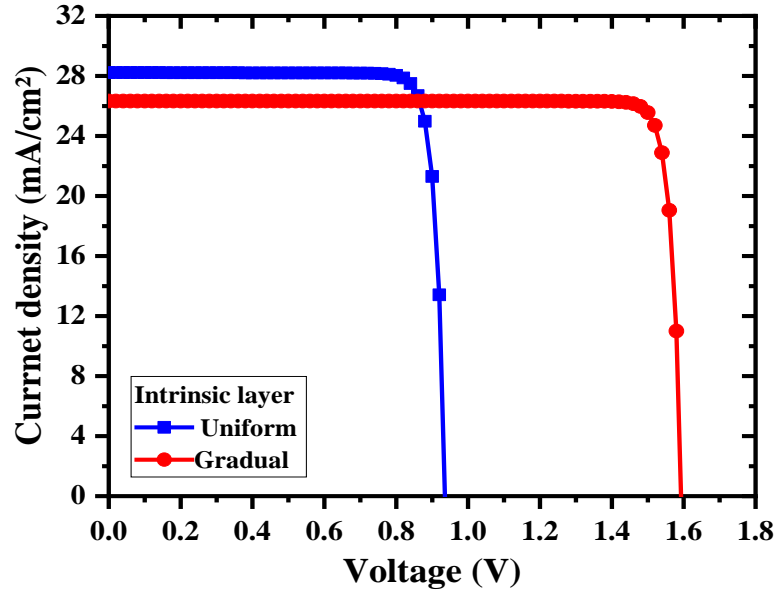


Figure III. 16: ($J - V$) characteristic for InGaN Schottky solar cell with a uniform intrinsic layer and gradual intrinsic layer.

Table III. 4: J_{SC} , V_{OC} , FF and η for InGaN schottky solar cell with uniform intrinsic layer and gradual intrinsic layer.

	J_{SC} (mA/cm ²)	V_{OC} (V)	FF (%)	η (%)
Uniform intrinsic layer	28.220	0.936	87.426	23.089
Gradual intrinsic layer	26.324	1.593	91.660	38.426

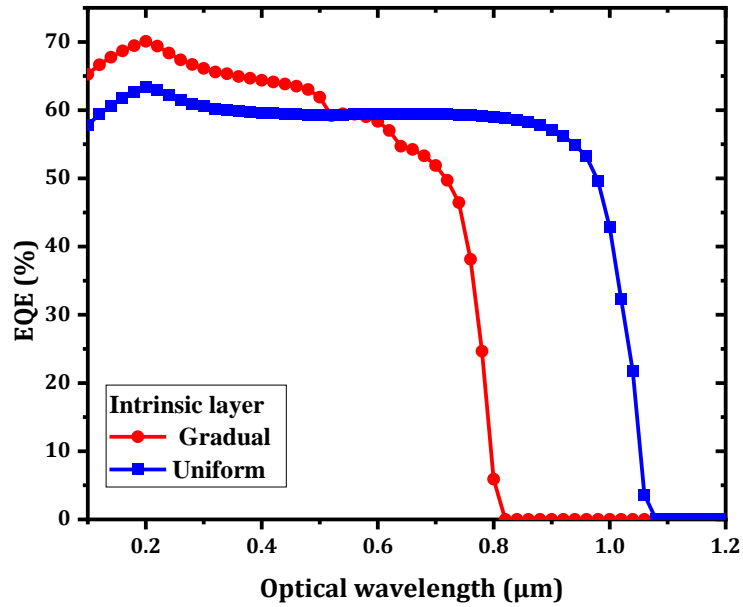


Figure III. 17: External quantum efficiency (EQE) for InGaN Schottky solar cell with a uniform intrinsic layer and gradual intrinsic layer.

Figure III.18 represents the effect of defects $E_c-0.39$ and $E_c-0.65$ on the efficiency of the gradual intrinsic layer solar cell. As we have seen previously, these two defects affect the efficiency of the cell negatively, as it decreases in this case from 38.42% to 28.89%. However, this efficiency remains high for the cell with the uniform intrinsic layer, whose efficiency after adding defects became 15.55%. Therefore, it is expected that this gradual layer will be effective in reducing the effect of defects on this type of solar cell. Although the density of defects may not reach this limit in InGaN if the surface is treated well.

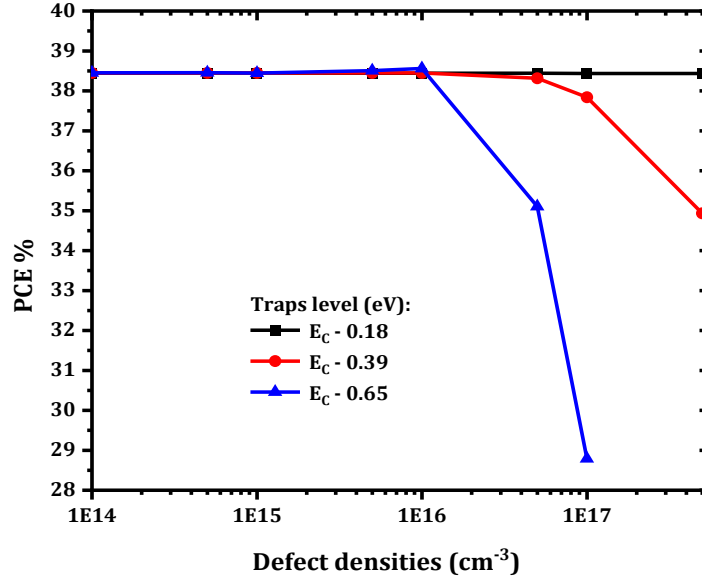


Figure III. 18: The gradual intrinsic layer solar cell efficiency η versus defect densities.

III.4.4 Influence of an insulating layer on the Schottky solar cell

In this part, we added an oxide layer of Schottky cell between the metal and the N-type semiconductor, to become a MIS solar cell (Metal-Insulator-Semiconductor) as shown in Figure III. 19. The oxide has a thickness of 1 nm [123] and is thin enough to allow a large number of electrons to tunnel through it. In addition, it used for the purpose of increasing the Schottky barrier height [124]. The comparison in the outputs of a Schottky cell and a MIS cell is shown in Table III.5, and the $J - V$ characteristic of the two solar cells is shown in Figure III.20.



Figure III. 19: InGaN based MIS solar cell structure.

From the curves in Figure III.20, it is clear that the MIS solar cell shows a higher open circuit voltage V_{oc} than the Schottky solar cell, due to the increase of the Schottky barrier height at the Pt/N-InGaN interface as expected. The short circuit current J_{SC} of the MIS solar cell decreases. This decrease may be due to the high Schottky barrier height which reduces the electrons passing over the Schottky barrier by thermionic emission (TE). However, this decrease does not affect the efficiency η , as Table III.5 shows. It is obvious that the efficiency of the MIS solar cell is much higher than the Schottky junction solar since it increases from 22.18% to 31.59% due to the increase in the open circuit voltage from 0.93 V to 1.39 V. Also, the fill factor FF has increased by almost 3%.

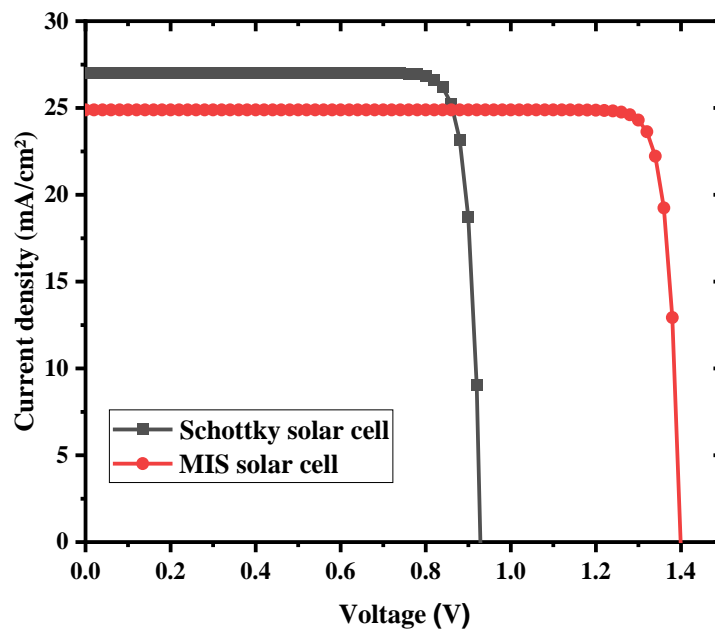


Figure III. 20: ($J - V$) characteristic for InGaN Schottky solar cell and MIS solar cell.

Table III. 5: J_{SC} , V_{OC} , FF and η for InGaN Schottky solar cell and MIS solar cell.

	J_{SC} (mA/cm^2)	V_{OC} (V)	FF %	η %
Schottky	27.009	0.9286	87.719	22.180
MIS	24.888	1.3994	90.703	31.590

III.4.5 Changing the Schottky solar cell to a MIS solar cell

In order to improve more the Schottky solar cell, we suggest to introduce an insulator material between the contact and the InGaN semiconductor.

Next to specify the appropriate oxide for an InGaN-based MIS solar cell, we suggest various prospective oxides, which are: SiO₂, Al₂O₃ and HfO₂. The parameters of the oxides are display in Table III.6.

Table III. 6: Parameters of oxides: Band gap, Affinity, Permittivity, electron and hole effective masses and fixed charge.

	E_g (eV)	χ (eV)	ϵ_{ox}	m_e/m_0	m_h/m_0	Fixed charge
SiO ₂	8.9[125]	0.9[126]	4[127]	0.4[128]	0.32[128]	positive[128]
Al ₂ O ₃	7[125]	1.9[126]	9[127]	0.46[125]	0.54[125]	negative[128]
HfO ₂	5.7[125]	1.88[129]	25[127]	0.42[125]	0.58[125]	positive[128]

Figure III.21 represents $J - V$ characteristic of MIS solar cell with different oxides. The output parameters are shown in Table III.7. According to the obtained results, we notice that SiO₂ oxide gives the highest value of J_{sc} (25.75 mA/cm²), while Al₂O₃ gives the highest value in V_{oc} , FF and η . The efficiency at Al₂O₃ oxide reaches 31.59% due to the high V_{oc} (1.39 V), while it reaches 28.85% and 25.82% for SiO₂ and HfO₂ respectively.

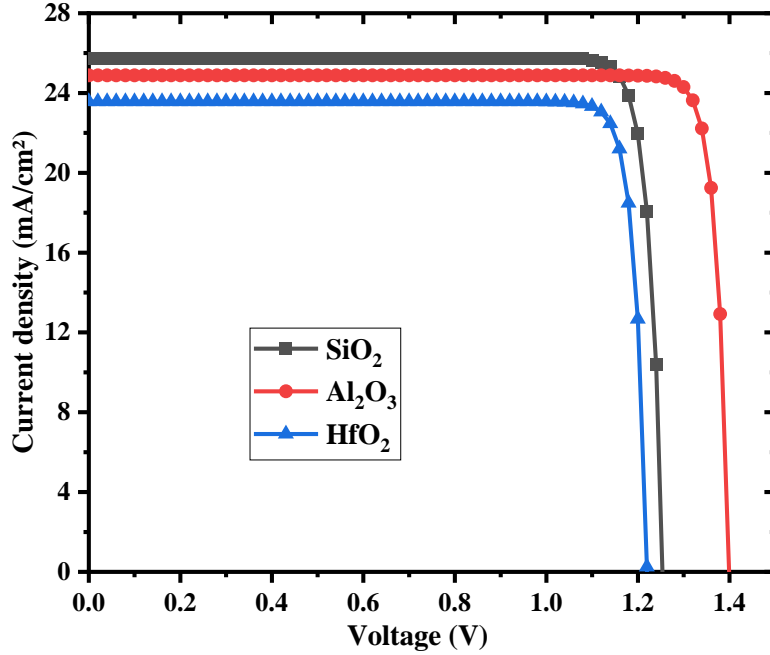


Figure III. 21: ($J - V$) characteristics of simulated structure for different oxides.

Table III. 7: J_{sc} , V_{oc} , FF and η for InGaN MIS solar cell with different oxides.

	J_{sc} (mA/cm^2)	V_{oc} (V)	FF %	η %
SiO₂	25.752	1.254	89.354	28.851
Al₂O₃	24.888	1.399	90.703	31.590
HfO₂	23.570	1.220	89.791	25.824

In order to explain why J_{sc} is different for each oxide, we extract the reflectance factor (R) from the refractive index (n) and extinction coefficient (k) according to the following expression[130]:

$$R = \frac{(n-1)^2 + \kappa^2}{(n+1)^2 + \kappa^2} \tag{III.2}$$

Figure III.22 presents the obtained reflectance factor. It is clearly that SiO₂ oxide, which recorded the highest short circuit current, has the lowest reflectance. The reflectance clearly affects the J_{sc} of the MIS cell, and the reason is that the cell structure contains a metal that

covers only 30% of the cell surface, thus, the oxide covers the remaining surface, which reflects a percentage of the light.

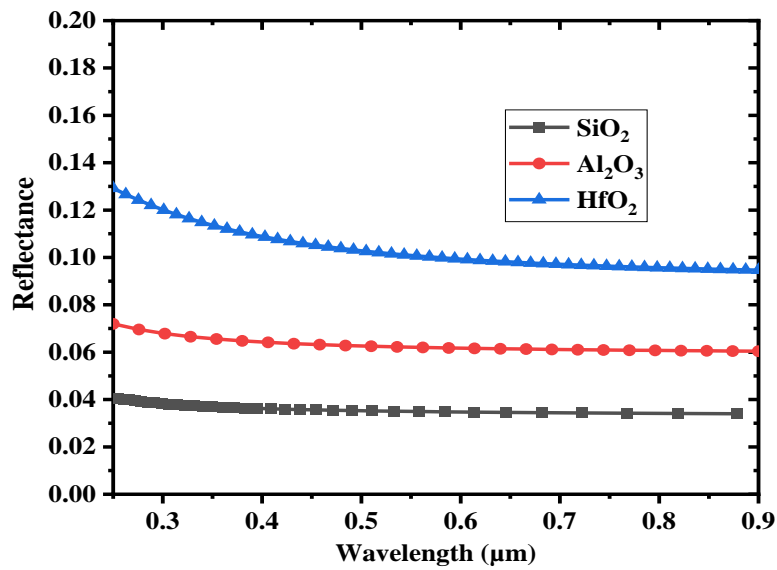


Figure III. 22: Reflectance factor of the oxides used in the simulation.

The External quantum efficiency (*EQE*) curves of the solar cell at the studied oxides are represented in Figure III.23. The obtained results prove the validity of the previous interpretation.

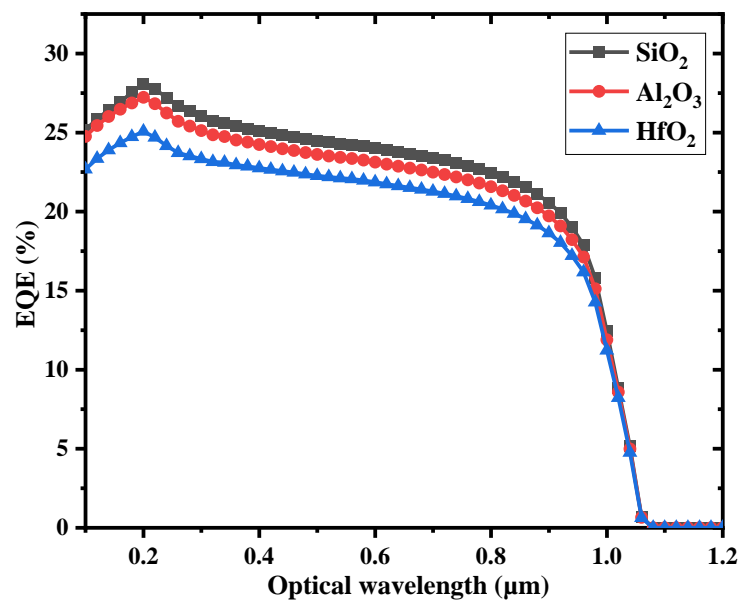


Figure III. 23: External quantum efficiency (*EQE*) for different oxides.

Al_2O_3 has negative fixed charges that are reduce surface recombination by repelling electrons[131], this is what makes this oxide give the highest V_{OC} as shown in Table III. 7 and Figure III. 21.

Figure III.24 presents the change in the output parameters as a function of negative fixed charges density in the oxide layer. The increase in the density of the fixed charges causes a significant increase in both the open circuit voltage V_{OC} and the cell efficiency η , which may reach 1.586 V and 36.186 %, respectively.

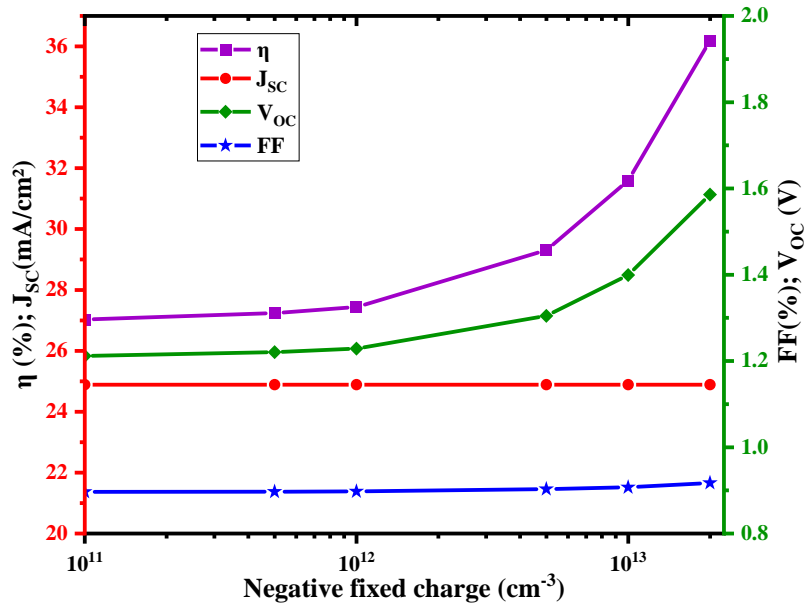


Figure III. 24: J_{sc} , V_{OC} , FF and η as a function of negative fixed charge density in Al_2O_3 oxide.

The second reason for the different V_{OC} values for oxides is the permittivity of the oxide. We notice in Figure III.25 that as permittivity increases, V_{OC} and η decrease. The permittivity does not affect much in the case of SiO_2 and HfO_2 positively charged oxides according to Figure III.21. The permittivity of the oxide ϵ_{ox} affects the ideality factor according to Equation I.10 mentioned earlier. So that the increase in permittivity leads to a decrease in the ideality factor and therefore the open circuit voltage according to the Equation I.11.

According to the obtained results, we conclude that Al_2O_3 oxide is the most suitable to provide a performant MIS solar cell since it is notable from the other suggested oxides in several properties.

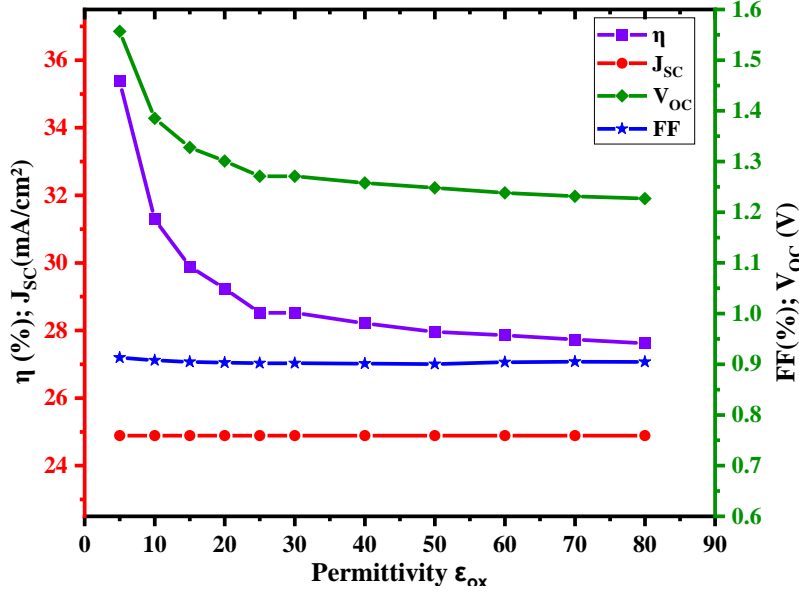


Figure III. 25: J_{sc} , V_{oc} , FF and η as a function of permittivity of Al_2O_3 oxide.

III.5. Summary

Schottky solar cells based on InGaN have faced many challenges in the design and material's manufacturing. Consequently, the study has focused on the appropriate parameters for good efficiency, in addition to a comprehensive improvement of the device.

The preliminary study of this type of solar cell depends on the selection of the suitable indium composition ($x_{In} = 0.54$) in the InGaN semiconductor and the suitable metal to form a good Schottky contact (platinum metal) given an efficiency of $\eta = 7.1\%$. The metal work function have been varied to 6.35 eV and better efficiency of $\eta = 22.08\%$ for In composition of $x_{In} = 0.7$ was obtained.

The next step was divided in several optimisation processes in the aim to improve the solar cell. First, adding an intrinsic layer between the $\text{In}_{0.7}\text{Ga}_{0.3}\text{N}$ semiconductor and the metal contact ($\text{Pt-}\phi_M = 6.35$ eV). We have noticed a significant increase in the efficiency. Then, we have considered the presence of traps in this layer and studied their effects. Under these consideration,

the efficiency has dropped dramatically to $\eta = 15.55\%$. The second step suggested in the improvement was the addition of intrinsic layer with a gradual composition to absorb larger amount of photon spectrum. The results show that the efficiency in the ideal case has increased significantly to $\eta = 38.42\%$ due to the noticeable increase in V_{OC} and with considering defects, the efficiency has again relatively reduced but remaining good enough for a solar cell.

The last suggested improvement that we have made on Schottky cells is to changing it to a MIS (Metal-Insulator-Semiconductor) solar cell, by adding an oxide layer between the metal and the semiconductor. An increase in the value of V_{OC} , was achieved, which led to an improvement in efficiency to approximately $\eta = 29.19\%$. Several oxides were studied to choose the most suitable one for the MIS junction. After analysing the obtained results, it was found that Al_2O_3 oxide gives the best efficiency of $\eta = 31.59\%$.

These studies, which included the selection of appropriate parameters in addition to the different improvements, constitute an appreciate contribution in the development of InGaN-based Schottky solar cells and improve their performance in the future.

General Conclusion

General Conclusion

InGaN material offers excellent properties in semiconductor devices and the development of InGaN-based solar cells is very important for future high-efficiency solar cells. However, these materials faced obstacles that may limit their capabilities and advantages and it is necessary to discover alternative methods such as structures without P-type semiconductor and methods for produce high-quality alloys with high indium content. Among the proposed solutions, Schottky barrier is a good alternative to the P- type layer, since this simple structure may achieve good efficiency with InGaN when the appropriate metal is provided.

The preliminary study of this type of solar cell depends on the selection of the suitable indium composition in the InGaN semiconductor and the suitable metal to form a good Schottky contact with high efficiency. The indium composition of $x_{In} = 0.54$ with platinum metal given an efficiency of $\eta = 7.1\%$. Then the metal work function have been varied to $\phi_M = 6.35$ eV and better efficiency of $\eta = 22.08\%$ for In composition of $x_{In} = 0.7$ was obtained.

The next step was divided in several optimisation processes in the aim to improve the solar cell. First, adding an intrinsic layer between the $In_{0.7}Ga_{0.3}N$ semiconductor and the metal contact (Pt- $\phi_M = 6.35$ eV). We have noticed a significant increase in the efficiency. Then, we have considered the presence of traps in this layer and studied their effects. Under these consideration, the efficiency has dropped dramatically to $\eta = 15.55\%$. The second step suggested in the improvement was the addition of intrinsic layer with a gradual composition to absorb larger amount of photon spectrum. The results show that the efficiency in the ideal case has increased significantly to $\eta = 38.42\%$ due to the noticeable increase in V_{OC} and with considering defects, the efficiency has again relatively reduced but remaining good enough for a solar cell.

The last suggested improvement that we have made on Schottky cells is to changing it to a MIS (Metal-Insulator-Semiconductor) solar cell by including an oxide layer between the metal and the semiconductor. An increase in the value of V_{OC} , was achieved, which led to an improvement in efficiency to approximately $\eta = 29.19\%$. Several oxides were studied to choose the most suitable one for the MIS junction. After analysing the obtained results, it was found that Al_2O_3 oxide gives the best efficiency of $\eta = 31.59\%$.

These studies, which included the selection of appropriate parameters in addition to the different improvements, constitute an appreciate contribution in the development of InGaN-based Schottky solar cells and improve their performance in the future.

References

- [1] A.G. Bhuiyan, K. Sugita, A. Hashimoto, A. Yamamoto, InGaN solar cells: Present state of the art and important challenges, *IEEE J. Photovoltaics*. 2 (2012) 276–293. <https://doi.org/10.1109/JPHOTOV.2012.2193384>.
- [2] K.N. Nwaigwe, P. Mutabilwa, E. Dintwa, An overview of Solar Power (PV Systems) Integration into Electricity Grids, *Mater. Sci. Energy Technol.* (2019). <https://doi.org/10.1016/j.mset.2019.07.002>.
- [3] P. Mahala, S.K. Behura, A.S. Kushwaha, A. Ray, O. Jani, C. Dhanavantri, A study on the 2D simulation of Pt/InGaN/GaN/metal Schottky junction solar cell, *Semicond. Sci. Technol.* 28 (2013). <https://doi.org/10.1088/0268-1242/28/5/055012>.
- [4] L. Dong, J. V. Mantese, V. Avrutin, Ü. Özgür, H. Morkoç, S.P. Alpay, Strain induced variations in band offsets and built-in electric fields in InGaN/GaN multiple quantum wells, *J. Appl. Phys.* 114 (2013). <https://doi.org/10.1063/1.4816254>.
- [5] Joachim Piprek, Nitride semiconductor device, Wiley-VCH, 2013. <http://www.google.com/patents/US5959307>.
- [6] X. Jun-Jun, C. Dun-Jun, L. Bin, X. Zi-Li, J. Ruo-Lian, Z. Rong, Z. You-Dou, Au / Pt / InGaN / GaN Heterostructure Schottky Prototype Solar Cell, 098102 (2009) 2007–2010. <https://doi.org/10.1088/0256-307X/26/9/098102>.
- [7] R. Kour, S. Arya, S. Verma, A. Singh, P. Mahajan, A. Khosla, Review—Recent Advances and Challenges in Indium Gallium Nitride (In x Ga 1-x N) Materials for Solid State Lighting , *ECS J. Solid State Sci. Technol.* 9 (2020) 015011. <https://doi.org/10.1149/2.0292001jss>.
- [8] G.F. S. Nakamura, S. Pearton, The Blue laser Diode, Second Edi, Springer-Verlag Berlin Heidelberg New York, USA, 2000. <https://doi.org/10.1007/978-3-662-04156-7>.
- [9] C. Yang, X. Wang, H. Xiao, J. Ran, C. Wang, G. Hu, X. Wang, X. Zhang, J. Li, J. Li, Photovoltaic effects in InGaN structures with p – n junctions, 4291 (2007) 4288–4291. <https://doi.org/10.1002/pssa.200723202>.
- [10] O. Jani, B. Jampana, I. Ferguson, H. Yu, E. Trybus, A. Doolittle, C. Honsberg, Effect of phase separation on performance of III-V nitride solar cells, in: *Proc. 22nd Eur. Photovolt. Sol. Energy Conf.*, 2007: pp. 64–67. <https://www.researchgate.net/publication/252262575>.
- [11] K.T. Chern, N.P. Allen, T.A. Ciarkowski, O.A. Laboutin, R.E. Welser, L.J. Guido, GaInN/GaN solar cells made without p-type material using oxidized Ni/Au Schottky

- electrodes, *Mater. Sci. Semicond. Process.* 55 (2016) 2–6. <https://doi.org/10.1016/j.mssp.2016.03.026>.
- [12] D.J. Chen, Y. Huang, B. Liu, Z.L. Xie, R. Zhang, Y.D. Zheng, Y. Wei, V. Narayanamurti, High-quality Schottky contacts to n-InGaN alloys prepared for photovoltaic devices, *J. Appl. Phys.* 105 (2009). <https://doi.org/10.1063/1.3099601>.
- [13] S. Lin, B.P. Zhang, S.W. Zeng, X.M. Cai, J.Y. Zhang, S.X. Wu, A.K. Ling, G.E. Weng, Preparation and properties of Ni/InGaN/GaN Schottky barrier photovoltaic cells, *Solid. State. Electron.* 63 (2011) 105–109. <https://doi.org/10.1016/j.sse.2011.05.001>.
- [14] S. Ould Saad Hamady, A. Adaine, N. Fressengeas, Numerical simulation of InGaN Schottky solar cell, *Mater. Sci. Semicond. Process.* 41 (2016) 219–225. <https://doi.org/10.1016/j.mssp.2015.09.001>.
- [15] R. Dahal, J. Li, K. Aryal, J.Y. Lin, H.X. Jiang, InGaN/GaN multiple quantum well concentrator solar cells, *Appl. Phys. Lett.* 97 (2010) 6–9. <https://doi.org/10.1063/1.3481424>.
- [16] D.V.P. McLaughlin, J.M. Pearce, Analytical model for the optical functions of indium gallium nitride with application to thin film solar photovoltaic cells, *Mater. Sci. Eng. B Solid-State Mater. Adv. Technol.* 177 (2012) 239–244. <https://doi.org/10.1016/j.mseb.2011.12.008>.
- [17] P. Schley, R. Goldhahn, A.T. Winzer, G. Gobsch, V. Cimalla, O. Ambacher, H. Lu, W.J. Schaff, M. Kurouchi, Y. Nanishi, M. Rakel, C. Cobet, N. Esser, Dielectric function and Van Hove singularities for In-rich $\text{In}_x\text{Ga}_{1-x}\text{N}$ alloys: Comparison of N- and metal-face materials, *Phys. Rev. B - Condens. Matter Mater. Phys.* 75 (2007) 1–8. <https://doi.org/10.1103/PhysRevB.75.205204>.
- [18] P. Mahala, S.K. Behura, C. Dhanavatri, A. Ray, O. Jani, Metal/InGaN Schottky junction solar cells: an analytical approach, *Appl. Phys. A Mater. Sci. Process.* 118 (2014) 1459–1468. <https://doi.org/10.1007/s00339-014-8910-5>.
- [19] A. Khetto, I. Zeydi, M. Chellali, M. Ben Arbia, S. Mansouri, H. Helal, H. Maaref, Simulation and optimization of InGaN Schottky solar cells to enhance the interface quality, *Superlattices Microstruct.* 142 (2020) 106539. <https://doi.org/10.1016/j.spmi.2020.106539>.
- [20] Y. Marouf, L. Dehimi, F. Bouzid, F. Pezzimenti, F.G.D. Corte, Theoretical design and performance of $\text{In}_x\text{Ga}_{1-x}\text{N}$ single junction solar cell, *Optik (Stuttg.)* 163 (2018) 22–32. <https://doi.org/10.1016/j.ijleo.2018.02.106>.
- [21] Joachim Piprek, Nitride semiconductor device, 2013. <http://www.google.com/patents/US5959307>.
- [22] R. Dahal, B. Pantha, J. Li, J.Y. Lin, H.X. Jiang, InGaN/GaN multiple quantum well solar cells with long operating wavelengths, *Appl. Phys. Lett.* 94 (2009). <https://doi.org/10.1063/1.3081123>.
- [23] C.A.M. Fabien, A. Maros, C.B. Honsberg, W.A. Doolittle, III-Nitride Double-Heterojunction Solar Cells with High In-Content InGaN Absorbing Layers: Comparison

- of Large-Area and Small-Area Devices, *IEEE J. Photovoltaics*. 6 (2016) 460–464. <https://doi.org/10.1109/JPHOTOV.2015.2504790>.
- [24] S.R. Routray, T.R. Lenka, InGaN-based solar cells: a wide solar spectrum harvesting technology for twenty-first century, *CSI Trans. ICT*. 6 (2018) 83–96. <https://doi.org/10.1007/s40012-017-0181-9>.
- [25] S. Rock, Modeling Schottky Barrier GaAs solar cell using Silvaco atlas, *NAVAL POST GRADUATE SCHOOL MONTEREY, CALIFORNIA*, 2018. <https://www.hsdl.org/?view&did=811367>.
- [26] C.O. Sullivan, J.A. Murphy, *Field Guide to Terahertz Sources, Detectors, and Optics*, Bellingham, Washington USA, 2012.
- [27] V. Prasad, *Electrical properties of n-GaN based MOS type schottky junctions*, Sri Venkateswara university, 2021.
- [28] B. L.Sharma, *Metal-Semiconductor Schottky Barrier Junctions and Their Applications*, 1 st editi, Plenum Publishing Corporation, Delhi, India, 1984. <https://doi.org/10.1007/978-1-4684-4655-5>.
- [29] S. M. SZE, M. K. LEE, *Semiconductor Devices Physics and Technology*, John Wiley & Sons Singapore Pte. Limited, Taiwan, 2016. <https://books.google.dz/books?id=gmmscQAACAAJ>.
- [30] H. Mathieu, H. Fanet, *Physique des semiconducteurs et des composants électroniques - 6ème édition: Cours et exercices corrigés*, 2009. https://books.google.fr/books/about/Physique_des_semiconducteurs_et_des_comp.html?id=vAXJsXS0yosC&pgis=1.
- [31] M. Grundmann, *The Physics of Semiconductors*, Third Edit, Springer International Publishing, Germany, 2016. <https://doi.org/10.1007/978-3-319-23880-7>.
- [32] B. Roul, M. Kumar, M.K. Rajpalke, T.N. Bhat, S.B. Krupanidhi, Binary group III-nitride based heterostructures: Band offsets and transport properties, *J. Phys. D. Appl. Phys.* 48 (2015). <https://doi.org/10.1088/0022-3727/48/42/423001>.
- [33] J.P. Ao, Y. Ohno, GaN-based Schottky diodes, *Handb. Light Emit. Schottky Diode Res.* (2009) 565–593. <https://doi.org/10.5772/intechopen.77024>.
- [34] J.R. Nicholls, S. Dimitrijević, P. Tanner, J. Han, The Role of Near-Interface Traps in Modulating the Barrier Height of SiC Schottky Diodes, *IEEE Trans. Electron Devices*. 66 (2019) 1675–1680. <https://doi.org/10.1109/TED.2019.2896216>.
- [35] J. Fan, S. Lee, Effect of Oxide Layer in Metal-Oxide-Semiconductor Systems, 06103 (2016) 0–4. https://doi.org/10.1051/mateconf/2016_6706103.
- [36] M. Farhat, S. Kais, F.H. Alharbi, Plasmonically Enhanced Schottky Photovoltaic Devices, *Sci. Rep.* 7 (2017) 1–9. <https://doi.org/10.1038/s41598-017-14528-0>.
- [37] S. Ju, B. Liang, J.Z. Wang, Y. Shi, S.L. Li, Graphene/silicon Schottky solar cells: Technical strategies for performance optimization, *Opt. Commun.* 428 (2018) 258–268. <https://doi.org/10.1016/j.optcom.2018.02.033>.

- [38] K.T. Chern, Dissertation, GaInN / GaN Schottky Barrier Solar Cells, Blacksburg, Virginia, 2015. <http://hdl.handle.net/10919/52899>.
- [39] I.M. Dharmadasa, *Advances in Thin-Film Solar Cells*, Second Edi, Jenny Stanford Publishing, Boulevard, 2018. <https://doi.org/10.1201/9780429020841>.
- [40] S.P. Electronics, *Semiconductor Physical Electronics*, 2006. <https://doi.org/10.1007/0-387-37766-2>.
- [41] ASTM G-173-03 (international standard ISO 9845-1,1995).
- [42] W.M. Haynes, *CRC Handbook of Chemistry and Physics*, 95 TH EDIT, CRC Press, 2014.
- [43] H.B. Michaelson, The work function of the elements and its periodicity, *J. Appl. Phys.* 48 (1977) 4729–4733. <https://doi.org/10.1063/1.323539>.
- [44] F.C. Walsh, Electrode reactions in metal finishing, *Trans. Inst. Met. Finish.* 69 (1991) 107–110. <https://doi.org/10.1080/00202967.1991.11870904>.
- [45] B.G. Baker, B.B. Johnson, G.L.C. Maire, Photoelectric work function measurements on nickel crystals and films, *Surf. Sci.* 24 (1971) 572–586. [https://doi.org/10.1016/0039-6028\(71\)90282-2](https://doi.org/10.1016/0039-6028(71)90282-2).
- [46] R.F. McOuat, D.L. Pulfrey, A model for Schottky-barrier solar cell analysis, *J. Appl. Phys.* 47 (1976) 2113–2119. <https://doi.org/10.1063/1.322857>.
- [47] J.K. Ho, C.S. Jong, C.C. Chiu, C.N. Huang, K.K. Shih, L.C. Chen, F.R. Chen, J.J. Kai, Low-resistance ohmic contacts to p-type GaN achieved by the oxidation of Ni/Au films, *J. Appl. Phys.* 86 (1999) 4491–4497. <https://doi.org/10.1063/1.371392>.
- [48] W.C. Chong, K.M. Lau, Comparison of Ni/Au, ITO, and ATO-based current spreading layers for near-ultraviolet light-emitting diodes, *Phys. Status Solidi Curr. Top. Solid State Phys.* 4 (2007) 2646–2649. <https://doi.org/10.1002/pssc.200674892>.
- [49] H.W. Jang, W. Urbanek, M.C. Yoo, J.L. Lee, Low-resistant and high-transparent Ru/Ni ohmic contact on p-type GaN, *Appl. Phys. Lett.* 80 (2002) 2937–2939. <https://doi.org/10.1063/1.1474609>.
- [50] T. Margalith, O. Buchinsky, D.A. Cohen, A.C. Abare, M. Hansen, S.P. DenBaars, L.A. Coldren, Indium tin oxide contacts to gallium nitride optoelectronic devices, *Appl. Phys. Lett.* 74 (1999) 3930–3932. <https://doi.org/10.1063/1.124227>.
- [51] S.D. Nehate, A. Prakash, P.D. Mani, K.B. Sundaram, Work Function Extraction of Indium Tin Oxide Films from MOSFET Devices, *ECS J. Solid State Sci. Technol.* 7 (2018) P87–P90. <https://doi.org/10.1149/2.0081803jss>.
- [52] J.W. Weber, V.E. Calado, M.C.M. Van De Sanden, Optical constants of graphene measured by spectroscopic ellipsometry, *Appl. Phys. Lett.* 97 (2010). <https://doi.org/10.1063/1.3475393>.
- [53] H.D. Cho, T. Yoon, S.U. Yuldashev, W. Kang, Electroluminescence in a rectifying graphene / InGaN junction, *RSC Adv.* (2017). <https://doi.org/10.1039/c7ra10672f>.

- [54] W. Zhang, L. Wu, Z. Li, Y. Liu, Doped graphene: Synthesis, properties and bioanalysis, *RSC Adv.* 5 (2015) 49521–49533. <https://doi.org/10.1039/c5ra05051k>.
- [55] M. Kim, N.S. Safron, C. Huang, M.S. Arnold, P. Gopalan, Light-driven reversible modulation of doping in graphene, *Nano Lett.* 12 (2012) 182–187. <https://doi.org/10.1021/nl2032734>.
- [56] R. Garg, N. Dutta, N. Choudhury, Work Function Engineering of Graphene, *Nanomaterials.* 4 (2014) 267–300. <https://doi.org/10.3390/nano4020267>.
- [57] T. Meng, Metal oxide heterovalence multijunctions for third generation solar cells, *Conf. Rec. 2006 IEEE 4th World Conf. Photovolt. Energy Conversion, WCPEC-4.* 1 (2006) 194–197. <https://doi.org/10.1109/WCPEC.2006.279415>.
- [58] A.A.M. Mazumder, M.S. Hasan, A.I.M. Iskanderani, M.R. Islam, M.T. Hasan, I.M. Mehedi, Analytical study of Metal-Insulator-Semiconductor contacts for both p- and n-InGaN, *Results Phys.* 19 (2020) 103679. <https://doi.org/10.1016/j.rinp.2020.103679>.
- [59] A.H.M. Shousha, Performance characteristics of thin film mis solar cells, *Sol. Wind Technol.* 6 (1989) 705–712. [https://doi.org/10.1016/0741-983X\(89\)90008-8](https://doi.org/10.1016/0741-983X(89)90008-8).
- [60] K.P. Pande, Characteristics of MOS Solar Cells Built on (n-Type) InP Substrates, (1980) 9–11. <https://doi.org/10.1109/T-ED.1980.19914>.
- [61] H.C. Card, E.H. Rhoderick, Studies of tunnel MOS diodes I. Interface effects in silicon Schottky diodes, *J. Phys. D. Appl. Phys.* 4 (1971) 1589–1601. <https://doi.org/10.1088/0022-3727/4/10/319>.
- [62] D.K. Simon, P.M. Jordan, T. Mikolajick, I. Dirnstorfer, On the Control of the Fixed Charge Densities in Al₂O₃-Based Silicon Surface Passivation Schemes, *ACS Appl. Mater. Interfaces.* 7 (2015) 28215–28222. <https://doi.org/10.1021/acsami.5b06606>.
- [63] O. Jani, I. Ferguson, C. Honsberg, S. Kurtz, Design and characterization of GaNInGaN solar cells, *Appl. Phys. Lett.* 91 (2007) 1–4. <https://doi.org/10.1063/1.2793180>.
- [64] V. Fiorentini, F. Bernardini, F. Della Sala, A. Di Carlo, P. Lugli, Effects of macroscopic polarization in III-V nitride multiple quantum wells, *Phys. Rev. B - Condens. Matter Mater. Phys.* 60 (1999) 8849–8858. <https://doi.org/10.1103/PhysRevB.60.8849>.
- [65] V. Fiorentini, F. Bernardini, O. Ambacher, Evidence for nonlinear macroscopic polarization in III-V nitride alloy heterostructures, *Appl. Phys. Lett.* 80 (2002) 1204–1206. <https://doi.org/10.1063/1.1448668>.
- [66] C.X. Ren, Polarisation fields in III-nitrides: effects and control, 0836 (2016). <https://doi.org/10.1179/1743284715Y.0000000103>.
- [67] M. Ferhat, F. Bechstedt, First-principles calculations of gap bowing in In_xGa_{1-x}N and In_xAl_{1-x}N alloys: Relation to structural and thermodynamic properties, (2002). <https://doi.org/10.1103/PhysRevB.65.075213>.
- [68] J. Wu, When group-III nitrides go infrared: New properties and perspectives *APPLIED PHYSICS REVIEWS – FOCUSED REVIEW* When group-III nitrides go infrared: New properties and perspectives, 011101 (2009). <https://doi.org/10.1063/1.3155798>.

- [69] Thi Huong NGO, Optimization of the internal quantum efficiency of luminescent devices based on GaN and operating from the yellow to the red, Montpellier, 2017. <https://tel.archives-ouvertes.fr/tel-01948385>.
- [70] A. Adaine, S. Ould Saad Hamady, N. Fressengeas, Simulation study of a new InGaN p-layer free Schottky based solar cell, *Superlattices Microstruct.* 96 (2016) 121–133. <https://doi.org/10.1016/j.spmi.2016.05.020>.
- [71] G.F. Brown, J.W.A. Iii, W. Walukiewicz, J. Wu, Finite element simulations of compositionally graded InGaN solar cells, *Sol. Energy Mater. Sol. Cells.* 94 (2010) 478–483. <https://doi.org/10.1016/j.solmat.2009.11.010>.
- [72] C.A.M. Fabien, W.A. Doolittle, Solar Energy Materials & Solar Cells Guidelines and limitations for the design of high-efficiency InGaN single-junction solar cells, *Sol. Energy Mater. Sol. Cells.* 130 (2014) 354–363. <https://doi.org/10.1016/j.solmat.2014.07.018>.
- [73] S.A. Kazazis, E. Papadomanolaki, E. Iliopoulos, Polarization-engineered InGaN/GaN solar cells: Realistic expectations for single heterojunctions, *IEEE J. Photovoltaics.* 8 (2018) 118–124. <https://doi.org/10.1109/JPHOTOV.2017.2775164>.
- [74] W. Shan, W. Walukiewicz, E.E. Haller, B.D. Little, J.J. Song, M.D. McCluskey, N.M. Johnson, Z.C. Feng, M. Schurman, R.A. Stall, Optical properties of In_xGa_{1-x}N alloys grown by metalorganic chemical vapor deposition, *J. Appl. Phys.* 84 (1998) 4452–4458. <https://doi.org/10.1063/1.368669>.
- [75] B.N. Pantha, J. Li, J.Y. Lin, H.X. Jiang, Single phase In_xGa_{1-x}N (0.25x0.63) alloys synthesized by metal organic chemical vapor deposition, *Appl. Phys. Lett.* 93 (2008) 13–16. <https://doi.org/10.1063/1.3006432>.
- [76] K.M. Chen, X. and Matthews, K. D. and Hao, D. and Schaff, W. J. and Eastman, L. F. and Walukiewicz, W. and Ager, J. W. and Yu, Characterization of MG-doped InGaN and InAlN alloys grown by MBE for solar applications, in: 2008 33rd IEEE Photovolt. Spec. Conf., 2008. <https://doi.org/10.1109/PVSC.2008.4922690>.
- [77] M. Gartner, C. Kruse, M. Modreanu, A. Tausendfreund, C. Roder, D. Hommel, Optical characterization of In_xGa_{1-x}N alloys, *Appl. Surf. Sci.* 253 (2006) 254–257. <https://doi.org/10.1016/j.apsusc.2006.05.077>.
- [78] Z. Xing, W. Yang, Z. Yuan, X. Li, Y. Wu, J. Long, S. Jin, Y. Zhao, T. Liu, L. Bian, S. Lu, M. Luo, Growth and Characterization of High In-content InGaN grown by MBE using Metal Modulated Epitaxy Technique (MME), *J. Cryst. Growth.* 516 (2019) 57–62. <https://doi.org/10.1016/j.jcrysgro.2019.03.021>.
- [79] A.G. Bhuiyan, A. Mihara, T. Esaki, K. Sugita, A. Hashimoto, A. Yamamoto, N. Watanabe, H. Yokoyama, N. Shigekawa, MOVPE growth of InGaN on Si(111) substrates with an intermediate range of In content, *Phys. Status Solidi C.* 672 (2012) 670–672. <https://doi.org/10.1002/pssc.201100355>.
- [80] K. Sasamoto, T. Hotta, K. Sugita, A.G. Bhuiyan, A. Hashimoto, A. Yamamoto, MOVPE growth of high quality p-type InGaN with intermediate In compositions, *J. Cryst. Growth.*

318 (2011) 492–495. <https://doi.org/10.1016/j.jcrysgro.2010.10.217>.

- [81] A. Syrkin, V. Ivantsov, O. Kovalenkov, A. Usikov, V. Dmitriev, Z. Liliental-Weber, M.L. Reed, E.D. Readinger, H. Shen, M. Wraback, First all-HVPE grown InGaN/InGaN MQW LED structures for 460–510 nm, *Phys. Status Solidi Curr. Top. Solid State Phys.* 5 (2008) 2244–2246. <https://doi.org/10.1002/pssc.200778647>.
- [82] H.M. Kim, W.C. Lee, T.W. Kang, K.S. Chung, C.S. Yoon, C.K. Kim, InGaN nanorods grown on (1 1 1) silicon substrate by hydride vapor phase epitaxy, *Chem. Phys. Lett.* 380 (2003) 181–184. <https://doi.org/10.1016/j.cplett.2003.09.020>.
- [83] K. Khan, M. Biswas, E. Ahmadi, Growth of high quality (In, Ga)N films on O-face ZnO substrates by plasma-assisted molecular beam epitaxy, *AIP Adv.* 075120 (2020) 6. <https://doi.org/10.1063/5.0012854>.
- [84] H. Turski, M. Siekacz, M. Sawicka, G. Cywinski, M. Krysko, S. Grzanka, J. Smalc-Koziorowska, I. Grzegory, S. Porowski, Z.R. Wasilewski, C. Skierbiszewski, Growth mechanism of InGaN by plasma assisted molecular beam epitaxy, *J. Vac. Sci. Technol. B, Nanotechnol. Microelectron. Mater. Process. Meas. Phenom.* 29 (2011) 03C136. <https://doi.org/10.1116/1.3590932>.
- [85] K. Prabakaran, R. Ramesh, P. Arivazhagan, M. Jayasakthi, S. Sanjay, S. Surender, S. Pradeep, M. Balaji, K. Baskar, Effects of indium flow rate on the structural, morphological, optical and electrical properties of InGaN layers grown by metal organic chemical vapour deposition, *J. Alloys Compd.* 811 (2019) 151803. <https://doi.org/10.1016/j.jallcom.2019.151803>.
- [86] O.K. Jani, Development of wide-band gap InGaN solar cells for high-efficiency photovoltaics, Georgia Institute of Technology, 2008. <https://doi.org/http://hdl.handle.net/1853/29627>.
- [87] I.H. Ho, G.B. Stringfellow, Solid phase immiscibility in GaInN, *Appl. Phys. Lett.* 69 (1996) 2701–2703. <https://doi.org/10.1063/1.117683>.
- [88] T. Nagatomo, T. Kuboyama, H. Minamino, O. Omoto, Properties of Ga_{1-x}In_xN Films Prepared by MOVPE, *J. Appl. Phys.* 28 (1989) 4. <https://doi.org/10.1143/jjap.28.11334>.
- [89] N. Yoshimoto, T. Matsuoka, T. Sasaki, A. Katsui, Photoluminescence of InGaN films grown at high temperature by metalorganic vapor phase epitaxy, *Appl. Phys.* 2251 (1991). <https://doi.org/10.1063/1.106086>.
- [90] V. Cardin, L.I. Dion-Bertrand, P. Grégoire, H.P.T. Nguyen, M. Sakowicz, Z. Mi, C. Silva, R. Leonelli, Recombination dynamics in InGaN/GaN nanowire heterostructures on Si(111), *Nanotechnology.* 24 (2013). <https://doi.org/10.1088/0957-4484/24/4/045702>.
- [91] S. Yamasaki, S. Asami, N. Shibata, M. Koike, K. Manabe, T. Tanaka, H. Amano, I. Akasaki, p-type conduction in Mg-doped Ga_{0.91}In_{0.09}N grown by metalorganic vapor-phase epitaxy, *Appl. Phys. Lett.* 1112 (1995) 1112. <https://doi.org/10.1063/1.113829>.
- [92] K. Kumakura, T. Makimoto, N. Kobayashi, Activation Energy and Electrical Activity of Mg in Mg-Doped In_xGa_{1-x}N (x < 0.2), *Jpn. J. Appl. Phys.* 39 (2000) 337–339. <http://iopscience.iop.org/1347-4065/39/4B/L337>.

- [93] K. Kumakura, T. Makimoto, N. Kobayashi, High hole concentrations in Mg-doped InGaN grown by MOVPE, *J. Cryst. Growth.* 221 (2000) 267–270. [https://doi.org/10.1016/S0022-0248\(00\)00697-7](https://doi.org/10.1016/S0022-0248(00)00697-7).
- [94] J.K. Kim, J. Lee, J.W. Lee, H.E. Shin, Y.J. Park, T. Kim, J.K. Kim, J. Lee, Low resistance Pd / Au ohmic contacts to p -type GaN using surface treatment, 2953 (2005) 20–23. <https://doi.org/10.1063/1.122641>.
- [95] J. Jang, S. Park, T. Seong, J. Jang, S. Park, T. Seong, Formation of low resistance Pt ohmic contacts to p-type GaN using two-step surface treatment, 2667 (2015). <https://doi.org/10.1116/1.591045>.
- [96] A. Ga, N. Gan, A.P. Zhang, B. Luo, J.W. Johnson, F. Ren, J. Han, S.J. Pearton, A.P. Zhang, B. Luo, J.W. Johnson, F. Ren, Role of annealing conditions and surface treatment on ohmic contacts to p- GaN and p- Al 0.1 Ga 0.9 N/GaN superlattices, 3636 (2001) 19–22. <https://doi.org/10.1063/1.1423387>.
- [97] K. Hestroffer, F. Wu, H. Li, C. Lund, S. Keller, J.S. Speck, U.K. Mishra, Relaxed c-plane InGaN layers for the growth of strain-reduced InGaN quantum wells, *Semicond. Sci. Technol.* (2015). <https://doi.org/10.1088/0268-1242/30/10/105015>.
- [98] Q.L. Zhang, F.Y. Meng, P.A. Crozier, N. Newman, S. Mahajan, Effects of stress on phase separation in In x Ga 1 - x N / GaN multiple quantum-wells, *Acta Mater.* 59 (2011) 3759–3769. <https://doi.org/10.1016/j.actamat.2010.11.020>.
- [99] F. Bernardini, V. Fiorentini, Nonlinear macroscopic polarization in III-V nitride alloys, *Phys. Rev. B - Condens. Matter Mater. Phys.* 64 (2001) 1–7. <https://doi.org/10.1103/PhysRevB.64.085207>.
- [100] A. Di Carlo, F. Della Sala, P. Lugli, V. Fiorentini, F. Bernardini, Doping screening of polarization fields in nitride heterostructures, (2000) 1–5. <https://doi.org/10.1063/1.126831>.
- [101] O. Jani, B. Jampana, M. Mehta, H. Yu, I. Ferguson, R. Opila, C. Honsberg, Optimization of GaN window layer for InGaN solar cells using polarization effect, *Conf. Rec. IEEE Photovolt. Spec. Conf.* (2008). <https://doi.org/10.1109/PVSC.2008.4922725>.
- [102] X. Chen, K.D. Matthews, D. Hao, W.J. Schaff, L.F. Eastman, Growth, fabrication, and characterization of InGaN solar cells, *Phys. Status Solidi Appl. Mater. Sci.* 205 (2008) 1103–1105. <https://doi.org/10.1002/pssa.200778695>.
- [103] L. Hsu, W. Walukiewicz, Modeling of InGaN/Si tandem solar cells, *J. Appl. Phys.* 104 (2008). <https://doi.org/10.1063/1.2952031>.
- [104] Y. Kuo, H. Lin, J.-Y. Chang, Y. Chen, Y. Chang, Polarization Effect on the Photovoltaic Characteristics of AlGaIn/InGaIn Superlattice Solar Cells, *IEEE Electron Device Lett.* 33 (2012) 1159–1161. <http://ieeexplore.ieee.org/lpdocs/epic03/wrapper.htm?arnumber=6230603>.
- [105] S.Y. Nam, Y.S. Choi, Y.H. Song, M.H. Jung, C.M. Kang, D.J. Kong, S.J. Park, J.Y. Lee, G. Namkoong, D.S. Lee, N-ZnO/i-InGaIn/p-GaN heterostructure for solar cell application, *Phys. Status Solidi Appl. Mater. Sci.* 210 (2013) 2214–2218.

<https://doi.org/10.1002/pssa.201329158>.

- [106] H.W. Wang, P. Yu, Y.R. Wu, H.C. Kuo, E.Y. Chang, S.H. Lin, Projected efficiency of polarization-matched p-In_xGa_{1-x}N/i-In_yGa_{1-y}N/n-GaN double heterojunction solar cells, *IEEE J. Photovoltaics*. 3 (2013) 985–990. <https://doi.org/10.1109/JPHOTOV.2013.2252953>.
- [107] J. Bai, C.C. Yang, M. Athanasiou, T. Wang, Efficiency enhancement of InGaN/GaN solar cells with nanostructures, *Appl. Phys. Lett.* 104 (2014) 1–5. <https://doi.org/10.1063/1.4864640>.
- [108] X. Zhang, X. Wang, H. Xiao, C. Yang, J. Ran, C. Wang, Q. Hou, J. Li, Simulation of In_{0.65}Ga_{0.35}N single-junction solar cell, 7335 (2007). <https://doi.org/10.1088/0022-3727/40/23/013>.
- [109] SILVACO, Int. ATLAS user's manual. Santa Clara, CA, Ver, 2011, vol. 5.
- [110] Shawn E. Green, Interdigitated back-surface-contact solar cell modeling using Silvaco Atlas, MONTEREY, CALIFORNIA, 2015. <http://hdl.handle.net/10945/45861>.
- [111] J. Baldomero Garcia, Indium gallium nitride multijunction solar cell simulation using silvaco atlas, MONTEREY, CALIFORNIA, 2007. <http://hdl.handle.net/10945/3423>.
- [112] TonyPlot User's Manual, 2015. www.silvaco.com.
- [113] H.U. Manzoor, M.A.M. Zawawi, M.Z. Pakhuruddin, S.S. Ng, Z. Hassan, High conversion and quantum efficiency indium-rich p-InGaN/p-InGaN/n-InGaN solar cell, *Phys. B Condens. Matter*. 622 (2021). <https://doi.org/10.1016/j.physb.2021.413339>.
- [114] N.D. Gupta, V. Janyani, M. Mathew, M. Kumari, R. Singh, Design and fabrication of InGaN/GaN superlattice-based solar cell using photonic crystal structure, *J. Nanophotonics*. 12 (2018) 1–15. <https://doi.org/10.1117/1.JNP.12.043505>.
- [115] T.H. Anderson, A. Lakhtakia, P.B. Monk, Optimization of nonhomogeneous indium-gallium-nitride Schottky-barrier thin-film solar cells, *J. Photonics Energy*. 8 (2018) 1–17. <https://doi.org/10.1117/1.JPE.8.034501>.
- [116] H.Y. Ryu, H.S. Kim, J.I. Shim, Rate equation analysis of efficiency droop in InGaN light-emitting diodes, *Appl. Phys. Lett.* 95 (2009) 8–11. <https://doi.org/10.1063/1.3216578>.
- [117] F. Bertazzi, M. Goano, E. Bellotti, A numerical study of Auger recombination in bulk InGaN, *Appl. Phys. Lett.* 97 (2010) 12–15. <https://doi.org/10.1063/1.3525605>.
- [118] W.M. Haynes, CRC Handbook of Chemistry and Physics, 95 TH EDIT, CRC Press, 2014. <https://doi.org/https://doi.org/10.1021/ja0336372>.
- [119] G.N. Derry, Z. Ji-Zhong, Work function of Pt(111), *Phys. Rev. B*. 39 (1989) 1940–1941. <https://doi.org/10.1103/PhysRevB.39.1940>.
- [120] L.A. DuBridge, The Photoelectric and Thermionic Work Functions of Outgassed Platinum, *Phys. Rev.* 31 (1928) 236–243. <https://doi.org/10.1103/PhysRev.31.236>.
- [121] A.Y. Polyakov, C. Haller, R. Butté, N.B. Smirnov, L.A. Alexanyan, A.I. Kochkova, S.A.

- Shikoh, I. V. Shchemerov, A. V. Chernykh, P.B. Lagov, Y.S. Pavlov, J.F. Carlin, M. Mosca, N. Grandjean, S.J. Pearton, Deep traps in InGaN/GaN single quantum well structures grown with and without InGaN underlayers, *J. Alloys Compd.* 845 (2020) 156269. <https://doi.org/10.1016/j.jallcom.2020.156269>.
- [122] E. Gür, Z. Zhang, S. Krishnamoorthy, S. Rajan, S.A. Ringel, Detailed characterization of deep level defects in InGaN Schottky diodes by optical and thermal deep level spectroscopies, *Appl. Phys. Lett.* 99 (2011) 2009–2012. <https://doi.org/10.1063/1.3631678>.
- [123] F. Oktasendra, R. Hidayat, R.I. Utama, Effects of interface state density on the carrier transport and performance of metal-insulator-semiconductor (MIS) type thin film solar cells, *J. Phys. Conf. Ser.* 1481 (2020). <https://doi.org/10.1088/1742-6596/1481/1/012005>.
- [124] S.A. and M.I.B.C. Md. Mehedi Hasan¹, Investigation of Graphene/Silicon-dioxide/Gallium Arsenide Based MIS Solar Cell Using Silvaco TCAD, in: 14th Glob. Eng. Technol. Conf. 29-30 December 2017, BIAM Found. 63 Eskaton, Dhaka, Bangladesh, 2017. <https://www.researchgate.net/publication/330090624%0AInvestigation>.
- [125] R.K. Chanana, BOEMDET-Band Offsets and Effective Mass Determination Technique applied to MIS devices on silicon to obtain the unknown bandgap of insulators, *IOSR J. Appl. Phys.* 6 (2014) 48–55. <https://doi.org/10.9790/4861-06634855>.
- [126] I. Shlyakhov, J. Chai, M. Yang, S. Wang, V. V. Afanas'ev, M. Houssa, A. Stesmans, Energy Band Alignment of a Monolayer MoS₂ with SiO₂ and Al₂O₃ Insulators from Internal Photoemission, *Phys. Status Solidi Appl. Mater. Sci.* 216 (2019) 1–7. <https://doi.org/10.1002/pssa.201800616>.
- [127] A. V. Korotun, A. V. Babich, Y. V. Karandas, On the influence of the effective mass of electrons on the Fermi energy of metal–insulator nanosandwiches, *Phys. Met. Metallogr.* 117 (2016) 426–429. <https://doi.org/10.1134/S0031918X16050112>.
- [128] T. Sugiura, S. Matsumoto, N. Nakano, Numerical analysis of tunnel oxide passivated contact solar cell performances for dielectric thin film materials and bulk properties, *Sol. Energy.* 214 (2021) 205–213. <https://doi.org/10.1016/j.solener.2020.11.032>.
- [129] A. Kumar, S. Mondal, K.S.R.K. Rao, Structural, electrical, band alignment and charge trapping analysis of nitrogen-annealed Pt/HfO₂/p-Si (100) MIS devices, *Appl. Phys. A Mater. Sci. Process.* 122 (2016) 1–8. <https://doi.org/10.1007/s00339-016-0569-7>.
- [130] N.S. Kozlova, A.P. Kozlova, Z.A. Goreeva, Spectrophotometric methods and their capabilities to study material optical parameters, in: Proc. - 2017 2nd Int. Ural Conf. Meas. Ural. 2017, 2017: pp. 281–288. <https://doi.org/10.1109/URALCON.2017.8120724>.
- [131] F. Kløw, E.S. Marstein, S.E. Foss, Tunneling Contact Passivation Simulations using Silvaco Atlas, *Energy Procedia.* 77 (2015) 99–105. <https://doi.org/10.1016/j.egypro.2015.07.015>.

Publications and conferences

- Benslim, A., Meftah, A., Labeled, M., Meftah, A., & Sengouga, N. (2021). Study and optimization of InGaN Schottky solar cell performance. *Optik*, 247, 167984.
- Simulation of schottky solar cell device based on Indium Gallium Nitride (InGaN); 8th international conference on materials science and nanotechnology for next generation held in Elazig, Turkey. 2021.
- Simulation and optimization of InGaN Schottky solar cells; 1st National Conference on the Physics of Materials and their Applications CNPMA'2021, November 27 and 28, 2021, Algiers, Algeria.
- Theoretical design and performance of $\text{In}_x\text{Ga}_{1-x}\text{N}$ schottky junction solar cell; 1st international Conference on Materials and Energies, September,13, 14,2021, Tamanghasset, Algeria.
- Numerical simulation of $\text{In}_x\text{Ga}_{1-x}\text{N}$ Schottky solar cell; 1st International Conference on Sustainable Energy and Advanced Materials IC-SEAM'21 April 21-22, 2021, Ouargla, ALGERIA



Contents lists available at ScienceDirect

Optik

Journal homepage: www.elsevier.com/locate/ijleo

Study and optimization of InGaN Schottky solar cell performance

Amina Benslim, Amjad Meftah, Madani Labeled, Afak Meftah, Nouredine Sengouga^{*}

Laboratory of semiconducting and metallic materials (LMSM), Mohammed Khider University, BP 145, Bliska 07000, Algeria

ARTICLE INFO

Keywords:
Solar cell
Schottky
Simulation
 $\text{In}_x\text{Ga}_{1-x}\text{N}$
Traps
Optimization

ABSTRACT

In this work, an extensive numerical simulation of an $\text{In}_x\text{Ga}_{1-x}\text{N}$ Schottky barrier solar cell is carried out using Silvaco ATLAS simulator. Firstly, the effect of different Schottky metals and Indium fraction (in $\text{In}_x\text{Ga}_{1-x}\text{N}$ compound) on the solar cell output parameters are studied. A standard Platinum (Pt) work function of 5.65 eV gave a low efficiency of about 7.10% for an Indium (In) molar fraction of 0.54. Since other studies have shown that Pt may have higher work function, this latter was scanned from 5.65 to 6.35 eV. Consequently, the efficiency increased from 7.10% to 22.18% for a work function of 6.35 eV and a 0.7 In fraction. Additional optimizations improved the cell efficiency to 23.3%, by introducing a 4 μm thick intrinsic $\text{In}_{0.7}\text{Ga}_{0.3}\text{N}$ layer between Pt and the doped $\text{In}_{0.7}\text{Ga}_{0.3}\text{N}$. Further improvement is achieved using a gradual band gap intrinsic layer. Furthermore, this gradual band gap intrinsic layer reduces the effect of interface traps which were found to induce serious degradation of the cell efficiency. The introduction of this gradual band gap intrinsic layer provides a cell efficiency of 38.42% at low trap densities and 28.8% at higher densities.

1. Introduction

Metal-semiconductor based devices find important applications in field effect transistors, detectors, phototransistors, bipolar transistors, and space solar cell. A high-performance Schottky barrier is important to the stability and reproducibility in device developments. The Schottky junction solar cell has been considered one among the unassuming photovoltaic device since it can be fabricated in simple manner and at low cost and is expected to give better spectral response in the shorter-wavelength region due to the close surface depletion region [1]. The semiconductor layer is placed between two metallic contacts. The first one in the front of the device and should form a Schottky barrier contact with the semiconductor while the second one is the end edge of the device and should form an Ohmic contact. In case of n-type semiconductor, the metal work function of the Schottky contact should exceed the one of the semiconductor while in Ohmic contact, metal work function should be lower [2].



CERTIFICATE OF ATTENDANCE

This is to certify that

Amina BENSLİM

Has attended

*8th international conference on materials science and nanotechnology
for next generation held in Elazığ, Turkey.*

14-16 July 2021

Prof. Dr. Fahrettin YAKUPHANOĞLU

Faculté de Physique

Département Matériaux et Composants

1^{ère} Conférence National sur la Physique des Matériaux et leurs Applications
(CNPMA'2021), 4 et 5 Décembre 2021, U.S.T.H.B, Alger, Algérie

Attestation de participation

Le Directeur du Laboratoire Physique des Matériaux «LPM» et le Président du comité d'organisation de la
1^{ère} Conférence National sur la Physique des Matériaux et leurs Applications (CNPMA'2021) attestent que :

Mme Benslim Amina

A présenté au CNPMA'2021 une communication intitulée :

Simulation and optimization of InGaN Schottky solar cells

Auteurs : Amina Benslim, Amjad Meftah, Madani Labeled, Afak Meftah and Nouredine Sengouga

Cette attestation est délivrée à l'intéressée pour servir et faire valoir ce que de droit.

Le Directeur du Laboratoire Physique des
Matériaux «LPM»

مدير مختبر الفيزياء للمواد،
الأستاذ بونقيدج بوطكديرت
Pr. Tarek BOUTKEDJIRT

Le Président du comité d'organisation /

Le Chef du Département Matériaux et Composants

رئيس قسم المواد والمكونات
الأستاذ شرفي رابع
Dr. Rabah CHERFI

Amine Elokka El Hadj Moussa Eg Akhamok University of Tamanghasset - Algeria



Sciences & Technology Faculty

Materials and Energies Research Laboratory- MERL

1st international Conference on Materials and Energies

September 13-14, 2021 - IC-ME '21 Online conference



CERTIFICATE

This certificate is awarded in recognition of attendance in oral /poster presentation

Name & Surname

Amina Benslim

Paper Title

Theoretical design and performance of InxGa1-xN schottky Junction solar cell

Professor Abderrahim Benmoussat
Conference chairman

Dr Mohammed Benattallah
Conference General Chair





PEOPLE'S DEMOCRATIC REPUBLIC OF ALGERIA
 MINISTRY OF HIGHER EDUCATION AND SCIENTIFIC RESEARCH
 UNIVERSITY OF KASDI MERBAH OUARGLA
 FACULTY OF MATHEMATICS AND MATTER SCIENCES



N° : IEMO728/2021

**1st International Conference on Sustainable Energy and Advanced Materials
 IC-SEAM'21 April 21-22, 2021, Ouargla, ALGERIA (Virtual conference)**

CERTIFICATE OF PARTICIPATION

The organizing committee of the first International Conference on Sustainable Energy and Advanced Materials
 IC-SEAM'21 April 21-22, 2021, Ouargla, ALGERIA, certifies that:

Amina Benslim

presented an Oral communication entitled:

Numerical simulation of InxGa1-xN Schottky solar cell

Co-author (s): Anjad Meftah, Madani Labed, Afak Meftah , Nouredine Sengouga

Dean of the Faculty
 Pr/Djamel BECHKI

IC-Coordinator of IC-SEAM'21
 Ouargla, Afak BENMEBROUK
 April 21-22, 2021

Chairman of the IC-SEAM'21
 Ouargla, Hajar MOHAMMEDI
 April 21-22, 2021